

**Protein Misfolding in Stroke-Heart Syndrome: A Molecular Bridge  
between Brain and Heart**

**Dissertation**

**zur**

**Erlangung der naturwissenschaftlichen Doktorwürde**

**(Dr. sc. nat.)**

**vorgelegt der**

**Mathematisch-naturwissenschaftlichen Fakultät**

**der**

**Universität Zürich**

**von**

**Thamonwan Diteepeng**

**aus**

**Thailand**

**Promotionskommission**

**Prof. Dr. Thorsten Buch (Vorsitz)**

**Prof. Dr. Giovanni Camici**

**Dr. Marco Luciani**

**Prof. Dr. Federica del Monte**

**Prof. Dr. Christian Grimm**

**Zürich, 2025**

## Table of Contents

TABLE OF CONTENTS .....	I
ABBREVIATIONS .....	III
ABSTRACT .....	1
STATEMENT OF AUTHORSHIP .....	4
1. INTRODUCTION.....	5
1.1 The growing burden of stroke .....	5
1.2 Neurological complications in stroke .....	6
1.3 Non-neurological complications in stroke.....	8
1.4 Stroke-heart syndrome.....	9
1.5 Protein misfolding and diseases .....	21
2. AIMS .....	31
3. MATERIAL AND METHODS .....	34
3.1 Animals and middle cerebral artery occlusion model of focal ischemia.....	34
3.2 ECG recordings .....	34
3.3 Echocardiography .....	35
3.4 Tissue harvesting .....	35
3.5 Assessment of the cerebral infarct volume .....	36
3.6 Measurement of biomarkers for myocardial injury and catecholamines .....	36
3.7 Proinflammatory cytokine profiling .....	36
3.8 STRING analysis.....	36
3.9 Immunofluorescence staining .....	37
3.10 Quantitative Real Time-Polymerase Chain Reaction (RT-PCR).....	37
3.11 Isolation of soluble and insoluble protein aggregates.....	38
3.12 Isolation of total proteins .....	38
3.13 Dot blot analysis .....	39
3.14 Western blotting.....	39
3.15 In vitro hiPSC-derived cardiomyocytes (iCM) culture and treatment .....	40
3.16 Cytotoxicity assay.....	41
3.17 Cell viability assay.....	41
3.18 Proteomic analysis using mass spectrometry .....	41
3.20 Buffers and solutions .....	42
3.19 Statistical analysis.....	42

4. RESULTS.....	43
4.1 AIS induces cardiac dysfunctions.....	43
4.2 AIS leads to myocardial stress and morphometric alterations.....	45
4.3 AIS alters systemic inflammatory response and autonomic dysregulation .....	46
4.4 AIS is associated with the increased presence of oligomers .....	48
4.5 AIS disrupts the local protein quality control (PQC) systems in the heart.....	51
4.6 AIS leads to the accumulation of ubiquitin aggregates in the ischemic brain but not the heart. ....	53
4.7 Sole effects of oligomers to the proteome in human iPSC-derived cardiomyocytes (iCM) .....	55
5. DISCUSSION .....	59
5.1 AIS-induced cardiac dysfunction and arrhythmias.....	60
5.2 AIS-induced autonomic dysregulation and systemic inflammatory responses .....	62
5.3 Systemic accumulation of oligomers and protein misfolding during AIS.....	62
5.4 Impairment of local PQC mechanisms in the post-stroke heart .....	63
5.5 Differential ubiquitin dynamics in the brain and heart.....	65
5.6 The biological relevance of oligomers on human cardiomyocytes .....	66
6. CONCLUSION AND FUTURE PERSPECTIVES .....	67
7. LIMITATION OF THE STUDY .....	68
8. APPENDIX I: SUPPLEMENTARY FIGURES.....	70
9. APPENDIX II: SUPPLEMENTARY TABLES .....	74
10. APPENDIX III: BUFFER PREPARATIONS .....	79
11. ACKNOWLEDGEMENTS.....	82
12. REFERENCES.....	83

## **Abbreviations**

A: Late diastolic mitral inflow velocity  
A': Late diastolic mitral annular velocity  
ACTH: Adrenocorticotrophic hormone  
AD: Alzheimer's disease  
AF: Atrial fibrillation  
AFDS: Atrial fibrillation detect after stroke  
AIS: Acute ischemic stroke  
ANOVA: Analysis of variance  
ANP: Atrial natriuretic peptide  
ATF4: Activating transcription factor 4  
ATF6: Activating transcription factor 6  
ATP: Adenosine triphosphate  
AXT: Protein kinase B  
A $\beta$ : Amyloid- $\beta$   
BBB: Blood-brain barrier  
BSA: Bovine serum albumin  
CHOP: C-EBP homologous protein  
CMA: Chaperone-mediated autophagy  
CNP: C-type natriuretic peptide  
CNS: Central nervous system  
CO: Cardiac output  
cTnT: Cardiac troponin T  
CXCL13: C-X-C chemokine ligand-3  
DALYs: Disability-adjusted life years  
DAMPS: Damage-associated molecular patterns  
DAPI: 4,6-diamidino-2-phenylindole hydrochloride  
DMSO: Dimethyl sulfoxide  
E: Early diastolic mitral inflow velocity  
E': Early diastolic mitral annular velocity

ECG: Electrocardiography  
EDV: End-diastolic volumes  
EF: Ejection fraction  
ER: Endoplasmic reticulum  
ERAD: Endoplasmic reticulum-associated degradation  
ESV: End-systolic volumes  
FS: Fractional shortening  
GAPDH: Glyceraldehyde-3-phosphate dehydrogenase  
GCs: Glucocorticoids  
GM1: Monosialogangliosides  
GRP: Glucose-regulated proteins  
HD: Huntington's disease  
hiCM: Human-induced pluripotent stem cells-derived cardiomyocytes  
hiPSC: Human-induced pluripotent stem cells  
HPA: Hypothalamic-pituitary-adrenal  
HSC: Heat-shock cognate proteins  
HSP: Heat shock protein  
HVA: Homovanillic acid  
ICAM-1: Intercellular adhesion molecule-1  
IFN- $\gamma$ : Interferon- $\gamma$   
IL: Interlukins  
IRE1: Inositol  
IRE1: Inositol-requiring enzyme 1  
kDa: Kilodalton  
LDH: Lactate dehydrogenase  
LV: Left ventricular  
LVIDd: Left ventricular end-diastolic internal diameter  
LVIDs: Left ventricular end-systolic internal diameter  
MCA: Middle carotid artery  
miR: MicroRNA

mTORC: Mammalian target of rapamycin complex  
MTT: 3-(4,5-dimethylthiazol-2-yl)-2,5-diphenyl tetrazolium bromide  
NT-proBNP: N-terminal pro-brain natriuretic peptides  
PAOs: Pre-amyloid oligomers  
PBS: Phosphate buffer saline  
PCA: Principle component analysis  
PD: Parkinson's disease  
PERK: PKR-like ER kinase  
PP2A: Protein phosphatase 2A  
PQC: Protein quality control systems  
PrP<sup>C</sup>: Prion protein  
SCD: Sudden cardiac death  
SD1: Short-term variability  
SD2: Long-term variability  
SHS: Stroke-heart syndrome  
SV: Stroke volume  
TBS: Tris-buffered saline  
TBST: Tris-buffered saline with 0.1% Tween-20  
TIMP-1: Tissue inhibitor of metalloproteinases-1  
TMAO: Trimethylamine-N-oxide  
tMCAO: Transient middle cerebral artery occlusion  
TNF- $\alpha$ : Tumor necrosis factor- $\alpha$   
TTC: 2, 3, 5-triphenyltetrazolium chloride  
TTS: Takotsubo syndrome  
UPR: Unfolded protein response  
UPS: Ubiquitin proteasome system  
XBP1: X-box binding protein 1

## **Abstract**

### **Introduction:**

Stroke remains a leading cause of mortality worldwide and the most prevalent cerebro-cardiovascular event in the Western world, yet effective therapies for improving prognosis remain limited. Beyond local neurological damage, stroke frequently triggers cardiovascular complications, collectively termed stroke-heart syndrome (SHS), which significantly worsen outcomes and increase mortality even in patients without pre-existing heart disease. This interconnection is not surprising as the brain and heart share a number of common risk factors (aging, hypertension, diabetes etc.) as well as overlapping pathophysiological responses such as excessive catecholamine release, endocrine dysregulation, oxidative stress, and inflammation. However, despite growing recognition of SHS, the mechanisms underlying brain-heart crosstalk remain largely elusive.

Emerging evidence suggests that protein misfolding, a mechanism implicated in both neurodegenerative and cardiovascular diseases, may represent a previously unrecognized contributor to ischemic injury, offering a potential novel target for therapeutic intervention. In nature, proteins must adopt a precise three-dimensional structure to maintain cellular function. Under pathological conditions, misfolding can occur, leading to the accumulation of toxic oligomers and amyloid aggregates, disrupting cellular homeostasis. Due to their physiochemical properties, misfolded proteins, particularly oligomers, interact with cell surfaces, alter intracellular homeostasis and possibly be transported beyond the tissue of origin, contributing to systemic complications, as in the case of transthyretin cardiac amyloidosis. The presence of amyloid- $\beta$  (A $\beta$ ) aggregates in the hearts of Alzheimer's patients along with their detrimental effects on cardiomyocyte function and metabolic homeostasis further supports a mechanistic link between protein misfolding in neurological and cardiac pathology.

Although traditionally associated with chronic neurodegenerative diseases, protein misfolding also plays a role in acute ischemic injury. Following stroke, ischemic tissues exhibit increased expression of molecular chaperones to correct misfolded proteins, however, when this adaptive mechanism becomes overwhelmed, misfolded proteins accumulate, ultimately exacerbating cellular dysfunction and tissue damage. This phenomenon, coupled with the increasing recognition of protein misfolding as a systemic process, challenges the conventional view of ischemic stroke as a localized neurological event. Instead, it raises the possibility that ischemic brain injury may propagate proteotoxic stress to peripheral organs

such as the heart. Understanding the role of protein misfolding in stroke-heart interactions provide critical insights into the systemic impact of ischemic stroke and establishes protein misfolding as a key contributor to neurocardiac dysfunction.

### **Main objectives:**

The present study investigates the systemic effects of acute ischemic stroke (AIS) on cardiac function and assesses the involvement of protein misfolding in SHS by evaluating oligomer presence and its biological relevance in the post-stroke myocardium. The sole effects of oligomers on human cardiomyocytes are also examined at transcriptional and translational levels.

### **Methods:**

Cerebral ischemia was induced in 3- to 4 months-old wild-type C57BL/6J male and female mice via 45-minute left-sided transient middle cerebral artery occlusion (tMCAO), followed by 48 hours of reperfusion. Cardiac function was evaluated using electrocardiography and echocardiography at baseline (pre-surgery) and 48 h post-surgery. Tissues were harvested to assess oligomer localization and myocardial proteostasis response through a set of molecular analyses. Plasma and urine were also collected to measure the levels of catecholamine metabolites, proinflammatory cytokines and cardiac injury biomarkers. To increase translational aspect of the present study and pinpoint the direct effects of oligomers on cardiomyocytes whether they actively contribute to stroke-induced cardiac injury or serve as bystanders in parallel to other stress factors, an *in vitro* model was established using hiPSC-derived cardiomyocytes (hiCM) from male and female donors. Following cardiac differentiation, hiCM were subjected to different stress conditions induced by synthetic A $\beta$ <sub>42</sub>-derived oligomers in parallel with other SHS-related mediators consisting of catecholamine modulators (epinephrine and haloperidol) and pro-inflammatory cytokines (IFN- $\gamma$ ). Vehicle-treated cells were used as negative controls while untreated cells represented baseline condition. To resemble the damage duration *in vivo*, these cells were exposed to these stressors for 48 h, followed by cell harvesting for transcriptional analysis using qPCR and proteomic profiling using Olink technology. This experimental approach allowed for a direct examination of the transcriptional and proteomic effects of oligomers on cardiomyocytes and their potential sex-specific responses.

**Results:**

AIS induced cardiac dysfunction characterized by bradyarrhythmias, reduced cardiac output and a tendency towards decreased stroke volume and fractional shortening. Systemic alterations included including dysregulated plasma pro-inflammatory cytokines, whose pattern is associated with A $\beta$  regulation, a key hallmark in a number of misfolding-related diseases including vascular dementia. Elevated oligomer and ubiquitin aggregate accumulation in the ipsilateral brain hemisphere confirmed localized ischemic proteotoxic stress. Notably, increased oligomer levels in the heart were also observed along with compromised cardiac proteotoxic resistance, as evidenced by reduced levels of the chaperone heat-shock protein 90 (HSP90) and impairment of activating transcription factor-6 (ATF6)-dependent unfolded protein response in both sexes. Concurrent activation of autophagic and antioxidant responses was also observed. Unlike the brain, the heart did not show ubiquitin aggregation, suggesting distinct proteostasis mechanisms between the two organs. In hiCM, A $\beta_{42}$ -derived oligomers broadly disrupted proteotoxic stress responses at the gene level, with potential sex-specific differences in certain markers. Principal component analysis plot further revealed distinct baseline proteomic profiles between sexes while showing a converging translational response to oligomer exposure.

**Conclusions:**

Our findings indicate the systemic effects of AIS on cardiac function in healthy young wild-type mice. The accumulation of oligomers in both brain and heart, along with impaired cardiac resistance to proteotoxicity, suggests a potential mechanistic link between post-stroke neurodegeneration and cardiac dysfunction. The complex response of hiCM to A $\beta_{42}$  oligomers underscores the unique feature of oligomers impact on the human myocardium with potential sex-specific divergence.

### **Statement of authorship**

I hereby declare that I am the main author of this dissertation and that I have not used any sources other than those listed in the bibliography and identified as references. I acknowledge some of the experiments shown in the present dissertation were performed by my colleagues from different research centers, specifically: murine models of ischemic stroke were conducted by Dr. Yustina Maria Puspitasari from the Center for Molecular Cardiology (CMC) at UZH under the animal license ZH040/2021. Echocardiography was performed with the help of Dr. Stefano Ministrini from CMC. Immunofluorescent staining in mouse tissues was performed with the help of Dr. Marialucia Telesca from the Center for Translational and Experimental Cardiology (CTEC). In vitro study in hiCM was performed with the collaboration with the group of Dr. Melanie Generali from the Institute for Regenerative Medicine (IREM) at UZH. The data analysis of Olink proteomics was performed by Dr. Shafeeq Ahmed Mohammed from CTEC. I performed all other experiments and am the sole responsible for writing the present dissertation. I further declare that I have not submitted this thesis at any other institution in order to obtain a degree.

## **1. Introduction**

### **1.1 The growing burden of stroke**

Stroke remains the second-leading cause of long-term disability and mortality globally, with the highest burden of the disease in low- and middle-income countries. The impact of stroke is remarkable, with over 100 million people worldwide affected and an annual mortality rate of 6.55 million. Between 1990 and 2019, the burden of stroke increased significantly in terms of the absolute number of the incidents (70%), prevalent (85%), stroke-related deaths (43%), and disability-adjusted life years (DALYs) (32%) at the global level<sup>1</sup> as shown in Figure 1. This large and rapid-growing stroke burden is attributed to various factors including population growth, ageing population and more prolonged exposure to modifiable risk factors such as arterial hypertension and diabetes.<sup>2</sup> In the absence of prompt implementation of effective primary prevention strategies, the stroke burden is likely to continue expanding worldwide, particularly in low-income countries. Notably, despite the common perception of stroke as a condition primarily affecting the elderly, over 12.2 million new stroke cases were reported in 2019 and 63% of which occurring in individuals under the age of 70. This indicates a shifting demographic trend in stroke occurrence towards younger populations.<sup>3</sup> Additionally, emerging research highlights age-dependent sex differences in stroke with evidence showing that men have higher incidence and mortality between the ages of 45 and 74 years old. Beyond this age, these rates dramatically rise in women influenced by factors such as sex steroid hormones (especially estrogen), genetic sex and epigenetics.<sup>4</sup>

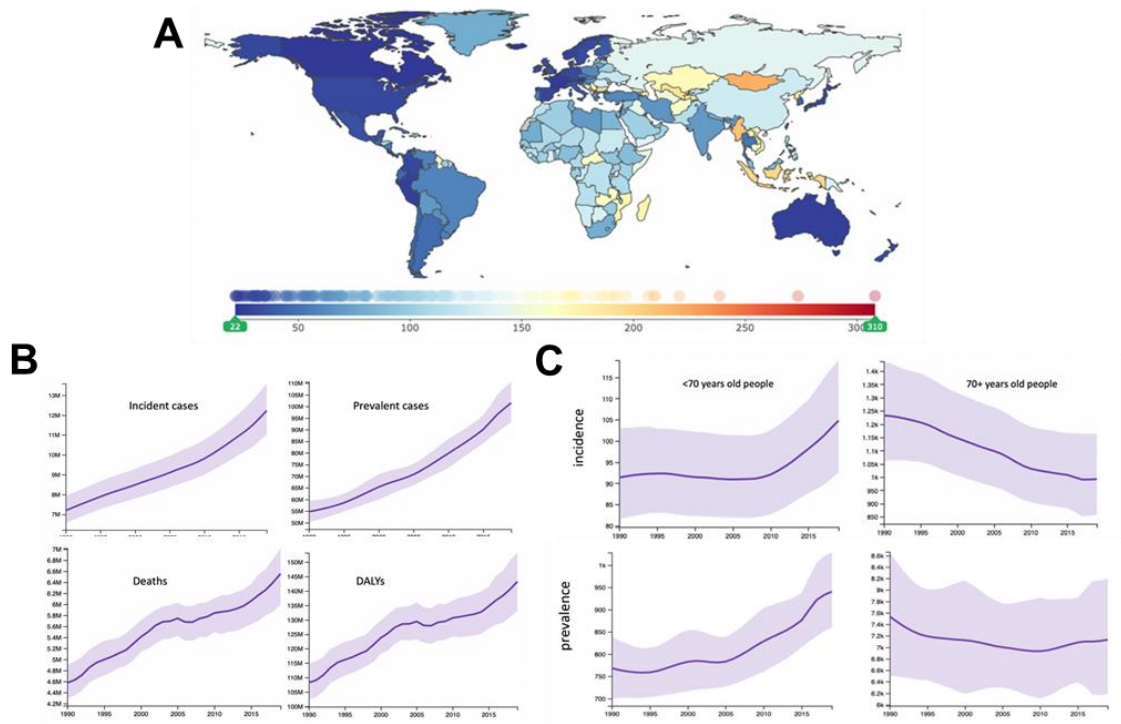


**Figure 1: Global burden of stroke.** (A) Age-standardized stroke death rates per 100,000 people by country in 2019, (B) Absolute number (in millions) of stroke incidence, prevalence, deaths and DALYs and (C) annual stroke incidence rate and prevalence per 100,000 people aged <70 and >70 years old by year from 1990 to 2019 (shadow areas are 95% uncertainty intervals). Adapted from Feigin et al. (2021).<sup>1</sup>

## 1.2 Neurological complications in stroke

Stroke is classified into five major subtypes: (1) ischemic stroke, (2) hemorrhagic stroke, (3) subarachnoid hemorrhage stroke, (4) cerebral venous thrombosis and (5) spinal cord stroke. Among these, ischemic stroke is the most prevalent, accounting for 87% of all stroke types.<sup>5</sup> This subtype is caused by blockage or narrowing of cerebral blood vessels supplying the brain, typically due to thrombotic or embolic events which limit blood flow to the brain. This results in the formation of an ischemic core with irreversible tissue damage, surrounded by the penumbra, a region of impaired but potentially salvageable neurons.<sup>6</sup> The insufficient supply of oxygen and blood to the ischemic region results in neuronal cell depolarization, the failure of energy metabolism, perturbed ionic homeostasis, pH imbalance and a concomitant increase in vascular permeability and leakage.<sup>7</sup> Although restoring blood flow to the ischemic lesions, known as reperfusion, is effective in providing oxygenation in the affected tissue, it paradoxically contributes to further injury. This phenomenon, known as reperfusion injury, is characterized by a complex series of pathophysiological events involving inflammation, oxidative stress, energy failure, calcium dysregulation, mitochondrial dysfunction, cellular

excitotoxicity, and increased blood-brain barrier (BBB) permeability (Figure 2). All these mechanisms collectively contribute to secondary brain damage, resulting in brain edema, neuroinflammation and neural cell death and ultimately severe neurological deficits.<sup>8</sup>

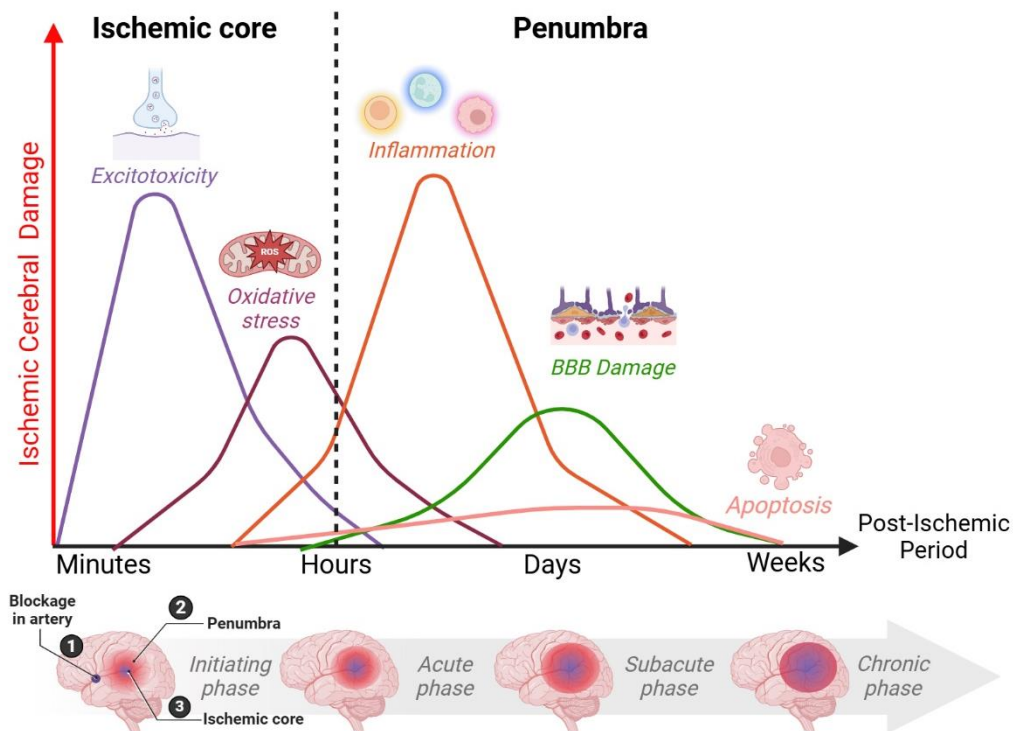


**Figure 2: Spatial and temporal progression of cerebral injury in ischemic stroke.** The ischemic core rapidly undergoes cellular excitotoxicity and oxidative stress within minutes due to oxygen and blood supply depletion, leading to irreversible neuronal death. In contrast, the penumbra, a surrounding brain region with reduced but salvageable blood flow, experiences neuroinflammation, BBB impairment and progressive cell death over hours to weeks. The lower panel illustrates the sequential phases of ischemic injury from the initiating phase (stroke onset) to acute, subacute and chronic phases, highlighting dynamic pathophysiological changes. Various signaling pathways are activated during these pathological transitions and their targeted regulation could serve as potential therapeutic strategies. Adapted from Qin et al. (2022).<sup>9</sup> This figure was created with BioRender.com.

The health and economic challenges posed by neurological deficits and long-term disability resulting from ischemic stroke prompt the development of various therapeutic strategies for reducing its severe impact. In the acute management of ischemic stroke, interventions aimed at reducing infarct volume and enhancing neuronal viability are widely employed.<sup>8</sup> These approaches include targeted modification of risk factors by primary and secondary prevention (i.e. hypertension, smoking, obesity, physical activity, alcohol consumption and diabetes mellitus) and therapeutic means such as pharmacological thrombolysis and mechanical endovascular thrombectomy. However, the effectiveness of these interventions is hindered by several factors such as a narrow therapeutic window for an effective rescue of ischemic

cerebral tissue suboptimal efficacy and safety of pharmacological drugs (e.g. fibrinolytics, anti-thrombolytics, anti-platelet agents, statins, edaravone, nerinetide<sup>10</sup>) and stringent criteria for patient selection thereby excluding frail patients with contraindications.<sup>11</sup> Despite the advancement in stroke treatment, the translation of these therapeutic approaches and neuroprotective agents for ischemic stroke from experimental settings to clinical practice has lagged behind the success observed in clinical trials for other medical conditions. This discrepancy is partly related to the complexity of ischemic stroke pathophysiology together with its multimorbid conditions presented in stroke patients.<sup>12</sup>

### **1.3 Non-neurological complications in stroke**

In recent years, there has been growing recognition of AIS as a systemic disease that extends its impact beyond the central nervous system (CNS), affecting multiple peripheral organs. Interestingly, only 6% of stroke patients occur without any additional pathophysiological conditions whereas the remaining 94% of patients present with at least one additional chronic predisposing medical condition such as hypertension, atrial fibrillation, atherosclerosis, diabetes mellitus, ischemic heart disease or chronic kidney disease which significantly impact both prognosis and functional recovery of stroke patients.<sup>13,14</sup>

Shortly following the onset of AIS, a multitude of organ systems beyond CNS experience a series of alterations, varying in severity from subclinical laboratory abnormalities to life-threatening complications.<sup>15</sup> This broad-reaching influence of adverse consequences extends across various tissues in human body including immune, respiratory, urinary, cardiovascular, gastrointestinal, musculoskeletal and endocrine systems, contributing to worse stroke outcomes, increased treatment burden and elevated mortality rates among stroke patients<sup>12</sup> (Figure 3).

The presence of multimorbidity, defined as the coexistence of two or more chronic medical conditions, in patients with AIS is believed to be influenced by shared common risk factors. For example, it has been shown that the association between multimorbidity and stroke predictably appears to increase with advanced age, female sex, smoking, frequent alcohol assumption and socioeconomic deprivation.<sup>16</sup> Furthermore, following the onset of AIS, the ischemic brain not only elicits local damages such as oxidative stress and inflammation within the cerebral tissue but also triggers pathological alterations outside the brain. These systemic responses are mediated by a complex network of mechanisms involving autonomic dysfunctions, activation of the hypothalamic-pituitary-adrenal (HPA) axis, systemic immune dysregulation, gut microbiome dysbiosis and other factors. Ultimately, these processes lead to

structural changes and functional impairments in distant organs. The extent and severity of these systemic effects are closely linked to both the volume and location of the cerebral ischemic lesion.<sup>12</sup>

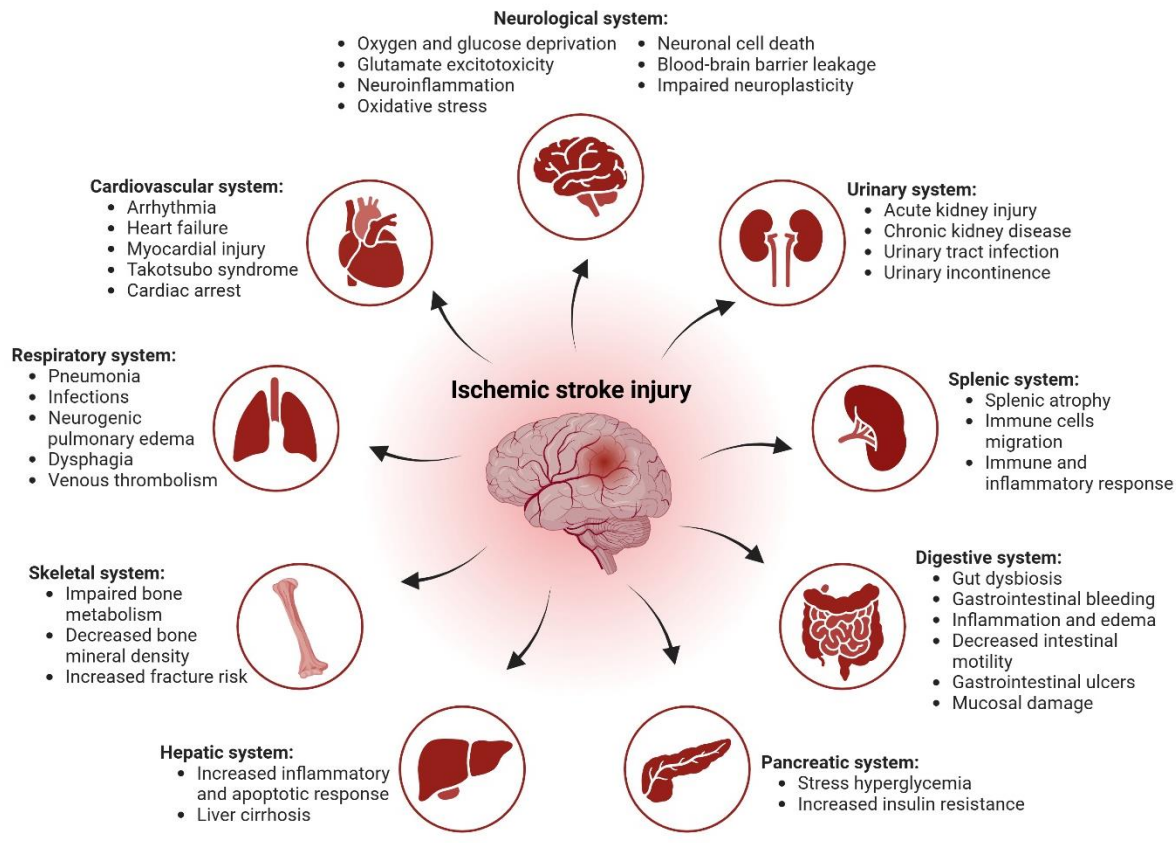


**Figure 3: Systemic effects of ischemic stroke injury in various peripheral organs.** The impact of ischemic stroke extends beyond the vascular injury occurring in the brain, triggering a cascade of detrimental processes such as inflammation, neurotoxicity and cell death. This multifaceted effect induces dysfunction across a spectrum of organ systems, including cardiac, respiratory, gastrointestinal, digestive, pancreatic, urinary and musculoskeletal tissues. This intricate interplay between the brain and each affected organ system underscores the systemic nature in stroke pathology, thereby emphasizing its influence beyond the confines of the cerebral nervous system. Adapted from Balch et al. (2020).<sup>15</sup> This figure was created with BioRender.com.

### 1.4 Stroke-heart syndrome

The occurrence of myocardial injury caused by cerebral vascular disease was firstly reported in 1947 by Byer et al., coining the term brain-heart syndrome.<sup>17</sup> Since then, the concept of brain-heart axis has gained prominence, underscoring the physiological and pathophysiological interactions between nervous and cardiovascular systems, leading to the emergence of the field known as ‘neurocardiology’.<sup>18</sup> Over the past decades, various neurological disorders such as subarachnoid hemorrhage, epilepsy, ischemic stroke, intracerebral hemorrhage, traumatic brain injury and dementia have been recognized to elicit

a broad spectrum of cardiovascular dysfunctions. These include subendocardial ischemia, electrocardiographic (ECG) changes, cardiac arrhythmias, autonomic dysfunction, Takotsubo syndrome and sudden cardiac death.<sup>19-21</sup>

In recent years, the incidence of heart injury following ischemic stroke has become increasingly significant. These cardiac complications have been observed in 20% of patients within the first few days following stroke events even in the absence of primary cardiac disease. Major adverse cardiovascular complications have been associated with a significantly worsened 5-year prognosis.<sup>22</sup> Furthermore, stroke patients experiencing early severe cardiac complications face a 2- to 3-fold increase of in-hospital mortality rates.<sup>23</sup> Distinguishing post-stroke cardiac complications from concomitants or preceding acute cardiovascular syndrome can be challenging although diagnostic strategies have been suggested. Thus, the term of SHS has been introduced to refer cardiac manifestations induced by acute ischemic stroke with an intention to increase clinical awareness, generating a common mechanistic framework as well as facilitating the development of research collaborations and efficient clinical management.<sup>24</sup>

#### 1.4.1 Clinical manifestations of SHS

A broad spectrum of cardiac complications after ischemic stroke can be categorized into 5 main groups including: (1) ischemic and non-ischemic acute myocardial injury with elevated cardiac troponin (cTn) levels, which are often asymptomatic; (2) post-stroke myocardial infarction; (3) left ventricular (LV) dysfunction, heart failure and post-stroke Takotsubo syndrome; (4) cardiac arrhythmias including atrial fibrillation (AF) and ECG changes; and (5) sudden cardiac death.<sup>25,26</sup> The clinical manifestations of SHS can occur spontaneously and even concomitantly, their incidence ranges from approximately 3% for myocardial infarction to over 50% for pathological ECG alterations.<sup>27</sup> The most serious complications are mostly developed in acute phase after stroke onset and associated with worsen neurological outcomes and increased mortality.<sup>28</sup>

##### 1.4.1.1 ECG changes and cardiac arrhythmia

The most common cardiac change after stroke is alterations in ECG parameters including corrected QT (QTc) prolongation, ST segment elevation, T-wave abnormalities, prominent U waves, pathological Q waves, and rhythm irregularities.<sup>29,30</sup> These alterations are often indicative of left ventricular (LV) systolic and diastolic dysfunctions, affecting approximately 50-80% of patients suffering from AIS. Such abnormal ECG and arrhythmias can be transient and occur early within 24 hours after ischemic stroke onset.<sup>30</sup> Patients exhibiting these

alterations experience elevated risk of mortality during hospitalization.<sup>31</sup> Prior investigations have demonstrated that prolonged QTc interval is associated with more severe manifestations of SHS, including myocardial injury with elevated cTn, severe arrhythmia, and cardiac sudden death after stroke.<sup>28,32</sup> Among patients affected by SHS, AF emerges as the most prevalent and persistent cardiac arrhythmia detected in up to one-quarter of AIS patients, defined as atrial fibrillation detected after stroke (AFDAS). AFDAS is acknowledged as a significant independent risk factor for ischemic stroke, increasing the stroke risk by 5-fold with a 2-fold increase in mortality.<sup>33,34</sup> AFDAS accounts for all cases of AF, either pre-existing or being triggered by the stroke with over 70% of cases diagnosed within the first 3 days of hospital admission and disappeared within few days thereafter.<sup>35,36</sup> Newly diagnosed AF following stroke may result from the underlying SHS itself and could be considered as primarily ‘neurogenic’. Nonetheless, AFDAS tends to have a lower prevalence of cardiovascular comorbidities and less severe cardiac structural abnormalities than AF diagnosed before stroke.<sup>37</sup> Consequently, the rapid initiation and continuous monitoring of cardiac function in patients following AIS onset are imperative for timely and effective diagnosis of post-stroke AF.<sup>38</sup>

#### 1.4.1.2 LV dysfunction and Takotsubo syndrome (TTS)

Post-stroke cardiac complications are not limited to myocardial injury but the occurrence of LV dysfunction, heart failure and Takotsubo syndrome is also associated with ischemic stroke depending on the underlying pathophysiological mechanisms.

Impairment of LV systolic function is relatively frequent in all three types of patients suffering from ischemic stroke<sup>39</sup>, intracerebral hemorrhage<sup>40</sup> and subarachnoid hemorrhage<sup>41</sup>. However, due to the lack of knowledge of baseline data on LV function prior to stroke, accurately determining the incidence of new-onset ventricular dysfunction remains challenging. Ventricular dysfunction is characterized by hypokinetic wall-motion alterations on ECG and is often clinically expressed as heart failure. Advanced age, high stroke severity, pre-existing cardiovascular disease, and elevated baseline cTn levels are identified risk factors for impaired LV function.<sup>42,43</sup> Echocardiographic evidence of systolic dysfunction is reported in 13-29% of the cases of ischemic stroke and is associated with a higher risk of in-hospital mortality.<sup>23</sup> In addition to systolic impairment, a dysfunction in the LV diastolic relaxation has also been reported in AIS patients and is considered as a prognostic marker of both functional recovery and the risk of recurrent stroke.<sup>44</sup>

TTS represents a distinct form of LV morpho-functional changes observed in AIS. It typically presents as an acute heart failure syndrome characterized by apical ballooning of the LV apex resembling a Japanese octopus trap known as a takotsubo.<sup>45</sup> This phenomenon is thought to result from increased sensitivity of apical myocytes to catecholamines.<sup>46</sup> Although the exact pathophysiology of TTS remains elusive, TTS is believed to arise from functional and structural impairments of the brain-heart axis.<sup>47</sup> Common triggers of TTS are acute neurological disorders such as ischemic stroke, intracranial hemorrhage and seizures. This syndrome predominantly affects postmenopausal women and is frequently preceded by intense emotional and physical stress.<sup>45</sup> Despite the presence of echo- and electrocardiographic abnormalities along with elevated cTn levels suggestive of systolic impairment, TTS patients often remain asymptomatic or fail to detect due to concurrent neurological deficits. Notably, the occurrence of TTS following stroke has been associated with increased in-hospital mortality.<sup>48</sup>

#### 1.4.1.3 Sudden cardiac death (SCD)

SCD is defined as an unexpected death occurring within 1 h from the start of symptoms when death is witnessed, or within 24 hours of being seen alive when death is unwitnessed.<sup>49</sup> SCD is presented frequently in patients with a pre-existing coronary artery disease as well as in those with neuropsychiatric disorder in the absence of cardiac diseases. SCD can be the consequence of various cardiac and non-cardiac conditions, including emotional stress, exposure to endogenous or exogenous catecholamines, cardiac arrest, subarachnoid hemorrhage, intracerebral bleeds, AIS (particularly infarctions in the insular cortex) and epileptic seizures.<sup>28</sup> Considering the potential mechanisms of stroke-induced SCD, neurogenic injury triggered by sympathetic hyperactivation following stroke has been known to cause SCD by inducing fatal cardiac arrhythmias, massive myocytolysis and myocardial infarction leading to death.<sup>50,51</sup> To assess the effects of ischemic lesion localization and SCD, Turkoglu and colleagues showed that stroke in the right insular led to decreased heart rate variability and increased of sudden death.<sup>52</sup> However, research on sudden death after stroke is complicated by the fact that many cases are not witnessed or sufficiently recorded. Additional challenging is identification of the actual cause of death in patients with SCD due to the scarcity of autopsy studies and availability of timely ECG recordings during events.

#### 1.4.2 Myocardial markers of SHS

Current guidelines for the early management of patients with AIS recommend the measurement of cardiac biomarkers upon admission to improve prognosis.<sup>53</sup> Comparing to other myocardial biomarkers, cTn is a preferred biomarker due to its high sensitivity and specificity in diagnosis of myocardial injury.<sup>54</sup> These proteins are primarily synthesized and released by ventricular cardiomyocytes in response to ventricular volume overload and increased ventricular wall stress. Notably, elevated serum cTn levels are detected in 13% of stroke patients even in the absence of overt coronary symptoms<sup>23</sup> and more prevalent in elderly patients, and those with existing structural cardiac conditions such as heart failure and atherosclerosis.<sup>55</sup> In addition, stroke characteristics particularly lesion location and severity may correlate with elevated cTn particularly lesions in the dorsal anterior insular cortex which can induce autonomic disbalance, sympathetic hyperactivity, and subsequent myocardial injury.<sup>56</sup>

Clinically, clinical differentiation between acute and chronic myocardial injury is distinguished by serial measurements of cTn levels; acute myocardial injury is manifested by a rising and/or falling pattern of cTn levels, whereas no such dynamic pattern is presented in chronic myocardial injury caused by structural heart disease.<sup>57</sup> Importantly, these dynamic cTn concentrations have been detected in approximately 5-20% of patients with ischemic stroke, indicating acute rather than chronic myocardial injury and are associated with an increased risk of in-hospital death<sup>55</sup>

An additional cardiac biomarker extensively investigated in the context of SHS manifestations is N-Terminal Pro-Brain Natriuretic Peptides (NT-proBNP). Elevated plasma levels of NT-proBNP have been reported in nearly two-thirds of acute stroke patients, reaching the highest level on the day following symptom onset and subsequently declining thereafter.<sup>58,59</sup> Elevated NT-proBNP levels are independently associated with greater stroke severity, poorer functional outcomes and increased risk of mortality.<sup>60,61</sup> Therefore, determining the underlying cause of acute myocardial injury after stroke in a timely manner is crucial to improve prognosis.

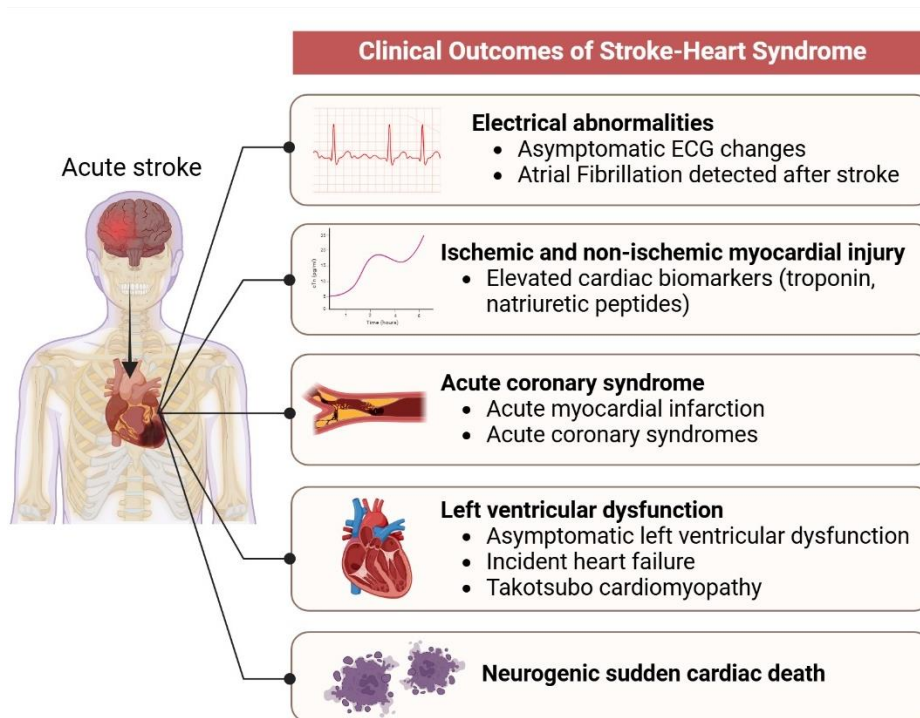


**Figure 4: Cardiac complications during acute phase following stroke.** The acute phase after stroke typically refers to the period between 24-72 hours after the event. Stroke-heart syndrome encompasses five main categories: 1) Electrocardiographic changes and cardiac arrhythmias including post-stroke atrial fibrillation; 2) Ischemic and non-ischemic acute myocardial injury presenting with elevated cardiac troponin, which is usually asymptomatic; 3) Post-stroke acute myocardial infarction; 4) Left ventricular dysfunction, heart failure, and post-stroke takotsubo syndrome; and 5) Post-stroke neurogenic sudden cardiac death.<sup>26</sup> This figure was created with BioRender.com.

### 1.4.3 Pathophysiology of SHS

AIS and cardiovascular complications share similar unmodifiable (e.g., age, sex, and ethnicity) and modifiable factors (e.g., physical activity, smoking, diet, diabetes, and hypertension) which are primarily involved in the pathogenesis of SHS. On top of these factors, multiple potential biological pathways contributing to the intimate crosstalk between the two organs in the setting of AIS have been identified, reinforcing the concept of the brain-heart axis. Key pathological mechanisms propelling the brain-heart crosstalk consist of autonomic nervous system, the HPA axis, inflammatory responses, and other contributing factors such as gut microbiome dysbiosis, microvesicles, microRNA as summarized in Figure 5.<sup>62</sup>

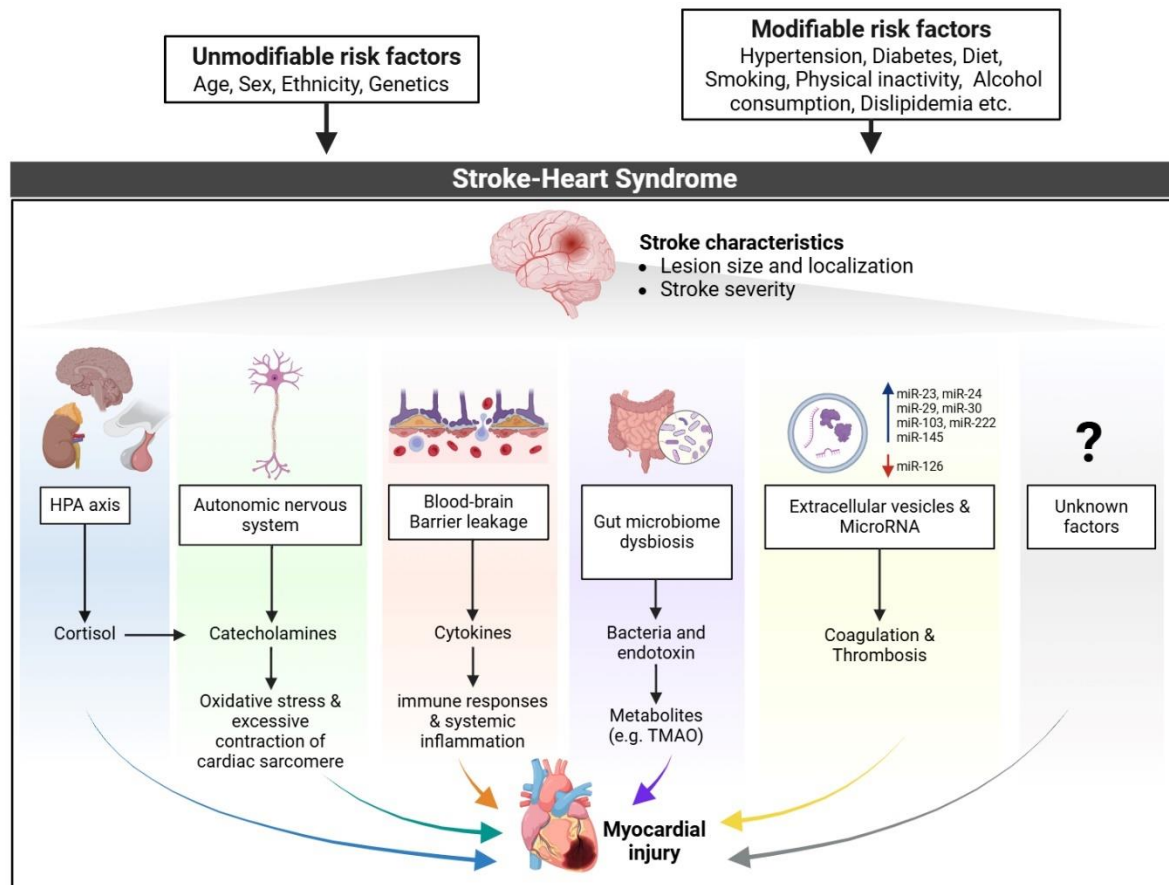


**Figure 5: Summary of pathological mechanisms and related risk factors in brain-heart interaction.** Stroke induces cardiac complications multiple pathophysiological mechanisms involved in the stroke-heart cross-talk including the alterations in HPA axis, autonomic nervous (sympathetic and parasympathetic) dysregulation, intestinal microbiota dysbiosis, inflammation as well as the release of microvesicles, and microRNA. Various risk factors, both modifiers and non-modifiers, in individuals contribute to the risk of developing SHS. Moreover, stroke-related factors such as ischemic lesion size, location involving certain brain areas of autonomic control (especially the right insular cortex) and stroke severity have been strongly correlated with the extent of subsequent myocardial injury. Adapted from Chen et al. (2017).<sup>63</sup> This figure was created with BioRender.com.

#### 1.4.3.1 Autonomic dysfunctions

Dysregulated autonomic activity after AIS has widespread effects on various organ systems including the heart, immune system, gastrointestinal tract and glucose metabolism. In the context of SHS, post-stroke cardiac injury is primarily driven by the alterations in the sympathetic and parasympathetic nervous systems with a shift towards sympathetic predominance.<sup>26,64</sup> Autonomic dysfunction is associated with adverse clinical outcomes in AIS patients, irrespective of the initial stroke severity.<sup>65</sup> Clinically, autonomic dysfunctions in AIS patients often manifest as changes in heart rate variability, baroreflex sensitivity, and levels of circulating/urinary catecholamines (including norepinephrine and epinephrine) or their metabolites (including metanephrine and normetanephrine).<sup>66</sup>

Cerebral ischemia is known to elevate sympathetic tone, accompanied by increased catecholamine release from the adrenal medulla and sympathetic nerve terminals into circulation.<sup>67</sup> Experimental animal study has shown that higher plasma concentrations of catecholamines after ischemic stroke are directly associated with the incidence of myocardial lesions and cardiac damage.<sup>68</sup> Catecholamines, including epinephrine and norepinephrine, act as neurotransmitters of the sympathetic and parasympathetic systems, and also play a role in regulating cardiovascular function via  $\beta$ 1- and  $\alpha$ 1-adrenergic receptors. Increased circulating catecholamines during cerebral injury stimulates  $\beta$ 1 adrenergic receptors in cardiomyocyte, activating adenylyl cyclase and increasing cytosolic cyclic adenosine monophosphate production. This leads to calcium release from the sarcoplasmic reticulum into the cells, causing calcium overload, oxidative stress and adenosine triphosphate (ATP) depletion, mitochondrial dysfunction and cardiomyocyte damage which can be reversible or result in cell death.<sup>69,70</sup>

Specific localizations of the ischemic lesion have been implicated in favoring the occurrence of cardiac injury. The insular cortex, a vital part of the central autonomic network in maintaining the balance between sympathetic and parasympathetic activity, is frequently affected in cases of cerebral ischemia within the middle cerebral artery (MCA) territory.<sup>71</sup> Structural changes in the forebrain, particularly the insular cortex, caused by ischemic stroke directly affect the autonomic nervous system, leading to cardiovascular abnormalities following AIS.<sup>72,73</sup> Considering the insular hemispheric differences in autonomic responses, ischemic lesions in the right hemisphere, associated with increased sympathetic tone, pose a higher risk of cardiovascular complications and mortality than left-sided insular lesions where parasympathetic activity increases.<sup>74</sup> To date, there is no evidence-based treatment for autonomic dysfunction after stroke. However, several therapeutic interventions such as  $\beta$ -blockers have the potential to modulate the autonomic function and ultimately improve outcomes.<sup>75,76</sup>

#### 1.4.3.2 HPA axis

The HPA axis constitutes an intricate network of direct influences and feedback interactions among the three endocrine glands: the hypothalamus, pituitary, and adrenal glands.<sup>77</sup> Activation of the HPA axis regulates a diverse array of neuronal and endocrine systems with the hypothalamic paraventricular nucleus serving as its primary control center, releasing corticotropin-releasing factors such as corticotrophin-releasing hormone and vasopressin. These factors stimulate the pituitary gland to release of adrenocorticotrophic hormone (ACTH)

into the systemic circulation which in turn stimulates the adrenal gland to release glucocorticoids (GCs) namely cortisol in humans and corticosterone in rats under the influence of stress.<sup>78</sup>

Ischemic stroke resulting from acute brain transient ischemic attack initiates a complex sequence of events in the HPA axis which has negative effects on organ's function, and may be a predictor of poorer functional outcome.<sup>79</sup> Numerous studies suggest that the HPA system undergoes one of the earliest measurable alterations as it gets activated within few hours after stroke onset, leading to neurohormonal dysfunction and neuronal death, thereby exacerbating the long-term prognosis following stroke.<sup>80</sup> For instance, early and persisting elevation of circulating cortisol levels after AIS has been correlated with greater stroke severity, elevated extent of insular damage, and increased post-stroke mortality.<sup>81</sup> Moreover, post-stroke secretion of GCs exerts multifaceted effects by modulating immune function, inflammation and metabolic processes as evidenced by the increased expression of pro-inflammatory cytokines and elevated blood glucose levels, ultimately contributing to stroke pathogenesis and progression.<sup>82</sup> Experimental animal study has further demonstrated that hypothalamic stimulation in response to ischemic stroke activates sympathetic output, leading to ECG ischemic-like changes and arrhythmias.<sup>83</sup> Importantly, HPA axis response to ischemic stroke is different between sexes. Women may exhibit an attenuated cortisol response to stroke due to the higher abundance of corticosteroid-binding globulin in plasma from female stroke patients relative to men which would act to limit the degree of post-stroke adaptive immune suppression.<sup>84</sup>

#### 1.4.3.3 Systemic immune dysregulation

The systemic immune dysregulation following stroke stems from a complex cascade of inflammatory responses triggered by the ischemic injury to the brain. Upon experiencing a deficiency in oxygen and nutrients during stroke, cerebral tissue releases immune-active biomolecules, termed damage-associated molecular patterns (DAMPs), within the brain parenchyma. This initiates local neuroinflammation, which occurs concomitantly with endothelial cell activation. Damaged endothelial cells contribute to increased oxidative stress and the disruption of BBB.<sup>85</sup> On the other hand, DAMPs can also enter the circulation, thereby promoting the recruitment of peripheral immune cells (e.g., neutrophils, monocytes, and lymphocytes) to the ischemic brain tissue through the compromised BBB. Subsequently, the activation of these immune cells results in the release of pro-inflammatory cytokines such as interleukins (e.g., IL-1 $\beta$ , IL-6), tumor necrosis factor- $\alpha$  (TNF- $\alpha$ ), and interferon- $\gamma$  (IFN- $\gamma$ )

as well as integrins, adhesion molecules, and chemokines into the circulation, thus facilitating systemic inflammation.<sup>86</sup> Several of these upregulated pro-inflammatory cytokines play pivotal roles in stroke-induced BBB disruption and are associated with increased vascular permeability and stroke severity.<sup>87</sup> They have also been implicated as potential mediators of cardiac damage based on their well-documented involvement in cardiac injury. Notably, cytokines such as IL-6, IL-1 $\beta$ , TNF- $\alpha$ , and IL-18 exert negative inotropic effects on the heart. Moreover, these pro-inflammatory cytokines along with other DAMPs are also known to activate cardiomyocytes via toll-like receptors, leading to further release of pro-inflammatory cytokines, sustaining the inflammatory milieu, and potentially promoting cardiac dysfunction.<sup>88,89</sup> Additionally, further studies indicate that alterations in gut microbiome composition contribute to the systemic pro-inflammatory immune activation by modulating the phenotype of immune cells during acute phase after stroke.<sup>90</sup> A comprehensive understanding these immune-mediated processes is of key importance for the development of targeted therapeutic interventions aimed at modulating the inflammatory response and attenuating the impact of SHS.<sup>86</sup>

#### 1.4.3.4 Gut microbiome dysbiosis

After an ischemic insult, gastrointestinal complications such as hemorrhage, dysphagia and intestinal paralysis develop in over 50% of AIS patients. These complications are strongly associated with deteriorated neurological outcomes and increased mortality rates. The underlying pathology of these disorders likely involves microbiota dysbiosis causing impaired gastrointestinal function after stroke.<sup>91</sup>

Under physiological conditions, the gut-blood barrier plays a crucial role in absorbing nutrients and water while preventing toxins and pathogenic microorganisms from the lumen of gastrointestinal tract into the blood. However, during disease pathogenesis, the integrity of the gut-blood barrier can be disrupted leading to increased intestinal permeability. This phenomenon enables the translocation of bacteria and endotoxin into the bloodstream, triggering inflammatory responses.<sup>92</sup> Furthermore, many experimental and clinical studies have established the association between the risk factors of cardiovascular diseases (e.g., hypertension, diabetes and obesity) and gut microbiota. Greater alterations in intestinal permeability result in more significant disruption of the central nervous system by enhancing the HPA axis and autonomic dysregulation. Apart from inflammatory responses, emerging evidence suggests that alterations in gut microbiota directly contribute to platelet hyperactivity and increased thrombosis risk through the production of trimethylamine-N-

oxide (TMAO), a metabolic byproduct of gut microbiota.<sup>91,93,94</sup> Clinical trials have indicated that TMAO levels can be served as a marker and predictor for cardiovascular diseases. Its level participates in gut microbiota-dependent changes and has been associated with myocardial infarction, heart failure, endothelial cell activation and ventricular remodeling.<sup>95</sup> Such interconnection between the gut, brain and heart establishes a complex brain-gut-heart axis through neural pathways and mechanisms, potentially contributing to the pathogenesis of SHS.<sup>96</sup> However, further investigations are necessary to elucidate the underlying mechanisms of the gut microbiome in mediating stroke-heart crosstalk. Understanding these mechanisms could provide promising therapeutic and preventive approaches, thereby promoting their potential use in clinical therapy.

#### 1.4.3.5 Microvesicles and microRNA

Circulating microvesicles, lipid bilayer-covered cell fragments present in the bloodstream, originate from various cells such as platelets and endothelial cells. Elevated levels of circulating microvesicles have been documented in patients experiencing ischemic stroke, correlating with worse clinical prognosis.<sup>97-99</sup> Circulating microvesicles in the stroke patients are released as a consequence of endothelial activation during inflammation which stimulate endothelial cells to release cytokine IL-6. Increased expression of IL-6 has been associated with a higher incidence of vasospasm, including those in the heart thereby increasing the risk of cardiovascular syndrome through peripheral blood vessels constriction.<sup>100</sup> Platelet-derived microvesicles, which exhibit greater procoagulant activity compared to activated platelets, exhibit elevated levels and correlates with the infarct volume in AIS, suggesting a possible role in the altered platelet activity observed in ischemic stroke patients.<sup>101</sup> Additionally, microvesicles released by neurons, astrocytes, microglia, and neural stem cells can exacerbate neurodegenerative and neuroinflammatory diseases.<sup>102</sup> Previous studies have shown that brain trauma can elevate circulating brain-derived mitochondrial particles, thereby promoting vascular leakage and thrombosis, which may lead to cardiac damage.<sup>103</sup> This finding suggests that the increased coagulation and thrombosis following stroke may have detrimental effects on the heart, warranting further research is needed for elucidation.

Moreover, alterations in the expression of circulating microRNAs (miRs), short sequences of noncoding RNA, have been identified as acute events in stroke patients, potentially impacting cardiac function through inflammatory responses. For example, the decrease in miR-126 expression is closely associated with vascular integrity and has been correlated with heart failure, atrial fibrillation and coronary artery disease after stroke.<sup>104</sup> Studies on endothelial

cell-specific miR-126 knockout mice have demonstrated exacerbated cardiac dysfunction, hypertrophy, fibrosis, and inflammation after ischemic stroke compared to control mice. Clinical evidence has shown that a decrease in serum and cardiac miR-126 expression levels following stroke, alongside the induction of post-stroke cardiac dysfunction, thus implying the involvement of miR-126 in SHS.<sup>105</sup> Furthermore, levels of miR-145 are elevated within 24 hours of cerebral ischemia, positively correlating with elevated plasma markers of inflammation including high-sensitivity C-reactive protein and inflammatory factor IL-6.<sup>106</sup> However, its potential involvement in brain-heart interaction needs to be further investigated.

## 1.5 Protein misfolding and diseases

On top of aforementioned mechanisms contributing to SHS, a growing body of literature has highlighted another potential mechanism associated with ischemic adverse events with possible therapeutic relevance, namely protein misfolding. In the recent past, defects in protein homeostasis and the subsequent occurrence of misfolded protein aggregations has been extensively studied and acknowledged as one of leading pathophysiological causes of over 50 human degenerative diseases involving either the central nervous system, giving rise to neurodegenerative conditions such vascular dementia, Alzheimer's disease (AD), Parkinson's disease (PD) and Huntington's disease (HD) or other tissues including the heart, spleen, liver and kidney, giving rise to systemic amyloidosis and a range of diverse conditions, for example, type II diabetes, renal amyloidosis, cardiac amyloidosis and some types of cancers.<sup>107-112</sup> These group of these protein misfolding-related diseases (termed as proteinopathies) are predominantly sporadic, with hereditary occurrence reported in some patients. In sporadic cases, the onset typically occurs at a relatively advanced age, indicating that protein aggregation and its associated symptoms primarily result from an age-related decline of regulatory mechanisms involving in protein homeostasis.<sup>113,114</sup>

### 1.5.1 The control of protein homeostasis

Proteins are highly versatile macromolecules, with mammalian cells synthesizing at least 20,000 distinct proteins.<sup>115</sup> Each protein must follow a specific folding sequence, regardless of localization, turnover, and molecular size to achieve its native conformation and perform its physiological functions.<sup>116</sup> Failure to properly fold can result in erroneous spatial conformation, potentially eliciting cell stress and leading to severe pathological phenotypes in tissues which termed as proteotoxicity.<sup>117</sup>

To counteract this event, cells have developed a sophisticated and highly coordinated network of cellular machinery known as the protein homeostasis or proteostasis to ensure the proper protein structure, promote cellular function, and prevent misfolded proteins from accumulating, thereby preserving cellular integrity and functionality. This network is operated by the coordinated functions of three main components: (1) the translational machinery for protein synthesis, (2) molecular chaperones and co-chaperones for protein folding, and (3) protein disaggregation and degradation such as the ubiquitin proteasome system (UPS), the autophagy-lysosome pathway and the endoplasmic reticulum (ER)-associated degradation (ERAD) stress response. Additionally, stress response pathways such as the heat shock

response in the cytosol and nucleus as well as unfolded protein response (UPR) in the ER and mitochondria are considered as essential modifiers in modulating the proteostasis network.<sup>118</sup>

#### 1.5.1.1 Protein folding and quality control

Protein folding is a critical process in which newly synthesized amino acid chains acquire their native three-dimensional structures, enabling proper biological function. Although the native state is thermodynamically favorable, proteins must navigate a complex energy landscape during folding, making them susceptible to kinetically stable misfolded states. Molecular chaperones act as the first line of defense in post-translational processes, ensuring proteins achieve the correct conformation and are properly localized within the cell. The chaperones have been grouped into distinct families including ribosome-binding chaperones, heat shock protein 40 (HSP40), HSP60, HSP70, HSP90, HSP100, prefoldins, small HSPs, and tetratricopeptide-domain containing cochaperone.<sup>116</sup>

In all types of cells, chaperones are constitutively expressed but can be upregulated in response to stress conditions to cope with protein folding defects.<sup>119</sup> Their primary function is to stabilize or assist protein folding in an ATP-dependent manner. Additionally, they can also refold aberrantly folded states and prevent aggregation by targeting hydrophobic amino acid side chains exposed by non-native proteins and directing them to degradation pathways.<sup>116</sup> The coordinated action of chaperones across various cellular compartments including the mitochondria (HSP60) and cytoplasm (e.g. HSP70, HSP90 and HSP100) is essential for maintaining proteostasis and preventing cellular dysfunction.<sup>120</sup>

In addition to HSP family, ER chaperones such as glucose-regulated proteins (GRPs) play a vital role in assisting the refolding of misfolded proteins within the ER and regulating the activity of the three primary ER transmembrane sensors of the UPR: PERK, IRE-1 and ATF6. The activation of these sensors initiates signaling cascades that promote protein homeostasis by increasing chaperone production and reducing overall protein synthesis, thereby mitigating ER stress. Another key component of these adaptive responses is ERAD, which employs the proteasome to degrade misfolded proteins.<sup>121</sup> However, this cellular state is sustainable for a limited period of time. Chronic stress, such as the constant production of misfolded proteins during disease or aging, can lead to persistent activation of the UPR, ultimately shifting towards apoptotic cell death mediated by factors such as C-EBP homologous protein (CHOP), human caspase-4 and rodent caspase-12.<sup>122–124</sup>

### 1.5.1.2 Protein degradation

Protein degradation is the second line of defense in maintaining the peptide's functional conformation by eliminating protein aggregates through two major proteolytic pathways: the UPS and the autophagosomal-lysosomal pathway.<sup>125,126</sup> In both systems, cytosolic chaperones cooperate in targeting aberrant proteins and maintain them in a soluble state compatible for degradation. The UPS-mediated proteolysis is the primary degradation system that removes ubiquitylated, soluble proteins that are misfolded or natively folded but no longer needed. This process involves ubiquitin machinery, consisting of ubiquitin-activating enzyme (E1), ubiquitin-conjugating enzymes (E2), and ubiquitin ligases (E3), which tags the target protein substrate via conjugation of ubiquitin molecules. Ubiquitinated proteins are then recognized and trafficked to the proteasome, a large proteolytic complex, for degradation.<sup>127</sup> In the ER, misfolded proteins are handled by the ERAD system which re-translocate them from the ER to the cytoplasm for UPS-mediated degradation.<sup>128</sup>

For large protein aggregates such as inclusion bodies or extracellular plaques which cannot be maintained in a soluble state and cleared by the chaperone machinery and the UPS defense, the autophagy pathway becomes essential. This pathway involves delivering the autophagic cargo to the lysosome, a membrane-bounded vesicle containing various proteases capable of degrading a range of molecules. Autophagy complements the UPS through three mechanistically distinct forms: macroautophagy, chaperone-mediated autophagy (CMA) and microautophagy. Microautophagy is a direct engulfment of cytosolic material at the lysosomal membrane while CMA involved the delivery of soluble proteins with the Lys-Phe-Glu-Arg-Gln (KFERQ) pentapeptide sequence to lysosomes for degradation via the heat-shock cognate protein of 70 kDa (HSC70). In contrast, macroautophagy, characterized by a double-membrane vesicle called the autophagosome, engulf damaged organelles and aberrant proteins before fusing with the lysosomal membrane for degradation into amino acids. In addition, the mammalian target of rapamycin complex 1 (mTORC1) and mTORC2 play a role in autophagy regulation, thereby integrating the proteostasis with the nutritional status of the organism, the cellular metabolic state, and protein synthesis rates.<sup>118,125</sup> The fidelity of this process is crucial to maintain cellular homeostasis; malfunction of proteosomal proteolysis will result in misfolded protein accumulation and ultimately cellular dysfunction.<sup>129</sup>

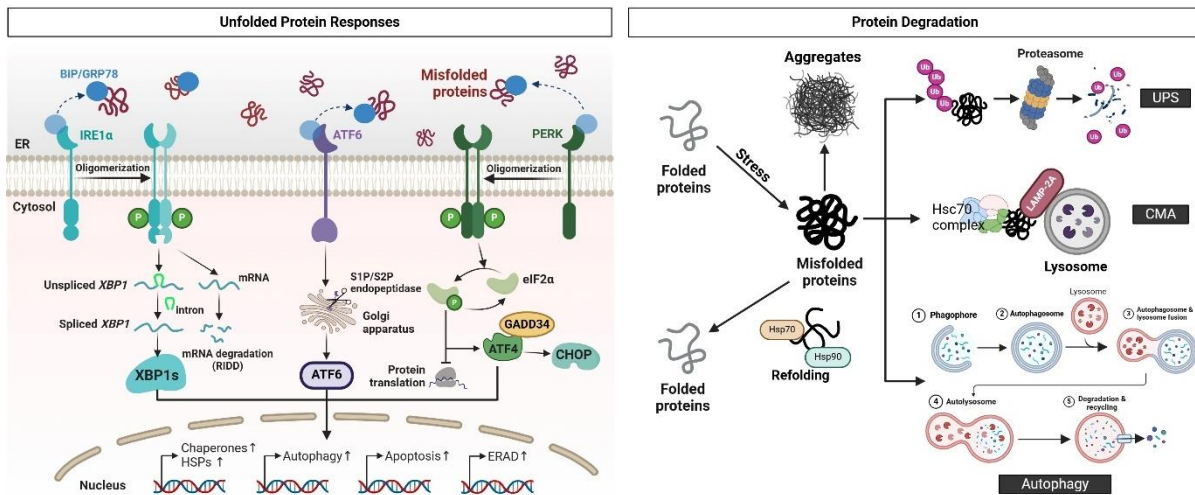


**Figure 6: The control of unfolded protein responses and protein degradation.** Protein homeostasis is maintained by unfolded protein responses (left panel). Misfolded proteins sequester ER chaperones (BiP/GRP78) away from the three transducers of the UPR (IRE1, ATF6 and PERK). This activation triggers various downstream signaling pathways to restore the protein homeostasis. The degradation of misfolded proteins (right panel) are regulated by three major pathways: the ubiquitin-proteasome system (UPS), chaperone-mediated autophagy (CMA) and autophagy depending on the nature, size and solubility of misfolded proteins. Failure in protein degradation leads to the accumulation of protein aggregates. Adapted from Ditepeng et al. (2021)<sup>130</sup> and Ciechanover and Kwon (2015).<sup>125</sup> This figure was created with BioRender.com

### 1.5.2 Mechanistic basis for protein aggregation toxicity

Many proteins are prone to misfold due to various cellular stresses either in the face of protein-dependent stimuli (i.e., genetic mutations, specific aminoacidic sequences, aberrant post-translational modifications, misfolded proteins load) or protein-independent factors (i.e., perturbations environmental conditions, aging, comorbidities and organ vulnerability).<sup>130</sup> When misfolded protein cannot be resolved due to proteostasis impairment, they accumulate and form larger structures known as prefibrillar oligomers or pre-amyloid oligomers (PAOs). In light of governing thermodynamic and kinetic factors, the soluble oligomers must undergo rearrangement to form highly ordered fibrils, representing the thermodynamic final state of the aggregation process<sup>131</sup> (Figure 7). Such fibrillar aggregates are also known as amyloid fibrils, a term derived from the Greek word “amyloidos” meaning “starch-like” due to their thread-like structure with a positive iodine staining reaction similar to starch.<sup>132</sup>

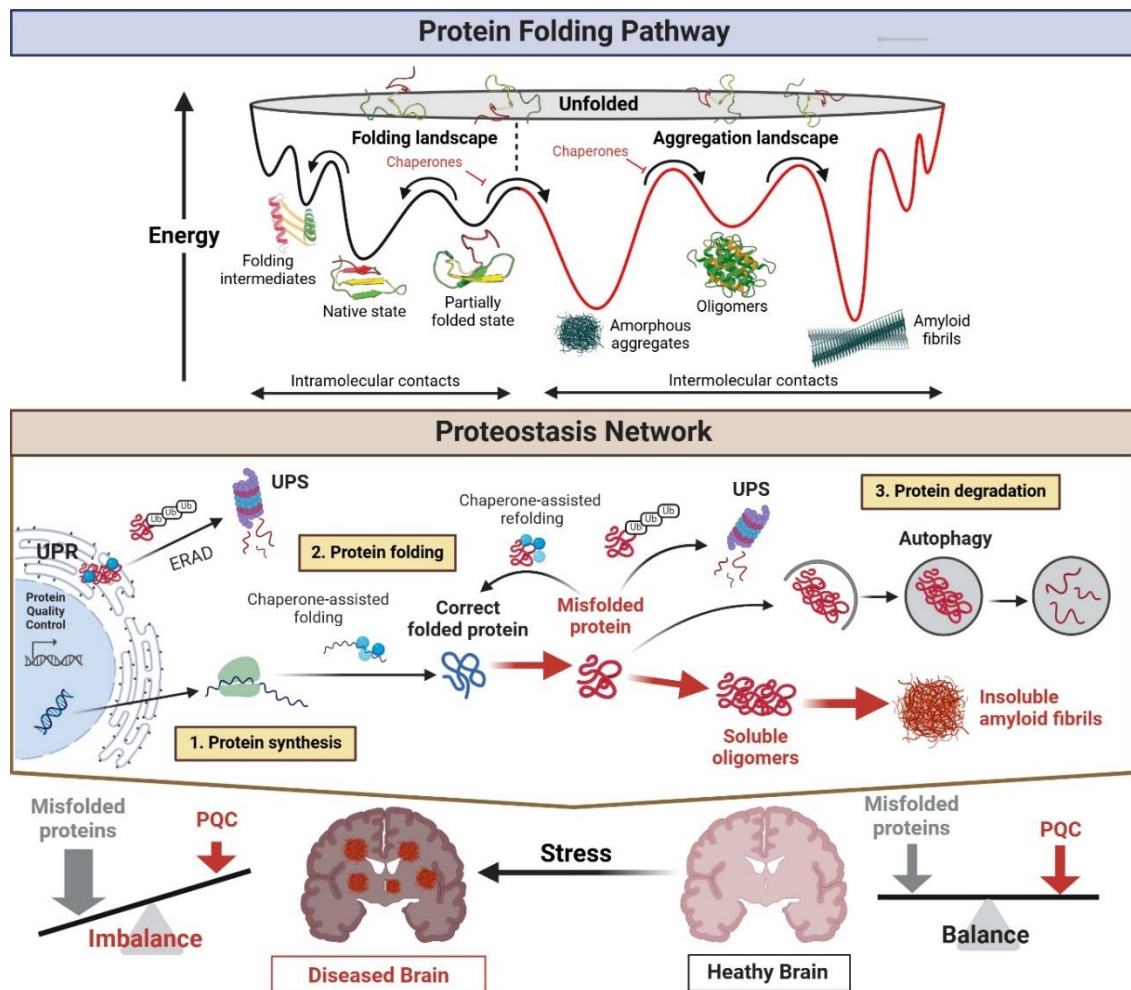


**Figure 7: The process of protein misfolding and proteostasis network during disease progression.** Top panel illustrates the funnel-shaped energy landscape model of protein folding. Unfolded polypeptides, which have the highest energy level and lowest stability, move down the funnel towards a low-energy native conformation at the bottom by forming energetically favorable intramolecular interactions (black funnel) with the assistance of chaperones. Ruggedness in the landscape can trap proteins in misfolded states, leading to aggregation (red funnel). The Proteostasis Network (middle panel) maintains protein homeostasis through three key processes: (1) Protein synthesis, where quality control mechanisms such as the unfolded protein response (UPR) and endoplasmic reticulum-associated degradation (ERAD), regulates nascent protein folding. (2) Protein folding, facilitated by chaperones to refold misfolded proteins. (3) Protein degradation, where misfolded proteins are eliminated via the ubiquitin-proteasome system (UPS) or autophagy. The bottom panel illustrates the balance between protein quality control (PQC) and misfolded proteins accumulation. In a healthy brain, PQC mechanisms maintain proteostasis, preventing toxic aggregation. Under pathological conditions, PQC failure leads to proteostasis imbalance, contributing to neurodegenerative diseases. Adapted from Herczenik and Gebbink (2008)<sup>131</sup> and Ditepeng et al. (2020).<sup>130</sup> This figure was created with BioRender.com.

These amyloid fibrils feature a characteristic cross- $\beta$  core, formed by  $\beta$ -strands arranged perpendicular to the fibril axis, creating an extensive hydrogen bond network that confers high stability to the amyloid state. The presence of such structures is typically

confirmed/assessed by the binding of dyes such as Congo red, thioflavin-T or their derivatives which produce specific spectral responses by forming ordered arrays along the fibril lengths.<sup>111,133</sup> Fibrillar aggregates formation and deposition within and around cells are well-characterized in age-dependent degenerative diseases like  $\alpha$ -synuclein in PD, A $\beta$  and tau in AD, and wild-type transthyretin in cardiac amyloidosis.<sup>134</sup>

To date, 37 proteins have been identified capable of misfolding and forming amyloid-like structures under certain conditions in various human tissues as either localized or systemic deposits.<sup>133</sup> Initially, mature amyloid fibrils were believed to be the most toxic aggregate forms in protein misfolding diseases, either by sequestering functional proteins (loss-of-function) or directly damaging cells and tissues where they deposit (toxic gain-of-function).<sup>135</sup> This concept however has been challenged by findings showing the inert nature of fibrillar aggregates in some cases and the poor correlation between their accumulation and disease severity.<sup>136,137</sup> Recent studies have introduced a paradigm shift proposing that PAOs are more strongly associated with disease phenotypes than monomeric and mature fibrils.<sup>138,139</sup> For instance, A $\beta$  oligomers, the first known biochemical change that occurs during AD progression, can cause cognitive deficits without the presence of amyloid plaques.<sup>140</sup> Additionally, the cytotoxicity of PAOs in the heart has been reported to induce cardiomyocyte loss, leading to heart failure.<sup>141</sup> These observations highlight PAOs as the most pathogenic species in the spectrum of proteinopathies. Consequently, targeting PAOs has emerged as a potential therapeutic strategy for effective drug screening while mature fibrillar aggregates remain important as pathological biomarkers and histological hallmarks.<sup>142</sup>

### 1.5.3 PAOs: the molecular origins of amyloid-related pathogenicity

A variety of PAOs, particular those derived from the well-known A $\beta$  peptides, have been isolated and characterized and given a wide range of names such as globulomers, pentamers, A $\beta$ \*56, amyloid-derived diffusible ligands, protofibrils, annular protofibrils, and spherical amyloid intermediates. Despite the diversity of these oligomeric species, they share a common sequence-independent conformation that can exert proteotoxicity through a uniform mechanism. Unlike monomers and fibrils, PAOs exhibit a distinct polypeptide backbone conformation with marked epitope formation independent of amino acid sequences which have been recognized by the oligomeric-conformational antibodies such as oligomer-specific A11 antibody.<sup>143,144</sup>

The transient nature of PAOs leads to structural polymorphism, resulting in a broad spectrum of sizes ranging from dimers to 24-mers and even higher-ordered assemblies as they progress through the aggregation process. Recent investigations emphasize the significance of oligomer size in determining their toxicity, with emerging evidence indicating an inverse correlation between the size of oligomeric species and the magnitude of their toxic effects. As oligomeric assemblies increase in size, their deleterious effects tend to decrease<sup>145</sup> (Figure 8). For example, studies on A $\beta$ <sub>40</sub> and A $\beta$ <sub>42</sub> oligomers reveal that small oligomers such as prefibrillar oligomers (18-90 kDa) and ADDLs (36-72 kDa) show maximum toxicity while larger oligomers such as fibrillar oligomers (approximately 68-104 kDa), annular protofibrils (approximately 250-400 kDa) and amyloid fibrils exhibit the least toxicity<sup>146</sup> The pronounced toxicity of small oligomers can be attributed to their high diffusional mobility and the exposure of hydrophobic protein parts on their surface, which are typically buried within the native structure or highly dispersed in intrinsically disordered aggregates. Such properties enable small oligomers to reach cell membrane more frequently and internalize into cells by interacting with the phospholipid components of cell membrane, thereby perturbing the membrane and inducing aberrant intracellular cascades.<sup>147,148</sup>

Exposure of neuronal and non-neuronal cell cultures as well as whole animals to these PAOs has been linked to various molecular and cellular perturbations including mitochondrial damage<sup>149</sup>, intracellular production of reactive oxygen species<sup>150</sup>, calcium influx into the cells, lipid peroxidation<sup>151</sup>, metal (i.e. copper, zinc, iron) dyshomeostasis<sup>152</sup> and induction of apoptotic pathways and inflammatory responses.<sup>153</sup> Beyond interacting with biological membranes, extracellular protein oligomers have been reported to bind directly and indirectly with a variety of receptors. These include the ionotropic glutamate receptors: NMDA (N-methyl-D-aspartate) and AMPA ( $\alpha$ -amino-3-hydroxy-5-methyl-4-isoxazole-propionate) receptors which regulate the calcium ions influx; the metabotropic glutamate receptor 5; the insulin receptor; the nicotinic acetylcholine receptor; the prion protein (PrP<sup>C</sup>); clusterin; and other cellular components.<sup>154</sup> However, oligomer-mediated cytotoxicity is not solely determined by the inherent properties of the oligomers and their ability to interact with the plasma membrane. The lipid composition of the interacting cell membrane also plays a crucial role. Evangelisti and colleagues revealed that cellular membranes enriched in monosialogangliosides, GM1, a key component of lipid rafts, exhibit higher membrane permeability, internalization and cytotoxicity of oligomers.<sup>155</sup>

Notably, oligomers are unlikely to exhibit a single molecular interaction, mechanism of action or a unique cascade of cellular events associated with a specific disease. Rather, their toxicity

which contributes to disease is likely due to their intrinsic misfolded nature and structural heterogeneity, causing them to engage in various aberrant interactions with multiple cellular components. However, due to the transient and heterogenous characteristics of PAOs, including variation in size, solubilities, and stabilities, investigating their biological and toxic properties in vitro and in vivo remains challenging.<sup>156</sup>

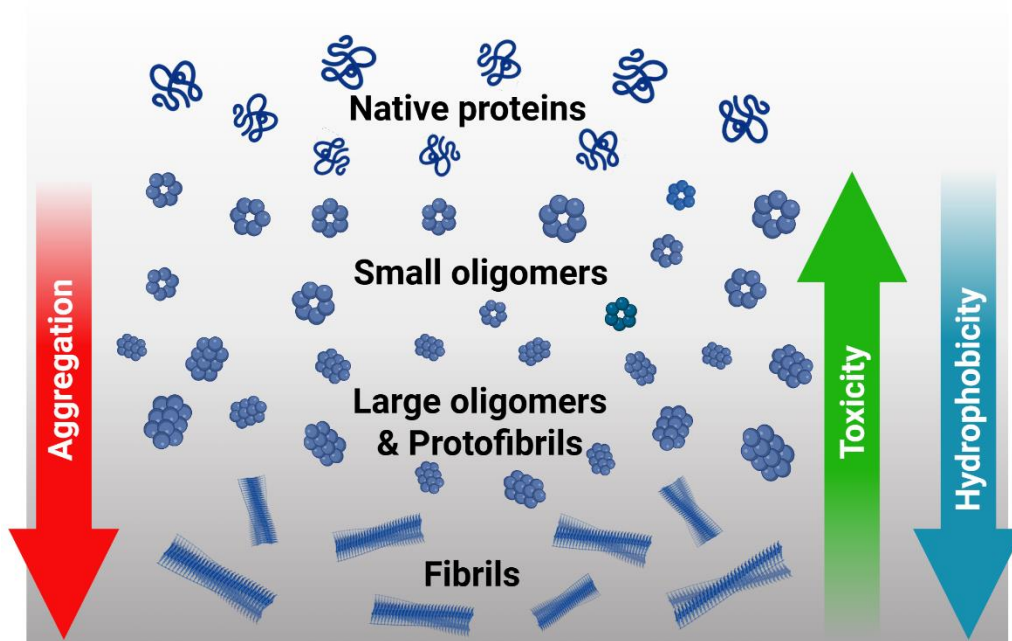


**Figure 8: Relationship between aggregate size and toxicity.** Misfolded proteins can form aggregates of different sizes and shapes. The toxicity of these aggregates typically increases with increasing hydrophobicity and smaller size, showing an inverse correlation between aggregate size and toxic potency. Adapted from Rinauro et al. (2004).<sup>148</sup> This figure was created with BioRender.com.

#### 1.5.4 Protein metastability and systemic pathology

When the protein homeostasis network becomes overwhelmed, intracellular accumulation of misfolded proteins is promoted and propagated following the seeding-nucleation model which begins with a slow and thermodynamically unfavorable nucleation phase that generates small and cytotoxic oligomers which act as seeds following by a rapid elongation stage, resulting in the formation of fibrils.<sup>157</sup> This model also accounts for their prion-like behavior as they aggregate into seeds and spread from cell to cell within the same tissue leading to progressive organ damages.<sup>158,159</sup> While aggregate spreading is a common feature of proteinopathies, the mechanism of internalization and transmission occur may be disease-specific and has been proposed to occur through various mechanisms including exocytosis, endocytosis, trans-synaptic transport, nanotubes, extracellular vesicles, exosomes and direct protein-protein interaction at the cell surface (Figure 9).<sup>160-162</sup> Due to the solubility of PAOs,

they are possibly carried distantly from the organ of origin to distant sites via the circular system of interstitial fluid, cerebral spinal fluid, or blood.<sup>163,164</sup>

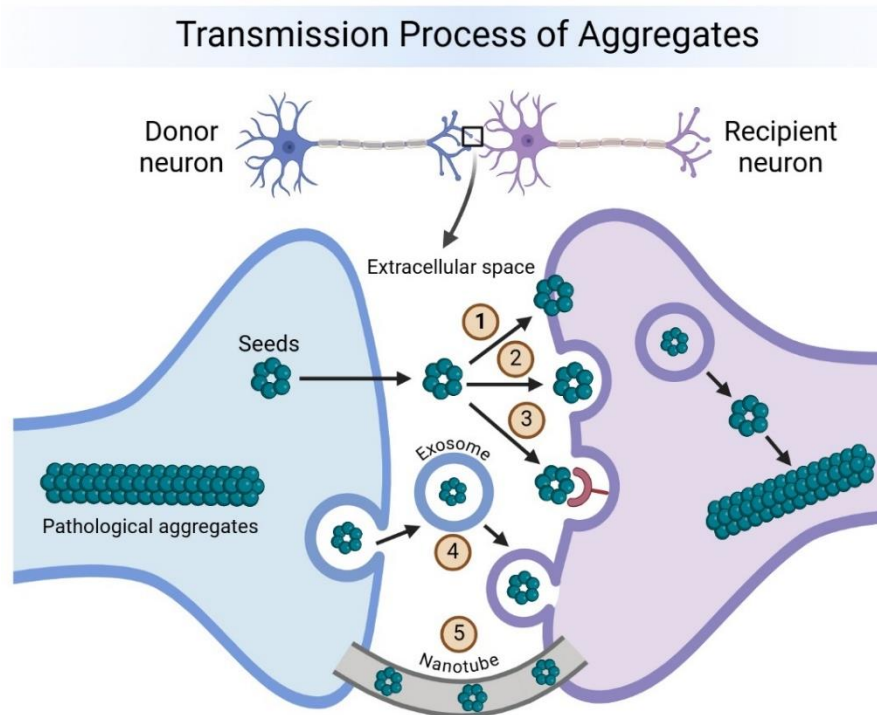


**Figure 9: Potential mechanisms mediating intracellular transmission of protein aggregates.** Misfolded proteins or seeds in the cytoplasm are released from the donor neurons and can be transmitted to recipient neurons through various pathways: (1) direct penetration of the plasma membrane, (2) fluid-phase endocytosis, (3) receptor-mediated endocytosis, (4) membrane-bound vesicles as exosomes or (5) tunnelling nanotubes that directly connect the two cells. Once internalized, these seeds can nucleate fibrillization in the cytoplasm of the recipient neurons. Adapted from Guo and Lee (2014).<sup>165</sup> This figure was created with BioRender.com.

Within the context of proteinopathies, a number of them are considered systemic in light of the metastatic spreading behavior of PAOs as in the case of cardiac amyloidosis associated to transthyretin mainly synthesized in the liver, or immunoglobulin light chains produced by bone marrow plasma cells.<sup>166</sup> Such systemic propagation leads to multiple organ dysfunctions, including the heart, classifying these conditions as systemic.

In addition, the systemic nature of neurodegenerative diseases, traditionally thought to be restricted to the central nervous system, has gained recognition with emerging evidence of amyloid deposits and hyperphosphorylated tau in myocardial tissue of patients with heart failure and/or Alzheimer's patients, in parallel to their accumulation in the brain.<sup>167,168</sup> Further study has demonstrated that plasma A $\beta$  is associated with a higher risk of new onset heart failure and mortality in general population, highlighting the systemic pathology of A $\beta$  beyond the brain.<sup>169</sup> In light of acute setting, protein aggregates have also been observed in damaged

cerebral tissues following AIS, although their potential transmission to other anatomical regions remains uncertain.<sup>170</sup> These systemic aspects of protein misfolding may represent an additional string in the web connecting brain and heart particularly during ischemic stroke, which warrant further investigation to address knowledge gaps in the SHS and facilitate the development of novel therapeutic strategies.

## 2. Aims

Post-stroke cardiac complications remain underrecognized in clinical practice, particularly in the decision-making process for implementing secondary prevention. This is mainly due to limited understanding of the mechanisms connecting stroke and cardiovascular disease as well as the lack of effective therapies for stroke-induced cardiac dysfunction. Addressing this knowledge gap is crucial to unravel the molecular pathways underlying brain-to-heart communication during ischemic stroke and to identify potential targets to protect the heart in stroke patients.

Emerging evidence points to protein misfolding as a potential mechanism implicated in this organ crosstalk with possible therapeutic relevance. This project hypothesizes that AIS triggers the accumulation of misfolded proteins, particularly oligomers, in the myocardium. These oligomers may either translocate from the ischemic brain to the heart or form locally in the myocardium in response to acute stress factors released upon cerebral damage such as catecholamines and inflammatory cytokines. This results in myocardial vulnerability which disrupts local protein homeostasis and subsequent molecular and functional alterations in the heart (Fig. 10).

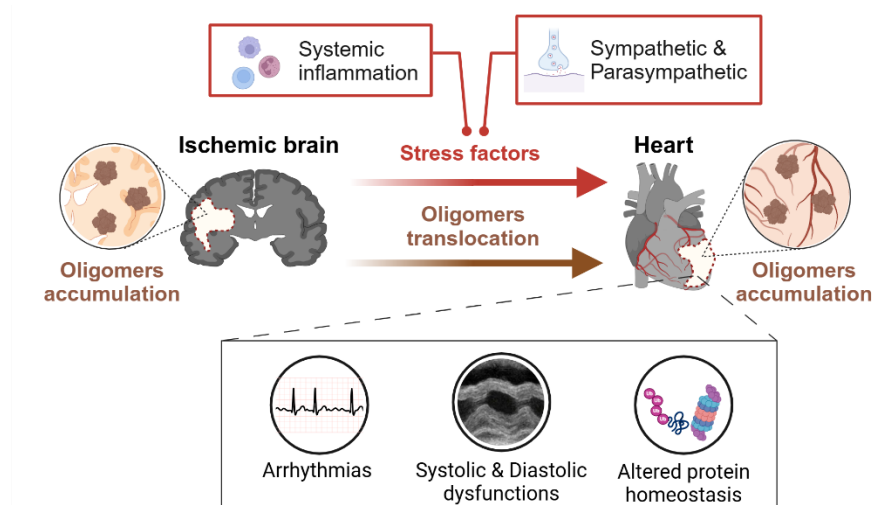


**Figure 10: Hypothesis of the current project.** This project investigates protein misfolding as a potential mechanistic link in the communication between ischemic brain and heart during AIS. Misfolded oligomers may either translocate between tissues or generate locally inside post-stroke myocardium in response to SHS-related stress factors such as systemic inflammation and autonomic dysregulation. These processes contribute to cardiac dysfunction and molecular alterations at local protein homeostasis. This figure was created with BioRender.com.

To test such hypothesis, the current study employs the following approaches:

**In vivo studies:** A murine model of tMCAO in young (3-4 months old) male and female C57BL/6J wild-type mice was used to assess the physiological and biological relevance in protein misfolding induced by AIS.

**In vitro studies:** Human-induced pluripotent stem cell (hiPSC)-derived cardiomyocytes was used to examine cardiac responses to misfolded proteins in the form of A $\beta$ <sub>42</sub> oligomers compared with other SHS-associated stress mediators. These experiments aim to dissect the role of oligomers in myocardial biology and determine their relevance as active players or bystanders in SHS.

Specifically, the aims of the present study are structured as follows:

**Aim 1: To investigate AIS-induced alterations of myocardial function**

- a) Myocardial injury, morphology, electrocardiography, echocardiography were assessed.

**Aim 2: To assess the alteration of SHS-related mechanisms of the systemic inflammation and autonomic nervous system**

- a) The levels of inflammatory cytokines in mouse plasma and circulating catecholamines metabolites (plasma metanephrine, plasma normetanephrine, urinary homovanillic acid) was quantified to evaluate the activation of systemic inflammation and autonomic nervous system triggered by AIS.

**Aim 3: To investigate the occurrence, localization of oligomers as well as the biological relevance of protein misfolding in the post-stroke heart**

- a) The presence and localization of oligomers in the myocardium and different anatomical structures (brain, lymph nodes and liver) were assessed.
- b) Alterations in molecular checkpoints regulating protein homeostasis in the myocardium were examined at both transcriptional and translational levels.
- b) The dynamics of ubiquitin-mediated protein degradation in response to AIS were evaluated in cerebral and myocardial tissues.

**Aim 4: Evaluation of the sole effect of oligomers in the SHS**

- a) The alterations to the proteome were investigated after 48 h of exposure to A $\beta$ <sub>42</sub> oligomers to male and female hiPSC-derived cardiomyocytes (hiCM) in comparison

to other SHS-related stress mediators, including catecholamines (epinephrine and dopamine inhibitors) and pro-inflammatory cytokines (IFN- $\gamma$ ).

### **3. Material and Methods**

#### **3.1 Animals and middle cerebral artery occlusion model of focal ischemia**

Male and female young wild-type C57BL/6J mice (3-4 months old) (Charles River, Germany) were used in this study. Animals were housed at  $21 \pm 2^\circ\text{C}$  under a 12 hour of light/dark cycle with ad libitum access to water and standard chow. Focal cerebral ischemia was induced by tMCAO for 45 min. In brief, mice were anesthetized with isoflurane (2-5%)/oxygen (1L/min). Following a midline neck incision, a silicone-coated 6-0 nylon monofilament (Cat. No. 602356PK5Re, Doccol Co., MA, USA) was inserted into the left internal carotid artery through the origin of the middle cerebral artery, where it remained for 45 min to induce cerebral ischemia. After 45 min, the occluding filament was carefully withdrawn to allow reperfusion which continued for 48 h. Throughout the surgery procedure, body temperature was maintained at  $37 \pm 0.5^\circ\text{C}$  using a thermostatic heating pad. The same surgical procedure was done for the sham-operated without insertion of the occluding filament. All procedures involving animals were conducted in accordance with institutional guidelines and were approved by the Cantonal Veterinary Office of Zurich, Switzerland (ZH040/2021). Echocardiography and ECG recordings were obtained prior to surgery to establish baseline values and at 48 h after the surgery to obtain acute effects after ischemia insults. Mice were subsequently euthanized for organ harvesting.

#### **3.2 ECG recordings**

The ECG signals were recorded non-invasively in conscious mice using the ECGenie system (Mouse Specifics, Inc.) in combination with Labchart7 software (ADInstruments). Mice were gently removed from their home cages and placed on the ECG recording platform equipped with disposable footpad electrodes embedded in the floor. Following an acclimation period of 20-minuts, ECG signals were collected for several minutes. Only data from continuous recordings of 15-20 ECG signals were chosen for analysis. Raw ECG signal was analysed using e-MOUSE<sup>TM</sup> software (Mouse Specifics, Inc.). The software uses a peak detection algorithm to find the peak of the R-waves. The heart rate was determined from the average of RR intervals. In addition, the PR, QRS and QT and corrected QT (QTc) intervals were calculated by the software. The heart rate variability was based on different parameters including SDNN; the standard deviation of the normal RR (NN) intervals, SD1; the short-term and SD2; the long-term variability derived from the Poincaré plots of the RR intervals.

### **3.3 Echocardiography**

#### 3.3 Echocardiography

The transthoracic echocardiography was performed using a Vevo 3100 (VisualSonics, Toronto, Canada) high-resolution imaging system equipped with a 22-55 MHz (MX400) linear array transducer to assess the cardiac function. This procedure was carried out in mice which were anesthetized by isoflurane (2-5%)/oxygen (1L/min). During anesthesia, the body temperature of mice was maintained at  $37\pm 0.5^{\circ}\text{C}$  by a temperature-controlled surgical table equipped with a rectal probe. To prepare the operated area, the chest hair was removed using a depilatory cream to minimize ultrasound attenuation. The echocardiography was performed using grayscale M-mode and B-mode images at the midpapillary level in the parasternal short-axis view. The Left ventricular (LV) function was evaluated through conventional echocardiographic techniques. Key measurements included end-diastolic (LVIDd) and end-systolic (LVIDs) internal diameters, anterior and posterior wall thicknesses, end-systolic (ESV) and end-diastolic volumes (EDV), and LV mass. These were used to derive fractional shortening (FS), ejection fraction (EF), stroke volume (SV), and cardiac output (CO). Trans-mitral inflow was assessed from the apical 4-chamber view to obtain early (E) and atrial (A) peak filling rates and their ratio (E/A). Furthermore, Tissue Doppler Imaging of the posterior LV wall in the short axis view yielded myocardial diastolic velocities (E' and A') and systolic velocity (S'). The E/E' ratio, a measure of LV end-diastolic pressure, was also calculated. All images were analyzed by an expert operator using the Visual Sonics software. The investigators performing and reading the echocardiograms were blinded to the group allocation.

### **3.4 Tissue harvesting**

Mice were deeply anesthetized with the overdose of isoflurane followed by sacrifice using terminal bleeding via cardiac puncture under continuous anesthesia. Before sacrifice, blood samples were directly collected from the heart and the diaphragm was incised to open the chest cavity. Then, the heart was perfused with 0.1 M phosphate buffered saline (PBS) and harvested by cutting great vessels. Organs including hearts, brains, livers and lungs were weighed, and relative weight was calculated as the ratio to the length of tibia. These organs were immersed in ice-cold PBS to clean the debris and preserved in 4% paraformaldehyde at 4°C overnight for histological analysis or snap-frozen in liquid nitrogen for molecular analysis.

### **3.5 Assessment of the cerebral infarct volume**

After 48 h of reperfusion, harvested brains were chilled at -80°C for 5 min to slightly harden the tissue. Brain tissues were cut into 2 mm coronal sections from the olfactory bulb to the cerebellum and then placed in pre-warm 2% 2, 3, 5-triphenyltetrazolium chloride (TTC) solution for 15-20 minutes at 37°C in the dark. Sections were scanned at 1,200 dpi, and the non-ischemic and ischemic hemisphere infarct areas were measured using ImageJ software. For the measurement of total infarct volume, all infarct area were calculated with a 2 mm distance between the slice. The subtraction of the ipsilateral from the contralateral hemisphere volume from the directly measured infarct volume was conducted to correct for brain edema.

### **3.6 Measurement of biomarkers for myocardial injury and catecholamines**

Blood samples were taken from sacrificed mice and centrifuged at 1,200 x g at 4°C for 15 min to obtain plasma. To evaluate the myocardial injury following stroke, ELISA kits of mouse cardiac troponin T type 2 (cTnT; MOES01677, Assay Genie) and brain-natriuretic peptide (BNP; abx574188, Abnova) were measured in plasma. Additionally, ELISA kits of mouse metanephrine (IML-BA-E-8100R, Immunosmol), normetanephrine (IML-BA-E-8200R, Immunosmol) and homovanillic acid (abx364786, Abnova) were used to measure circulating byproducts of catecholamines including metanephrine and normetanephrine levels in plasma and homovanillic acid levels in urine. All the ELISA measurements were performed in accordance with the manufactures' instructions. All the samples and standards were performed in duplicates to confirm reproducibility.

### **3.7 Proinflammatory cytokine profiling**

Post-stroke induced inflammatory responses in plasma was assessed with a proteome profiler mouse cytokine array kit, Panel A (ARY006, R&D Systems). Plasma samples from 5 mice of each group were pooled together and subjected to protein array analysis according to the manufactures' instructions to quantify 33 chemokines and cytokines in plasma of tMCAO mice compared with sham controls. To generate a protein profile, the array data were quantitated using Image J software and presented as average signal (pixel density) of the pair of duplicate spots which represent each cytokine or chemokine.

### **3.8 STRING analysis**

STRING protein-protein interaction ([string-db.org](http://string-db.org)) was performed to investigate the network of identified cytokines and chemokines. The interaction of proteins was analyzed by

considering high confidence (0.700), and protein-protein interaction enrichment p-value was 0.00113. In addition, their associated biological processes were assessed by Gene Ontology from the STRING data set.

### **3.9 Immunofluorescence staining**

Paraformaldehyde-fixed heart tissues were transferred into 30% (w/v) sucrose and incubated overnight at 4°C before being embedded in OCT and frozen at -80°C. For brain tissues, frozen ipsilateral and contralateral hemisphere of brains were directly embedded in OCT and frozen at -80°C. Embedded tissues were cut (10 µm thick for heart and 7 µm thick for brain) and along the coronal plane for the heart and the sagittal plane for the brain. Sections were blocked with 10% normal goat serum and 1% bovine serum albumin (BSA) in PBS for 1 h at room temperature and incubated with primary antibodies diluted in the blocking buffer overnight at 4°C in a humid chamber. Following primary antibody incubation, sections were washed with 1x PBS supplemented with 0.1% Tween-20 for four times and with 1x PBS for four times (4 min for each wash), following by incubation with Alexa Fluor conjugated respective secondary antibodies for 1 h and counterstaining of the nuclei with DAPI (4,6-diamidino-2-phenylindole hydrochloride, Invitrogen) for 15 min in a humid chamber at 37°C. Next, slides were washed again and mounted with Vectashield Hardset antifade mounting media (Vector Laboratories).

Negative controls were processed in a similar fashion with primary antibody omitted, or nonspecific IgG substituted for primary antibody. Stained sections were examined by fluorescence microscopy. The primary and secondary antibodies we used were Anti-Oligomer A11 (1/200 dilution; AHB0052; Life Technologies), Alexa Fluor 488 (1/500 dilution, #A11034, Invitrogen), and Alexa Fluor 549 (1/500 dilution, #A11031, Invitrogen).

### **3.10 Quantitative Real Time-Polymerase Chain Reaction (RT-PCR)**

Total RNA from animal tissues as well as hiCM was isolated using RNeasy Midi kit (Qiagen) according to the manufacturer's recommendations. Prior to RNA extraction, 10 mg of tissue samples were homogenized using a tissue grinder. cDNA conversion was carried out by RT<sup>2</sup> First Strand kit (Qiagen) using 400 ng of cDNA according to the manufacturer's recommendations.

Real-time PCR was performed using the RT<sup>2</sup> SYBR Green qPCR Mastermix (Qiagen) on a Quant Studio 7 cycler (Life Technologies) according to the manufacturer's instructions. The amplification program consisting of 1 cycle at 95 °C (10 min), followed by 40 cycles with a

denaturing phase at 95°C (15 sec) and an annealing and elongation phase at 60°C (1 min). A melting curve was then analyzed to verify the accuracy of the amplicon. All experiments were performed in duplicates to confirm reproducibility and analysis of relative gene expression data was performed using the  $2^{-\Delta\Delta CT}$  method. Samples with a Ct SD > 0.5 were excluded from the final analysis. To normalize RNA concentration,  $\beta$ -actin was used as endogenous control. All primers used in this study were designed using PrimerQuest™ tool (Integrated DNA Technologies, Inc.) which are reported in Table S1.

### **3.11 Isolation of soluble and insoluble protein aggregates**

Frozen tissues were homogenized in a Dounce homogenizer in ice-cold lysis buffer (15 mM Tris-HCl pH 7.6, 250 mM sucrose, 1 mM MgCl<sub>2</sub>, 2.5 mM EDTA, 1 mM EGTA, 1% Triton X-100, 150 mM KCl, 20 mM N-ethylmaleimide, 0.1 mM Na<sub>3</sub>VO<sub>4</sub>, 5 mM NaF, 0.01 mM leupeptin, 1.5  $\mu$ M aprotinin and 1 mM PMSF). The homogenates were sonicated (20% amplitude for 5 seconds) and shaken at 550 rpm on the vertical shaker at 4°C for 1 h prior to being ultracentrifuged at 100,000 g at 4°C for 1 h. Supernatant was collected to serve as Triton-soluble fractions which contains soluble and membrane-bound proteins and frozen at -80°C for downstream analysis. To prepare Triton-insoluble extract, obtained pellets were washed with 1x PBS and centrifuged again at 100,000 x g at 4°C for 1 h. Pellets were then resuspended in room-temperature lysis buffer containing 2% SDS and 1 mM dithiothreitol (DTT) before subjecting them to sonication. The lysates were incubated for 30 min at 37°C to fully solubilize the pellet and centrifuged at 10,000 x g for 10 min at room temperature to discard cell debris. Supernatant was collected as Triton-insoluble fractions and stored at -80°C in multiple aliquots to avoid repeated freeze-thaw procedures.

### **3.12 Isolation of total proteins**

Mouse frozen tissues and hiCM were lysed for immunoblotting with ice-cold lysis buffer (150 mM NaCl, 50 mM Tris-HCl, 0.5% NP-40, 1 mM EDTA, 1 mM DTT, 1 mM NaF, 0.01 mM leupeptin, 1.5  $\mu$ M aprotinin, 0.1 mM Na<sub>3</sub>VO<sub>4</sub> and 1 mM PMSF). Homogenates were subsequently sonicated and incubated on ice for 30 min with vortexing at every 10 minutes prior to being centrifuged at 13,300 x g at 4°C for 10 min to regard cell debris. Supernatant containing the total protein was collected for immunoblotting analysis and stored at -80°C. Protein concentrations of all samples were determined by detergent compatible Bradford protein assay (Bio-Rad).

### 3.13 Dot blot analysis

To measure the level of prefibrillar oligomers and fibrils, Triton-soluble (5 µg/dot) and Triton-insoluble fractions (8 µg/dot) were spotted in triplicate onto pre-wet 0.45 µm nitrocellulose membrane using the Bio-Dot microfiltration apparatus (Bio-Rad) and filtered under vacuum. The membrane was dried at room temperature prior to washing with tris-buffered saline (TBS) and stained with Ponceau S solution (Thermo Scientific) to assess the total protein on the membrane. The membrane was washed with 1x TBS supplemented with 0.1% Tween-20 (TBST) and subsequently blocked with 5% BSA in 1x TBST at room temperature for 1 hour. The membrane was then incubated overnight at 4°C under agitation in diluted primary antibody in TBST as follows: anti-oligomer A11 antibody (1/5,000 dilution, #AHB0052, Invitrogen), anti-fibril OC antibody (1/10,000 dilution, #AB2286, Millipore). After incubation and washing three times with TBST, membrane was probed with anti-rabbit IgG, HRP-linked antibody (1/30,000 dilution, SouthernBiotech) for 1 hour at room temperature. Blots were visualized using Immobilon Crescendo Western HRP substrate (Millipore). The intensity of each dot was quantified by Dot Blot Analyzer in the ImageJ software. All signals were normalized with Ponceau S staining solution (#A40000279, Thermo Scientific). To subtract non-specific background, a duplicate membrane was prepared in the same way except that the primary antibody was excluded. Human synthetic Aβ<sub>42</sub> oligomers (#SPR-488, StressMarq) and fibrils were used as A11-specific positive and negative controls respectively.

### 3.14 Western blotting

For Western blot (WB) detecting ubiquitin in Triton-insoluble fractions, equal amounts of Triton-insoluble proteins were mixed in NuPage™ LDS sample buffer (4x) (Invitrogen) and heated at 70°C for 10 min. Proteins were loaded and separated by 8% NuPAGE Bis-Tris mini protein gels (Invitrogen) using Bolt™ MES SDS running buffer (Invitrogen) under the constant current at 120 V at room temperature. Proteins were then transferred to Immobilon-P PVDF membranes (0.45 µm pore size) (Millipore) under a constant current of 20 V for 60 min at room temperature using Bolt™ transfer buffer (Invitrogen). Next, membranes were blocked in 5% BSA in 1x TBST at room temperature for 1 hour and incubated overnight at 4°C with anti-ubiquitin antibody (1/1,000 dilution, #13-1600, Invitrogen) or anti-β-actin antibody (1/10,000 dilution, #A1978, Sigma-Aldrich) which was used as a loading control. Membranes were subsequently washed in 1x TBST three times for 10 min each on a shaker at

room temperature and incubated for 1 h at room temperature with either Horseradish Peroxidase (HRP)-conjugated anti-mouse or anti-rabbit secondary antibodies (SouthernBiotech). Membrane was washed again three times on a shaker with 1x TBST.

For the rest WB analyses, equal amounts of total proteins from each sample were subjected to 8% or 10% NuPAGE Bis-Tris mini protein gels (Invitrogen) followed by the same process as described above. After the protein transfer, the membranes were blocked with 5% non-fat dry milk or 5% BSA in 1x TBST at room temperature for 1 h and incubated with primary antibodies overnight at 4°C. Following primary antibody incubation, the membranes were washed three times with 1x TBST (10 min each) and subsequently incubated with HRP-conjugated respective secondary antibodies. Anti-vinculin antibody (1/10,000 dilution, #MA5-11690, Invitrogen), and anti-glyceraldehyde-3-phosphate dehydrogenase (GAPDH) (1/40,000 dilution, #MAB374, Millipore) were used as loading controls.

The immunoreactive bands were developed using Immobilon Crescendo or Forte Western HRP substrates (Millipore) and detected by a digital chemiluminescence system (Amersham Imager 600). Densitometric quantification for the protein level changes were performed using Image J software. Data was normalized with loading controls. All primary antibodies used in this study are listed in Table S2.

### **3.15 In vitro hiPSC-derived cardiomyocytes (iCM) culture and treatment**

In vitro experiments were performed using female and male iCM which were kindly provided by the group of Prof. Hoerstrup from Institute of Regenerative Medicine (IREM), University of Zurich. Before the analysis of cytotoxicity and cell viability, cells were seeded at the density of 10,000 cells/well using RPMI medium 1640 supplemented with B-27<sup>TM</sup> (serum-free) (Thermo Fisher) and 1 μM of Y27632 (Miltenyi Biotec) in 96-well plates coated with Cultrex<sup>TM</sup> basement membrane extract (Biotechne) diluted in DMEM/F12 (Gibco) and incubated at 37°C and 5% (v/v) CO<sub>2</sub>. Media was changed every other day. On day 7, contracting iCM were exposed for 48 h to synthetic Aβ<sub>42</sub> oligomers (#SPR-488, StressMarq), epinephrine (#E4250, Sigma-Aldrich), haloperidol (#HY-14538, MedChemExpress) and IFN-γ (#300-02, Peprotech) at various concentrations in RPMI/B27 medium. This approach aimed to identify the optimal concentration of each compound capable of inducing cellular damage with minimal cell death. The respective dissolved solvent for each compound were used as a negative control.

### **3.16 Cytotoxicity assay**

After 48 h of exposure, cytotoxicity was quantified by measuring lactate dehydrogenase (LDH) activity released in cell culture supernatant using LDH cytotoxicity detection kit (11644793001, Roche) according to the manufactures' instructions. Absorbance was measured at 490 nm using the microplate spectrophotometer. All the samples were performed in duplicates. LDH activity was expressed as the percentage cytotoxicity compared to hiPSC-derived cardiomyocytes treated with 1% Triton X-100 serving as a positive control.

### **3.17 Cell viability assay**

After 48 h of exposure, cell viability was quantitated by measuring cellular metabolic activity using the MTT (3-(4,5-dimethylthiazol-2-yl)-2,5-diphenyl tetrazolium bromide) assay (#M2128, Sigma-Aldrich) according to the manufactures' instructions. A freshly made solution of 0.5 mg/mL thiazolyl blue tetrazolium bromide in 1x PBS was prepared. The media was removed. Then, the prepared MTT medium was added and incubated for 3 h at 37°C and 5% (v/v) CO<sub>2</sub>. After the incubation period, the wells were resuspended in dimethyl sulfoxide (DMSO) and placed on a shaking table for 15 min at room temperature to dissolve the formazan crystals. Absorbance was measured at 590 nm using the microplate spectrophotometer. All the samples were performed in duplicates. Cell viability was expressed as a percentage of the control.

### **3.18 Proteomic analysis using mass spectrometry**

Before the analysis of protein profiling, male and female hiCM were seeded at the density of 75,000 cells/well in 24-well coated plates using RPMI medium 1640 supplemented with B-27<sup>TM</sup> (serum-free) and 1 μM of Y27632 and incubated at 37°C and 5% (v/v) CO<sub>2</sub>. Media was changed every other day. On day 7, contracting hiCM were exposed for 48 h to each compound at selected concentration as following: 20 μg/ml of synthetic Aβ<sub>42</sub> oligomers, 40 μM of epinephrine, 10 μM of haloperidol and 400 ng/ml of IFN-γ. The respective dissolved solvent for each compound were used as a negative control. Untreated cells were used for negative control. All the samples were performed in singlicate.

At 48 h of exposure, media was collected, aliquoted and frozen at -80°C until used. Cells were then washed twice with cold 1x DPBS prior to harvested from the plate using a cell scraper and transferring to a LoBind<sup>®</sup> Eppendorf microcentrifuge tube. Cell suspension was centrifuged at 240 *x* g at 4°C for 5 min. Pellets were resuspended in RIPA buffer (50 mM Tris-HCl pH 7.4, 150 mM NaCl, 1 mM EDTA pH 7.4, 1% Triton X-100, 0.1% deoxycholate

supplemented with protease inhibitors (1 mM NaF, 1.5  $\mu$ M aprotinin, 10  $\mu$ M leupeptin, 0.1 mM Na<sub>3</sub>VO<sub>4</sub> and 1 mM PMSF) and incubated on ice for 30 min with vortexing at every 10 minutes prior to being centrifuged at 13,000 rpm at 4°C for 10 min to regard cell debris. Supernatant containing the total protein was collected in a LoBind<sup>®</sup> Eppendorf microcentrifuge tube for Olink proteomic analysis. Protein concentrations of all samples were determined by Bradford protein assay (#A6932, PanReac AppliChem). Samples were normalized to 0.5 mg/ml total protein concentration in RIPA lysis buffer and 30  $\mu$ l aliquots of each sample randomized into wells of 96-well plate.

Proximity extension assay technology with the Olink Cardiovascular II panel was used to profile the cell lysates proteomics. This panel includes 92 oligonucleotide-labelled antibody probe pairs that can bind to their respective targets in the sample and quantified using standard real-time PCR (Table S3). Data was analyzed and graphed in the R package of OlinkAnalyze.

### **3.20 Buffers and solutions**

All buffers and solutions used in this study were prepared using analytical-grade reagents and distilled water or ultrapure water for in vitro experiments. Detailed compositions and preparations methods are provided in Appendix III.

### **3.19 Statistical analysis**

All data in this study are presented as mean  $\pm$  SD. An unpaired Student's t-test was used for two-group comparisons. Two-way analysis of variance (ANOVA) was used with 2 independent variables; tMCAO and timepoint or tMCAO and sex followed by Bonferroni's *post-hoc* test for multiple comparisons. Statistically significance was defined as  $p < 0.05$ . Statistical analysis was performed using GraphPad Prism software (version 9.0) and Microsoft Office Excel.

## 4. Results

### 4.1 AIS induces cardiac dysfunctions

To assess cardiac functions in the acute phase of ischemic stroke, we established a murine model of left-sided tMCAO and performed electrocardiography and echocardiography at baseline (pre-operation) and 48 h post-operation (Fig. 11A). This study takes an advantage of using healthy young mice of both sexes to isolate AIS-induced cardiac effects from aging or pre-existing cardiovascular conditions while also allowing for the examination of potential sex-specific differences in post-stroke cardiac alterations. Besides, employing wild-type mice eliminates confounding factors associated with genetic modification in transgenic models. Cerebral infarction following AIS was observed in both sexes of tMCAO groups, confirming the successful establishment of our stroke model (Fig. 11B, C). Cardiac function impairment was evident in the mice at 48 h after stroke, characterized by slower heart frequencies (Fig. 11D). Representative RR-interval tachograms (Fig. 11E), Poincaré plots of consecutive RR intervals (Fig. 11F) and HRV assessments (Fig. S1A, B) demonstrated irregular RR intervals in tMCAO mice, compared to their pre-operative baseline and sham-operated controls, suggesting a tendency toward arrhythmias. Consistent with the bradycardia observed in tMCAO mice, echocardiographic analysis showed a significant reduction in cardiac output (Fig. 11G). Although changes in systolic and diastolic functions were minimal (Fig. S1C), the observed trend toward reduced stroke volume and fractional shortening suggest their potential contribution to cardiac dysfunction particularly in the clinical setting of individuals with borderline and previously impaired conditions, despite the lack of statistical significance.



(See figure on the previous page)

**Figure 11: Impaired cardiac functions after AIS.** (A) Schematic presentation of the murine study with the experimental designs and the timeline. Left-sided tMCAO was induced in 3-4 months old wild-type C57BL/6J mice at both sexes for 45 min to induce ischemic injury, followed by 48 h of reperfusion. Cardiac functions were assessed by electro- and echo-cardiography at baseline (pre-operation) and at 48 h-post operation. After that, the animals were euthanized for tissue harvesting. (B) Representative images of brain sections stained with TTC to visualize cerebral infarcts. Each group shows five consecutive brain sections from one mouse. White: Infarct, Red: Viable tissue. (C) Quantification of infarct sizes (N=4/group). In this bar graph, statistical comparisons between tMCAO and sex were performed by two-way ANOVA followed by Bonferroni's *post-hoc* test. (D) Heart rate (beats/min) (N=9/per group). (E) Representative electrocardiographic recordings and (F) Poincaré plots of consecutive RR intervals time series in the heart of male and female undergoing tMCAO and sham controls at baseline (pre-operation) and 48 h after tMCAO (N=5/group). (G) Cardiac output, stroke volume, fractional shortening and ejection fraction were assessed for systolic function by echocardiography in tMCAO and sham control mice at baseline (pre-operation) and 48 h after tMCAO (N=10/group). Data is presented as mean  $\pm$  SD. Each dot in the graph corresponds to individual data points from each mouse. In these graphs, statistical comparisons between tMCAO and timepoint were performed by two-way ANOVA followed by Bonferroni's *post-hoc* test. A *p*-value  $<0.05$  was considered significant. \**p*  $< 0.05$ ; \*\**p*  $< 0.01$ ; \*\*\**p*  $< 0.001$ ; \*\*\*\**p*  $< 0.0001$  sham vs. tMCAO. ns, Not significant; p.o., Post-operation; h, hours; ms, Milliseconds; tMCAO, Transient-middle carotid artery.

## 4.2 AIS leads to myocardial stress and morphometric alterations

To further evaluate myocardial injury following AIS, the plasma levels of cardiac troponin T (cTnT) were measured as key biomarker of cardiac damage. Our results revealed a trend towards increase in plasma cTnT from tMCAO mice after AIS compared with sham-operated animals (Fig. 12A). Additionally, we assessed BNP as a representative member of natriuretic peptides, typically upregulated in response to cardiac stress.<sup>171</sup> Both plasma BNP levels and local BNP transcript levels (*NPPB*) in the myocardium of mice subjected to AIS remained unchanged in comparison to their sham counterparts in our models (Fig. 12B, D). In contrast, we observed a significant reduction in atrial natriuretic peptide (ANP) expression while C-type natriuretic peptide (CNP) gene expression remained stable in the myocardium upon AIS, indicating potential dysregulation of natriuretic peptides (Fig. 12C, E).

Both male and female tMCAO mice experienced substantial weight loss after AIS (Fig. 12F). However, there is no alteration in the heart weight/tibia length ratio in both sexes of stroke mice (Fig. 12G). Interestingly, a significant reduction in the liver weight/tibia ratio was observed with the potential of sex-specific differences, suggesting differential hepatic-specific responses to AIS between sexes (Fig. 12H). Furthermore, the normal lung wet-to-dry weight ratio observed in our study suggests that overt heart failure has not yet developed at this stage (Fig. S2A).

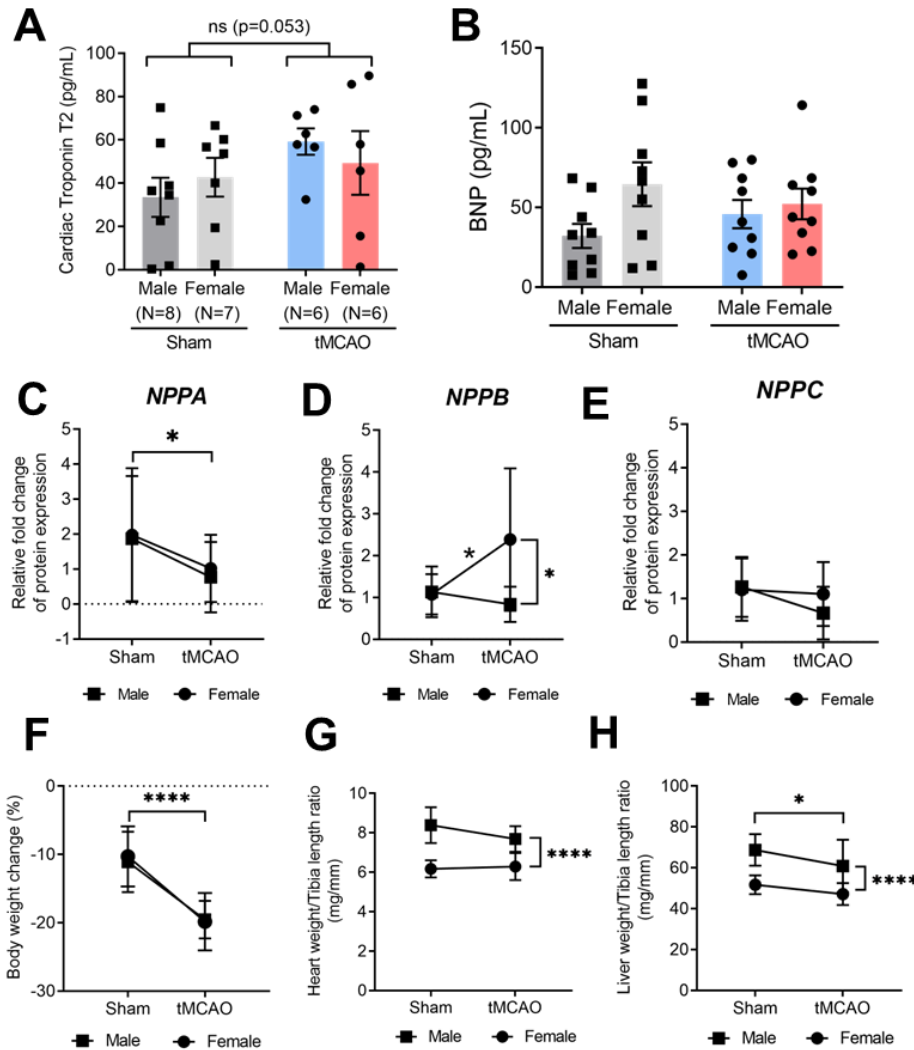


**Figure 12: Myocardial damage and morphometric changes as consequences of AIS.** (A) ELISA showing cTnT (N=6-9/group) and (B) BNP levels (N=9/group) in plasma of male and female mice at 48 h after tMCAO versus sham controls. Bar graphs represents mean  $\pm$  SD. Each dot in the graph corresponds to individual data points from each mouse. Real-time PCR showing relative expression of genes encoding (C) ANP (*Nppa*), (D) BNP (*Nppb*) and (E) CNP (*Nppc*) in the heart of male (closed square) and female (closed circle) undergoing tMCAO versus sham controls (N=10/group). (F) Changes of body weight after the operation in tMCAO mice versus sham controls (N=11/group). (G) The ratio of heart weight/tibia length and (H) liver weight/tibia length in tMCAO and sham control mice (N=11/group). Data represents mean  $\pm$  SD. Statistical comparisons between tMCAO and sex were performed by two-way ANOVA followed by Bonferroni's *post-hoc* test. A *p*-value <0.05 was considered significant. \**p* < 0.05, \*\*\*\**p* < 0.0001 sham vs. tMCAO; ns, Not significant; tMCAO, Transient-middle carotid artery.

### 4.3 AIS alters systemic inflammatory response and autonomic dysregulation

The pathophysiology of cardiac dysfunction following stroke is mediated by a complex interaction among multiple biological mechanisms within the brain-heart axis, including inflammatory and immune responses as well as autonomic nervous system regulation.<sup>172</sup> We,

therefore, explore the potential involvement of these mechanisms in our murine model of AIS.

To examine AIS-induced inflammatory responses, cytokine profiling in mouse plasma was performed. Among the identified circulating cytokines and chemokines, we found that the expression of CXCL13 (C-X-C chemokine ligand-3), ICAM-1 (intercellular adhesion molecule-1) and TIMP-1 (tissue inhibitor of metalloproteinases-1) altered profoundly in both male and female tMCAO mice compared to sham-operated controls (Fig. 13A). Protein-protein interaction analysis further revealed that such combinations of detected cytokines interacted with each other, potentially acting as downstream mediators of TNF- $\alpha$  and IFN- $\gamma$  signaling. Notably, this particular cytokine pattern appears to be involved in the biogenesis and buildup as well as clearance of A $\beta$ , one of the histological hallmarks in Alzheimer's disease<sup>173</sup> (Fig. 13B). These findings suggest an interplay between the systemic inflammation and A $\beta$  accumulation which may be relevant to the oligomer accumulation observed in the post-stroke myocardium in our murine model.

To further investigate autonomic nervous system activity during SHS, we quantified catecholamine byproducts, including plasma levels of metanephrine and normetanephrine levels as well as urinary levels of homovanillic acid (HVA) which are catabolites of epinephrine, norepinephrine and dopamine, respectively. At 48 h post-AIS, both male and female tMCAO mice exhibited a significant reduction in HVA levels (Fig. 13C). This reduction may be attributed to impaired dopamine production and/or altered enzymatic activity of dopamine metabolism. However, plasma concentrations of metanephrine and normetanephrine, remained unchanged (Fig. 13D, E). Together, these results demonstrate that while systemic sympathetic activation remains unaltered in this tMCAO model, AIS selectively disrupts dopaminergic activity, potentially contributing to autonomic dysfunction in SHS.

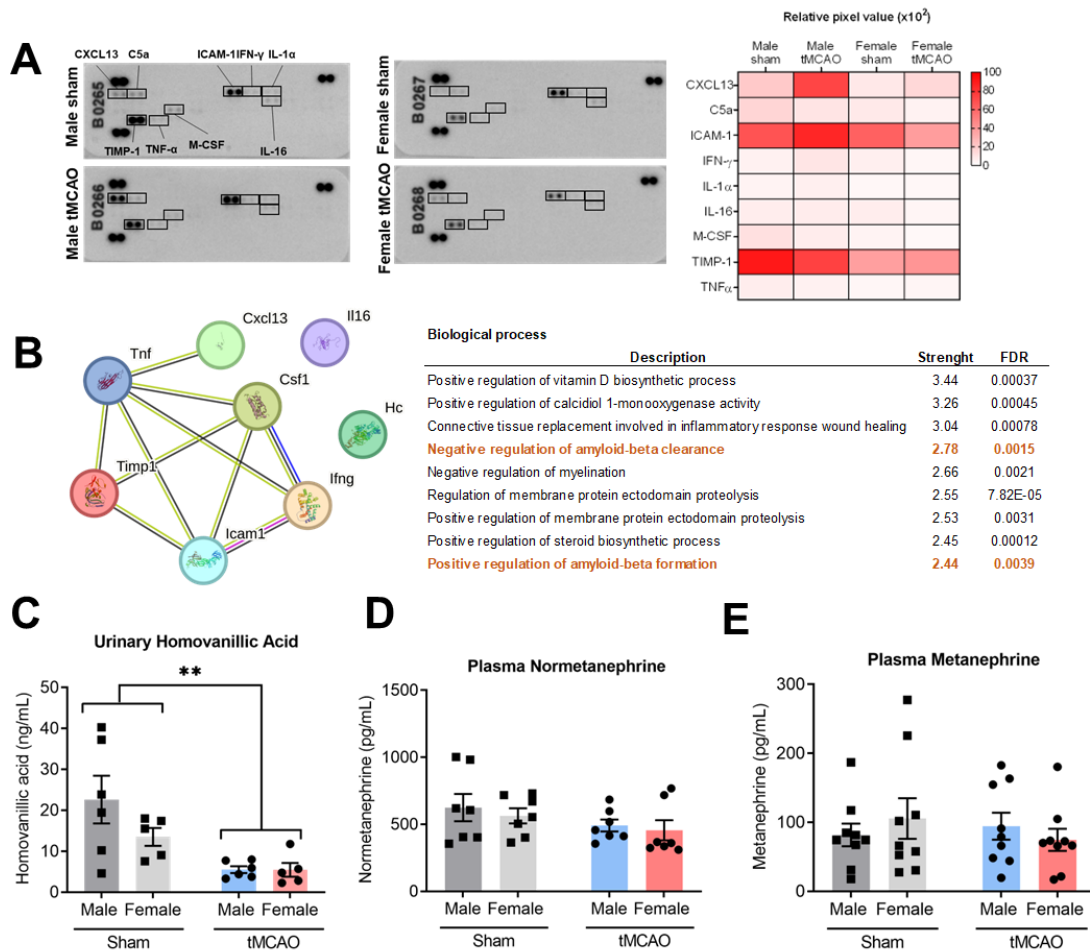


**Figure 13: Post-stroke induced systemic inflammatory response and autonomic imbalance.** (A) Representative dot blot showing the expression of proinflammatory cytokines and chemokines expression in pooled plasma from 5 male or 5 female mice following 48 h of AIS or sham surgery. Heat map showing the differential relative quantification of detected proinflammatory cytokines and chemokines on the blot as visualized by chemiluminescence (N=5 pooled mice/group). (B) Protein-protein interaction analysis of identified cytokines and chemokines in mice from the STRING database. Proteins are represented as nodes. The diagram shows their top-ranking regulated biological processes. (C) ELISA showing levels of circulating urinary homovanillic acid (N=5/group), (D) plasma metanephrine (N= 9/group) and (E) plasma normetanephrine (N=7/group) at 48 h after AIS versus sham controls in both male and female mice. Bar graph represents mean  $\pm$  SD. Each dot in the graph corresponds to individual data points from each mouse. Statistical comparisons between tMCAO and sex were performed by two-way ANOVA followed by Bonferroni's *post-hoc* test. A *p* value  $<0.05$  was considered significant. \*\**p*  $< 0.001$  sham vs. tMCAO; tMCAO, Transient-middle carotid artery.

#### 4.4 AIS is associated with an increased presence of oligomers

Protein misfolding has emerged as a key pathological factor in acute ischemic events with growing evidence suggesting its involvement in organ crosstalk through the spreading capability of misfolded proteins.<sup>159,174</sup> However, the involvement of protein misfolding to brain-heart axis in the context of AIS remains largely unexplored. This study aims to

investigate the unrecognized contributions of misfolded proteins, particularly oligomers, in post-stroke brain-heart interactions and to elucidate their associated molecular mechanisms.

To assess the presence and localization of oligomers, immunohistochemical analysis was performed using the A11 antibody, which specifically recognizes oligomeric conformations independent of amino acid sequence while excluding monomers or fibrils. In tMCAO mice, A11-positive oligomers were observed as small dots distributed throughout different areas including midbrain and cortex of the injured ipsilateral brain hemispheres at 48 h post-surgery. No such signal was detected in the corresponding regions of sham controls or negative staining controls. (Fig. 14A). Notably, similar oligomeric structures were also detected in the myocardial tissues of tMCAO mice, despite the presence of high intrinsic autofluorescent background (Fig. 14B). These findings indicate that misfolded oligomers are not restricted to the local damaged brain but are also present in peripheral organs like the heart.

To further quantify the oligomers detected in cerebral and myocardial tissues, we employed a dot blot assay using the oligomer-specific A11 antibody. Typically, oligomer populations are studied from the detergent-soluble fraction due to their small and less organized structure compared to fibrillar aggregates, which allows them to remain soluble in detergents.<sup>175</sup> We therefore isolated the Triton-soluble fraction from the brain and heart tissues of both tMCAO and sham-operated mice to assess oligomer levels.

Consistent with the immunostaining images, dot blot analysis revealed a significant elevation of soluble oligomers in the ipsilateral brain hemispheres of tMCAO mice, while no detectable increase was observed in the contralateral ones (Fig. 14C). These findings reinforce the concept of localized ischemic insult. Soluble oligomer levels were also significantly increased in the myocardium of both male and female tMCAO mice compared to sham-operated controls (Fig. 14D). Comparing between sexes, no sex-specific differences was observed in the levels oligomer accumulation in either tissue. Together, the data further supports the systemic presence of AIS-related misfolded oligomers and suggests their potential involvement in the SHS pathology. Beyond the brain and heart, higher levels of oligomers were observed in axillary lymph nodes isolated from tMCAO male mice at 24 h after AIS followed by a decrease at 48 h (Fig. S3A). This transient elevation suggests a possible route of oligomers spreading especially during the early phase upon ischemic injury. However, no detection of increased oligomers in liver following AIS may suggest limited

systemic dissemination or efficient clearance mechanisms in such organs, preventing oligomer accumulation (Fig. S3B).

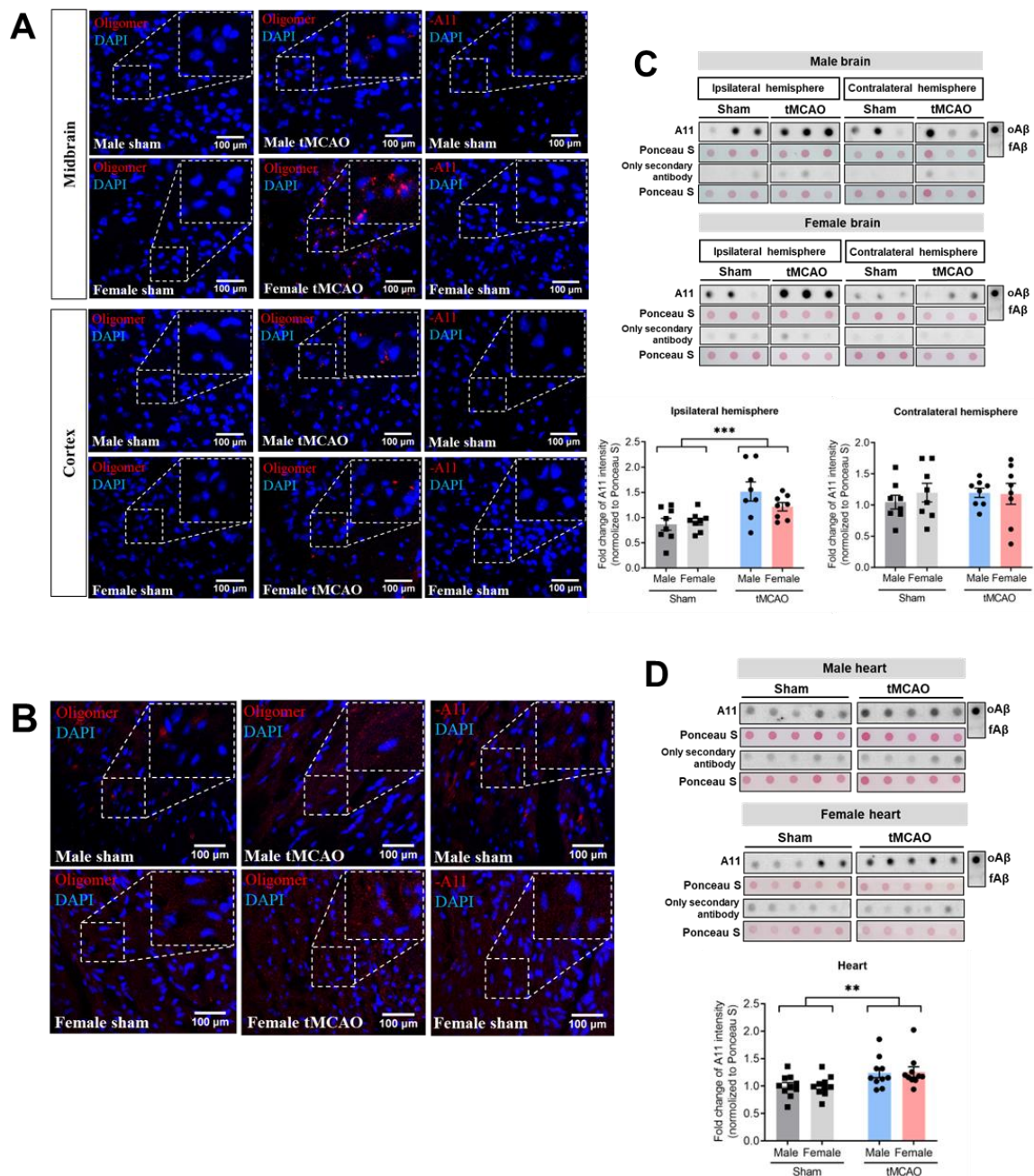


**Figure 14: Localization and elevated levels of oligomers after AIS.** (A) Representative immunofluorescence images showing the presence of oligomers by staining with oligomer-specific A11 antibody (*red*) observed in cerebral tissues at midbrain and cortex region and (B) heart sections of both sexes of tMCAO and sham control mice. DAPI (*blue*) was used to counterstain nuclei. Tissue was processed through the same staining protocol in the absence of A11 antibody (-A11) to reveal background autofluorescence. Original magnification 20x. Scale bars = 100 μm. (C) Representative dot blot images and their relative densitometric quantification for the expression of oligomers using A11 antibody in the Triton-soluble fraction of both injured ipsilateral and non-injured contralateral hemispheres of the cerebral tissues and (D) myocardial tissues from tMCAO versus sham controls mice at 48 h post-surgery (N=10/group). Bar graph represents mean ± SD. (*Figure legend continued*)

**Figure 14:** (*Figure legend continued*) Each dot in the graph corresponds to individual data points from each mouse. Statistical comparisons between tMCAO and sex were performed by two-way ANOVA followed by Bonferroni's *post-hoc* test. A *p* value <0.05 was considered significant. \*\**p* < 0.01, \*\*\**p* < 0.001 sham vs. tMCAO; tMCAO, transient-middle carotid artery; oA $\beta$ , Human synthetic A $\beta$ <sub>42</sub> oligomers; fA $\beta$ , Human synthetic A $\beta$ <sub>42</sub> fibrils.

#### 4.5 AIS disrupts the local protein quality control (PQC) systems in the heart

Next, we examined the potential impact of AIS on myocardial PQC by conducting transcriptional and translational analyses of key molecular checkpoints involved in this complex system, including protein folding, UPR, proteasome, autophagy, antioxidative stress and oligomer-binding receptors. Our findings show that both male and female tMCAO mice exhibited a susceptibility to cardiac proteotoxicity as evidenced by transcriptional alterations in multiple molecular makers of protein homeostasis (Fig. 15A).

We further investigated alterations of cardiac protein homeostasis at the protein level by Western blot analysis (Fig. 15B). Among the three main UPR branches namely ATF6, IRE1 and PERK, we observed a significant downregulation of the cleaved (activated) form of ATF6 (cATF6) in both sexes of tMCAO mice compared to sham-operated controls while site-1-protease (S1P), an enzyme responsible for ATF6 processing, was reduced only in male tMCAO mice. A small shift toward decreased GRP78, a chaperone regulated by ATF6, was also noted in post-stroke hearts. In contrast, the activation of IRE1 and PERK, as reflected by their phosphorylated forms (p-IRE1 and p-PERK), remained unchanged. However, a downstream PERK signaling was affected as shown by a trend towards increased expression of activating transcription factor 4 (ATF4) in the post-stroke heart of male mice.

Concurrently, AIS led to autophagic induction in the heart as reflected by a significantly increased LC3-II/I ratio, a marker of autophagosome formation. This was accompanied by a significant downregulation of key autophagic inhibitors, including phosphorylated AKT (p-AKT) and HSP90 in both male and female mice following AIS compared to sham controls. We further observed protein phosphatase 2A (PP2A), an enzyme responsible for AKT dephosphorylation. However, its expression showed no significant difference in both sexes of tMCAO mice, compared to sham controls. On the other hand, AIS triggered an upregulation of catalase, an oxidative stress inhibitor, in the hearts of both sexes. These findings underscore the complexity of myocardial responses following ischemic stroke. Moreover, cleaved ATF6 and LC3B exhibited significant sex-specific differences in their responses together with a potential trend toward sex-specific differences in phosphorylated mTOR at Ser2448 and

ATF4. These findings suggest a divergent regulation of cardiac protein quality control pathways between males and females following stroke.

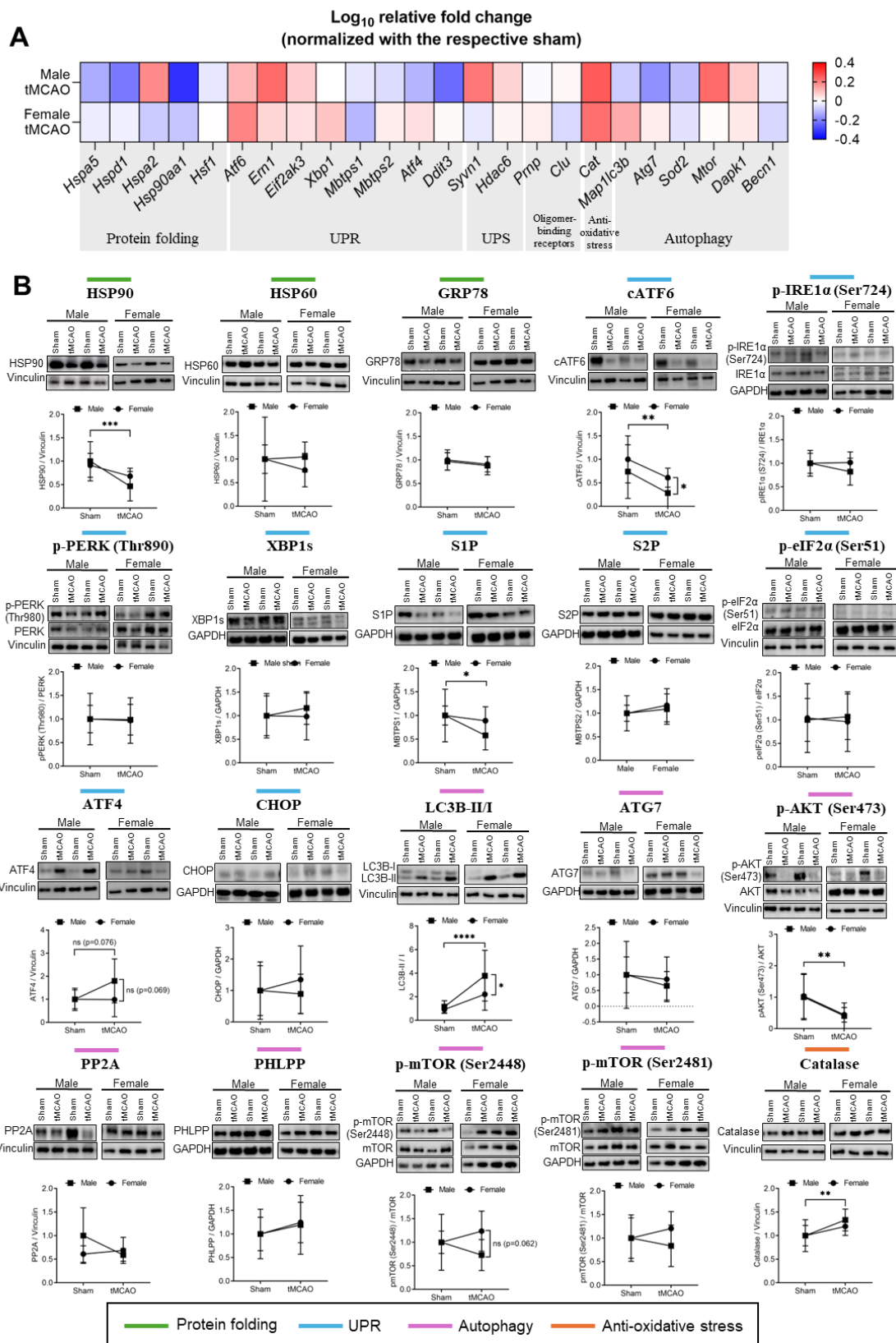


Figure 15 (See legend on the next page)

(See figure on the previous page)

**Figure 15: Systemic responses in myocardial proteostasis after AIS.** (A) Heat map showing differential expression of several genes involving in proteotoxicity in the post-stroke heart from both male and female tMCAO mice versus their corresponding sham controls. (B) Representative Western Blot and their respective densitometric quantification for the expression of proteins involved proteotoxic resistance in the post-stroke heart from male (closed square) and female (closed circle) tMCAO and sham control mice (N=9-10/group). Each dot in the graph represents mean  $\pm$  SD. Statistical comparisons between tMCAO and sex were performed by two-way ANOVA followed by Bonferroni's *post-hoc* test. A  $p$  value  $<0.05$  was considered significant. \* $p < 0.05$ , \*\* $p < 0.01$ , \*\*\* $p < 0.001$ , \*\*\*\* $p < 0.0001$  sham vs. tMCAO; ns; Not significant; tMCAO, Transient-middle carotid artery.

#### **4.6 AIS leads to the accumulation of ubiquitin aggregates in the ischemic brain but not the heart.**

Upon the presence of misfolded oligomers in the post-stroke brain and heart, we further investigated the downstream handling of such oligomers in these tissues. Under physiological condition, ubiquitination typically targets abnormal proteins for degradation via the UPS or autophagy-lysosomal pathways.<sup>176</sup> However, excessive proteotoxic stress, such as that induced by stroke, can overwhelm these degradation mechanisms, resulting in the sequestration of ubiquitinated proteins into insoluble aggregates. This process depletes the pool of available or free ubiquitin, thereby reducing the capacity of cells to protect against stress condition.<sup>177-179</sup>

To assess ubiquitin dynamics in response to AIS, Western immunoblotting with an anti-ubiquitin antibody was performed to evaluate the accumulation of ubiquitinated proteins in the Triton-insoluble fraction as well as the levels of free ubiquitin in the Triton-soluble fraction. The results revealed a significant increase in ubiquitin aggregates in the injured ipsilateral brain hemisphere of both male and female tMCAO mice compared to sham-operated controls (Fig. 16A). In contrast, no such accumulation was observed in the post-stroke heart (Fig. 16B). Despite the differential ubiquitin sequestration in the brain and the heart, the levels of free ubiquitin remain unchanged in both tissues (Fig. 16C, D). These findings suggest the disruption of ubiquitin-mediated protein degradation in the ischemic brain, while the heart appears to employ a distinct response to stroke-induced proteotoxicity such as autophagy.

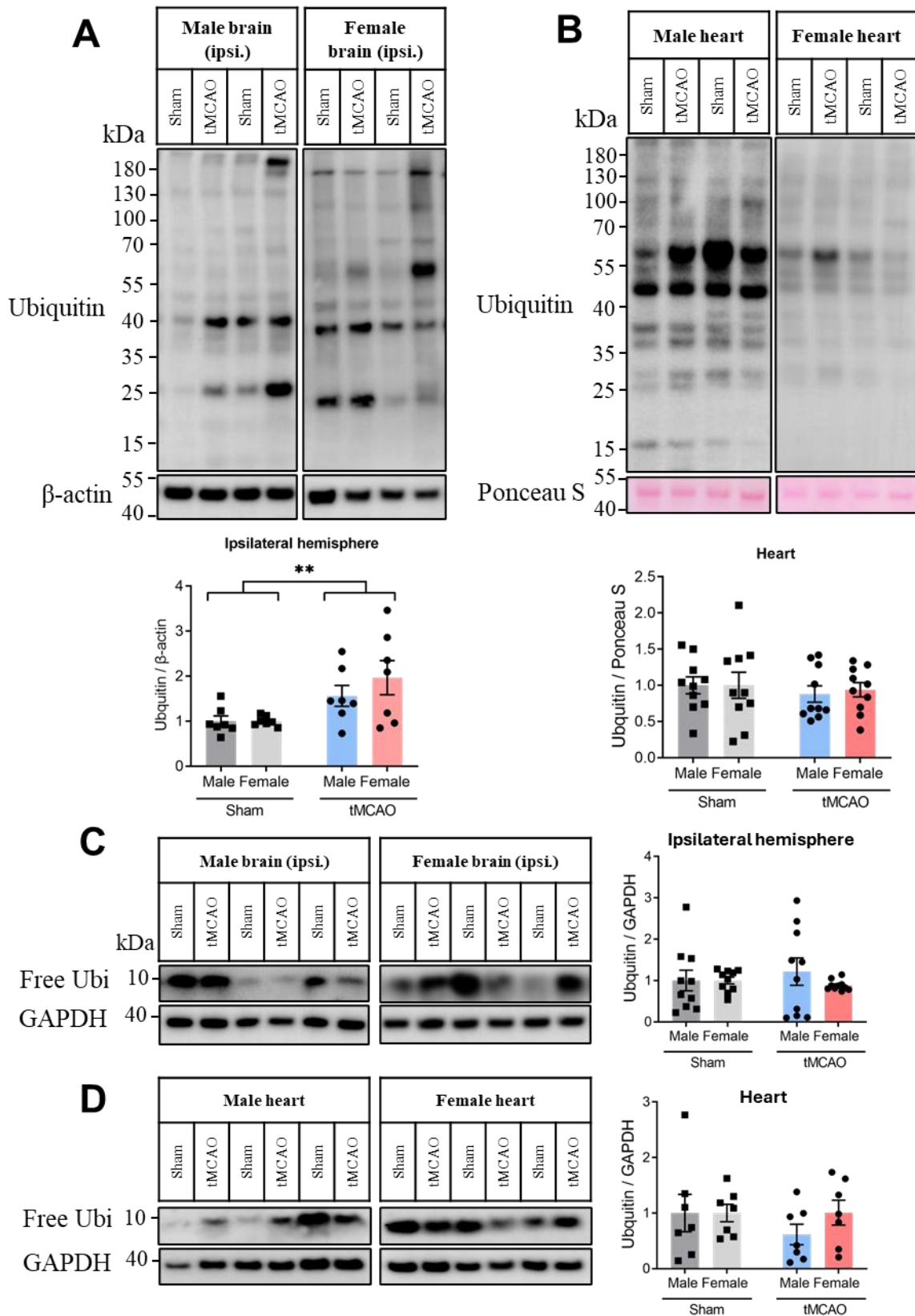


**Figure 16: Changes in insoluble ubiquitin aggregates in the ipsilateral brain hemisphere but not the heart after AIS (A) Representative Western Blot of insoluble ubiquitin (Figure legend continued)**

**Figure 16:** (*Figure legend continued*) containing aggregates and their respective densitometric quantification for the expression of ubiquitin-stained bands in Triton-insoluble proteins isolated from the ipsilateral (ipsi.) brain hemisphere (N=7/group) and (B) the heart of male and female tMCAO mice and sham controls (N=10/group). (C) Representative Western Blot images of free ubiquitin isolated from Triton-soluble proteins from the ipsilateral brain hemisphere (N=7/group) and (D) the heart of male and female tMCAO mice and sham controls (N=10/group) and their respective densitometric quantification for the expression of free ubiquitin. Bar graph represents mean  $\pm$  SD. Each dot in the graph corresponds to individual data points from each mouse. Statistical comparisons between tMCAO and sex were performed by two-way ANOVA followed by Bonferroni's *post-hoc* test. A *p* value  $< 0.05$  was considered significant. **\*\**p* < 0.01**; Ubi, Ubiquitin.; kDa, Kilodalton; tMCAO, Transient-middle carotid artery.

#### **4.7 Sole effects of oligomers to the proteome in human iPSC-derived cardiomyocytes (iCM)**

In order to dissect the role of oligomers and clarify their biological relevance as active players or bystanders within a complex milieu of released stress factors (inflammatory cytokines, neurohormones etc.), we employed an *in vitro* model using hiCM as a human-relevant model which enhances both mechanistic insights and the translational relevance of our findings to human cardiac biology. hiPSC derived from male and female donors were differentiated into hiCM and subsequently subjected to various stress conditions (Fig. 17A). These included exposure to human A $\beta_{42}$ -derived oligomers, a key hallmark of protein misfolding-related diseases including vascular dementia<sup>180</sup> as well as other stress mediators which have been implicated in SHS pathology consisting of autonomic regulators (epinephrine and haloperidol; a dopamine receptor antagonist), and pro-inflammatory cytokines (IFN- $\gamma$ ). To confirm the oligomeric confirmation of A $\beta_{42}$ -derived oligomers prior to exposure to the cells, we performed Western blot using oligomer-specific A11 antibody and anti-A $\beta$ -6E10 antibody (Fig. S4).

To recapitulate the experimental conditions of our murine model, contracting male and female hiCM were exposed with these mediators for 48 h. Initially, a titration assay was performed by exposing hiCM to different concentrations of each mediator for 48 h and subsequently analyze for cell viability and cytotoxicity using MTT and LDH assay respectively. The results are shown in Fig. 17B-E. This approach enables the identification of optimal concentration that induced cellular stress with minimal cell death induction (approximately less than 10%), ensuring appropriate conditions for subsequent proteomic analysis. After the MTT and LDH analysis, the optimal concentration of each stress mediator was selected according to the above-mentioned criteria as following: 20  $\mu$ g/ml oligomer, 400 ng/ml IFN- $\gamma$ , 10  $\mu$ M haloperidol and 40  $\mu$ M epinephrine.

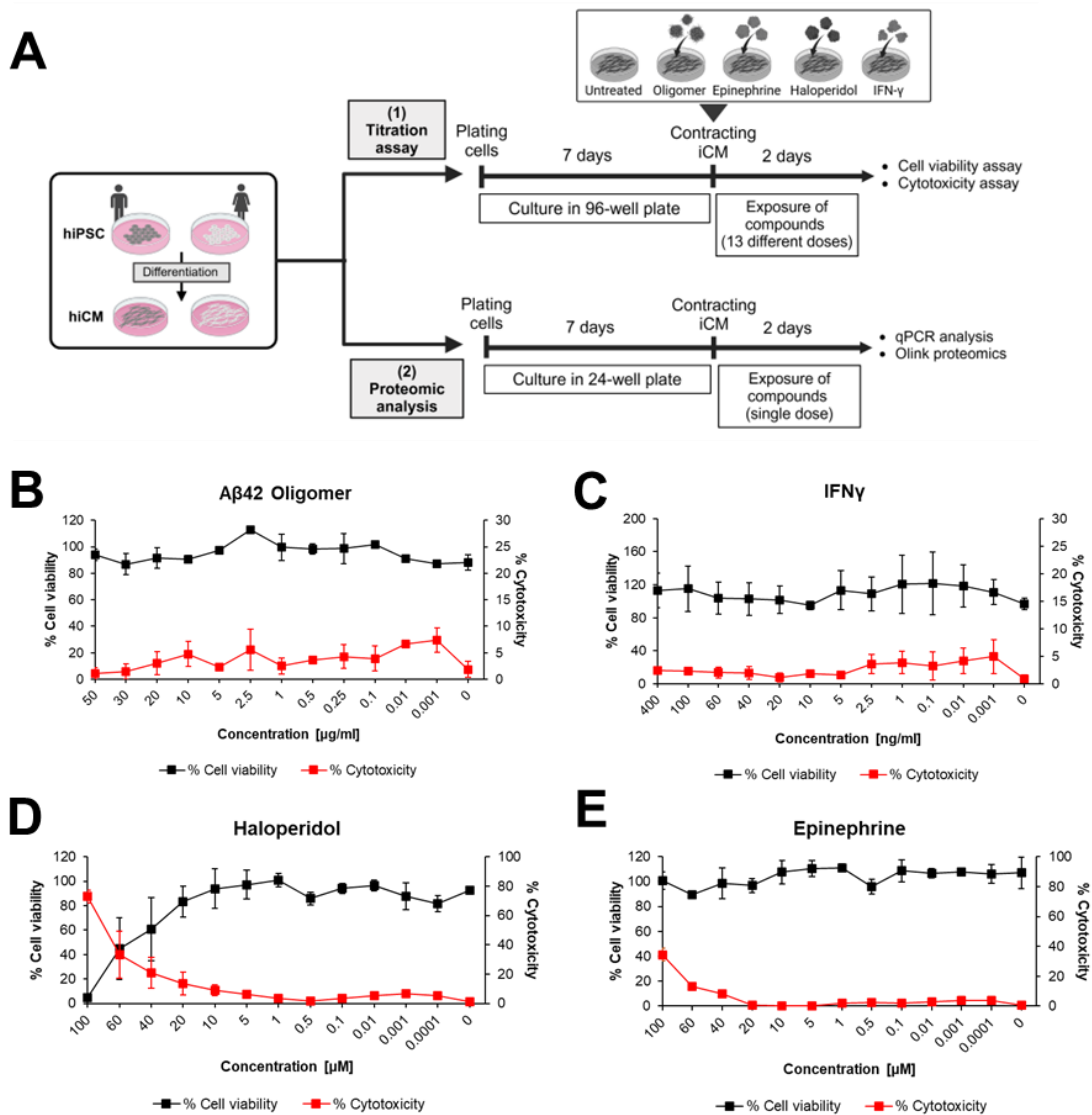


**Figure 17: Cell viability and cytotoxicity of iCM after various treatments.** (A) Schematic representation of cell preparation, experimental design, timeline and assays used in an in vitro model employing iCM derived from male and female human donors. Briefly, after cardiac differentiation, iCM were initially seeded at defined densities into new culture plates and maintained for 7 days. Cells were then exposed to various stressors (oligomer, epinephrine, haloperidol and IFN- $\gamma$ ) for 48 h, with untreated cells serving as negative controls. Experiments were conducted into 2 separate settings for the titration assay and Olink proteomic analysis, each requiring different cell numbers. The line graph showing the percentage of cell viability by MTT assay and cytotoxicity by LDH assay of iCM after 48 h of exposure to (B)  $A\beta_{42}$  oligomers, (C) IFN- $\gamma$ , (D) haloperidol and (E) epinephrine across 13 different concentrations (N=2/group). Data are presented as mean $\pm$ SD.

We next investigated the effects of  $A\beta_{42}$ -derived oligomers and other stressors on proteotoxic stress responses in hiCM at the transcriptional level. The results demonstrated that  $A\beta_{42}$ -derived oligomers induced broad dysregulation of proteostasis-related pathways and exhibited a gene expression profile comparable to that observed under other stress conditions. Despite the limited sample size, a potential sex-specific difference was observed with male hiCM

exhibiting broad upregulation of gene expression across multiple stressors, whereas female hiCM showing a downregulation of certain markers including the chaperone encoding genes (*HSPA5*, *HSPD1*, *HSPA2*), UPR-related genes (*ATF6*, *EIF2AK3*, *XBP1*, *MBTPS1*, *ATF4*), oligomer receptor-encoding gene (*PRNP*) and autophagy-related gene (*MAP1LC3B*) (Fig. 18A).

To further explore the translational relevance of our findings and gain unbiased insights into the effects of A $\beta$ <sub>42</sub>-derived oligomers and other stressors on the cardiac proteome, proteomic analysis using the Olink Cardiovascular (CVD) II panel was employed to assess proteomic changes in cardiovascular and inflammatory markers in hiCM lysates following stress induction. Principal component analysis (PCA) revealed distinct clustering of proteomic responses by sexes across treatments. In response to A $\beta$ <sub>42</sub>-derived oligomers, male and female hiCM samples initially formed separate clusters following vehicle treatment, however, oligomer exposure reduced this separation, shifting the proteomic profiles toward a more convergent state (Fig. 18B). Furthermore, hierarchical clustering of cardiovascular and inflammatory markers further highlights distinct patterns of differentially regulated proteins across different stress conditions with identification of potential sex-specific differences in certain proteins (Fig. 18C). These data implies that A $\beta$ <sub>42</sub>-derived oligomers actively modulate cardiac stress pathways, given their significant impact at both transcriptional and translational levels.

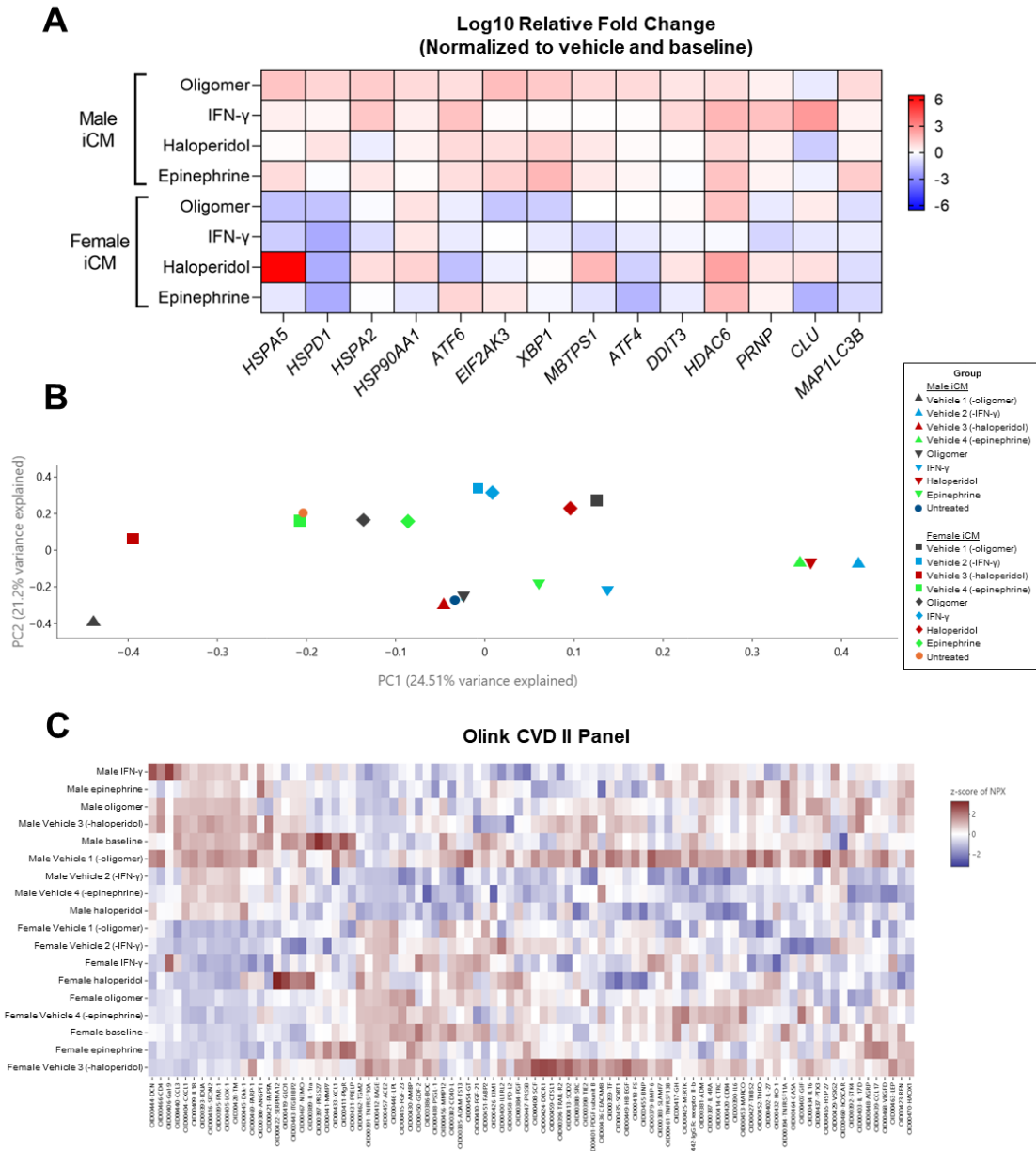


**Figure 18: Differential transcriptional and translational responses to various stressors in male and female hiCM** (A) Heatmap showing the differential gene expression of proteotoxic resistance markers in male and female-derived hiCM following 48-h exposure to different stressors including oligomer, epinephrine, haloperidol and IFN- $\gamma$ . Data in each group was normalized to the combination of their vehicles and baseline (untreated) conditions. (B) PCA plot illustrating the distribution of samples based on their normalized protein expression (NPX) across all 92 assays in the Olink CVD II panel. (C) Heatmap presenting z-scored protein expression in male and female hiCM exposed to different stressors, vehicles or baseline (untreated) conditions as measured by Olink technology. Each column represents differentially expressed protein targets clustered and shown in Table S3. Each row shows a different sample condition. Positive values (*red*) indicate higher expression and negative values (*blue*) indicate lower expression. iCM, human induced-pluripotent stem cells derived cardiomyocytes.

## 5. Discussion

This study provides novel insights into previously unrecognized systemic effects of ischemic stroke on the heart during an acute injury in both sexes, emphasizing the interplay between protein misfolding, systemic inflammation, and autonomic dysregulation in the SHS pathology. In detail, we found (1) post-stroke cardiac dysfunction, characterized by bradyarrhythmias and impaired cardiac output, (2) AIS-induced systemic inflammatory response and autonomic dysregulation, (3) the presence of misfolded proteins, particularly oligomers, locally in the injured brain and systemically in the heart, in conjunction with disruptions in cardiac resistance to proteotoxicity and (4) the unique transcriptional and proteomic profiling upon  $A\beta_{42}$  oligomers in hiCM with potential sex-specific divergence as illustrated in Fig. 24.

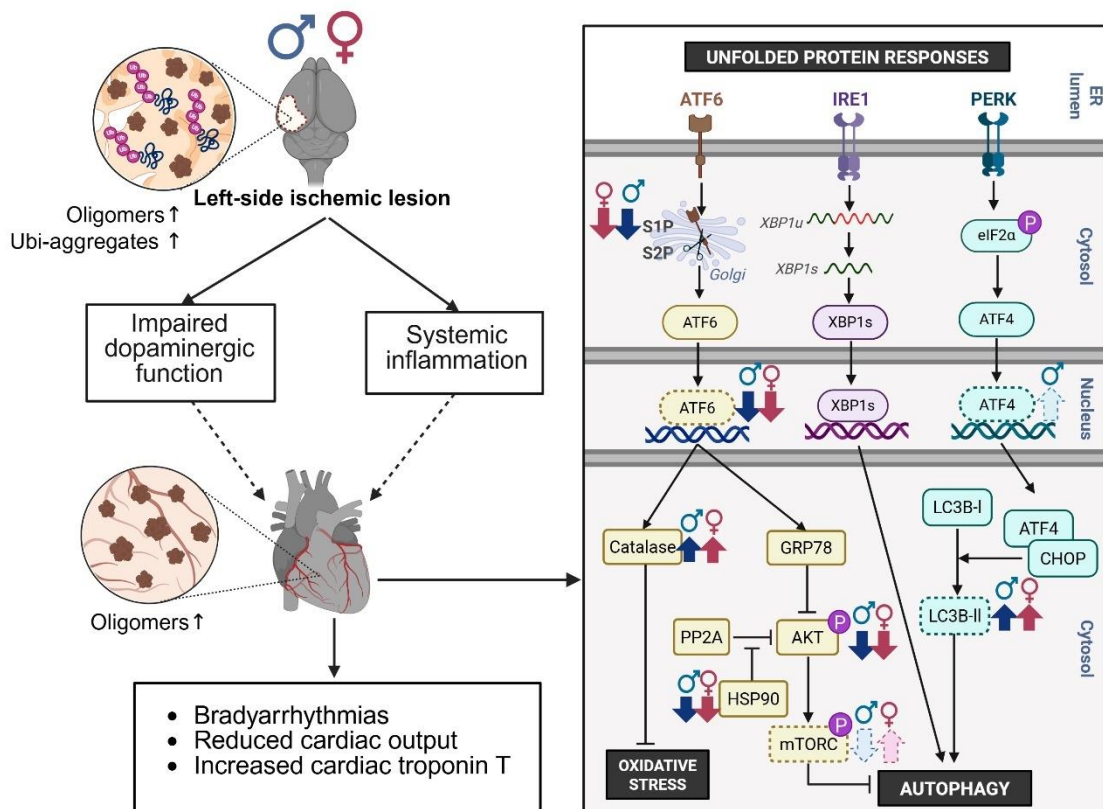


**Figure 24: Schematic summarizing the main study findings.** A left-sided ischemic lesion induces cardiac dysfunction in young wild-type mice of both sexes, characterized by bradyarrhythmia, reduced cardiac output and elevated cardiac troponin T levels. Additionally, systemic alteration is triggered including autonomic dysregulation with a selective impairment of dopaminergic activity and inflammation responses. These molecular changes are linked to post-stroke cardiac injury in our murine model (dashed arrow). AIS is associated with the accumulation of oligomers in both ischemic cerebral and myocardial tissues while ubiquitin aggregation is selectively observed in the ischemic brain. Concomitantly, post-stroke myocardial tissue exhibits compromised (*Figure legend continued*)

**Figure 24:** (*Figure legend continued*) cardiac proteotoxic resistance with broad disruptions in PQC mechanisms, characterized including HSP90 reduction, selective impairment of the ATF6-dependent UPR, AKT inactivation, autophagy induction, and oxidative stress adaptation. Solid arrows indicate statistically significant changes in protein expression in the heart of male (blue) and female (red) mice following stroke, reflecting either upregulation or downregulation. Dashed arrows represent trend in protein expression that did not reach statistical significance. Dashed boxes represent proteins with a potential of sex-specific difference in expression. This figure was created with BioRender.com.

### 5.1 AIS-induced cardiac dysfunction and arrhythmias

Our *in vivo* murine model of left-sided tMCAO demonstrated significant alterations in cardiac electrophysiology and function within 48 h post-stroke, characterized by bradycardia and arrhythmic events. The fact that such profound cardiac effects occurred even in young and wild-type mice of our tMCAO model underscores the acute impact of cerebral ischemia on the heart, independent of aging-related factors or pre-existing cardiovascular conditions. These findings align with previous experimental study showing early cardiac dysfunction and damage after left insular lesion in young male mice as evidenced by bradycardia, rapid cardiomyocyte atrophy and cardiac weight loss.<sup>181</sup>

Notably, the observed bradycardia in our tMCAO model points toward the direction of parasympathetic dominance rather than the more commonly reported sympathetic overactivation, which typically leads to tachycardia observed in stroke patients.<sup>182</sup> This response is primarily influenced by the laterality of insular cortex involved, as left insular cortex injury is associated with decreased sympathetic tone and increased vagal activity, ultimately contributing to parasympathetic overactivity and arrhythmic bradycardia which is in accordance with some findings of previous studies<sup>181,183–185</sup>, while in contrast by others.<sup>186</sup> This discrepancy could be explained by other factors including the model species and type (reperfused vs. non-reperfused), the severity and duration of ischemic insult. Due to the influence of hemispheric autonomic control on baroreflex regulation<sup>187</sup>, these results reinforce the impact of autonomic dysfunction in stroke-induced cardiac rhythm disturbances. The translational significance of this study is further highlighted by the observed arrhythmic patterns which suggests a potential link to atrial fibrillation, a prevalent post-ischemic stroke complication<sup>188</sup>, and revealed hints of autonomic disbalance. In light of this variability, further clinical and translation studies are deemed for a better understanding of this medical condition.

AIS affects not only heart rate but also cardiac function, as demonstrated by a significant reduction in cardiac output which can be caused by bradycardia in conjunction with reduced

stroke volume as observed in our model. The underlying mechanisms may involve altered myocardial contractility, potentially driven by autonomic dysregulation<sup>189</sup>, inflammatory responses<sup>190</sup>, or ischemia-induced cardiac stress.<sup>191</sup> Unlike other stroke models with prominent systolic dysfunction, our mice showed no significant changes in systolic and diastolic function, likely due to parasympathetic overactivation following left-hemispheric stroke. This exerts less detrimental effects on ventricular contractability<sup>192</sup> than tMCAO models in the presence of sympathetic stimulation which is a major drive of systolic dysfunction.<sup>193</sup> Although changes in systolic and diastolic markers were not significant, the downward trend in stroke volume and fractional shortening suggests a subtle yet functionally relevant impairment in cardiac performance, warranting further investigation into its long-term consequences.

Plasma biomarker analysis provided additional evidence of post-stroke myocardial injury, as indicated by the trend toward increase in cardiac troponin T (cTnT) even in the absence of coronary artery disease in mice following AIS. However, no significant alteration presented in this study which likely due to small sample size. Plasma levels of BNP, another biomarker of cardiac stress, remained unchanged, indicating that the observed cardiac dysfunctions may not progress to overt heart failure at this early stage particularly in healthy mice. This is supported by observed normal lung wet/dry weight ratio, a measure of pulmonary congestion which is commonly associated with heart failure. However, the significant downregulation of ANP and the unchanged expression of CNP point toward a selective disruption within the natriuretic peptide system. Considering the physiological roles of ANP in regulating fluid balance, vascular tone, and cardiac remodeling,<sup>194</sup> its reduction may indicate early maladaptive changes in cardiac homeostasis after stroke.

Moreover, the significant weight loss observed in both sexes post-AIS highlights a systemic response to cerebral ischemia, which may involve metabolic disturbance, reduced food intake, or systemic inflammation.<sup>195,196</sup> Despite this, unaltered heart weight/tibia length ratio suggests no occurrence of myocardial hypertrophy or atrophy at this time point. In contrast, the significant reduction in liver weight/tibia length ratio, along with indications of sex-specific differences, suggests a greater hepatic susceptibility to AIS. This observation is supported by previous studies showing stroke-induced liver damage and hepatocyte apoptosis.<sup>197</sup> Collectively, these findings emphasize the importance of examining peripheral organ involvement in stroke pathology with particular attention to sex differences, which may influence disease progression and therapeutic outcomes.

## **5.2 AIS-induced autonomic dysregulation and systemic inflammatory responses**

Catecholamines and inflammatory cytokines are key circulating mediators of AIS-induced cardiac dysfunction.<sup>198</sup> In our murine model, we observed catecholamine imbalance, reflected by reduced urinary HVA levels, alongside a systemic inflammatory response in the early phase of ischemic injury. This reduction in urinary HVA levels suggests a selective impairment in dopaminergic activity, accompanied by a subtle increase in metanephrine levels in males.

This observation may result from ischemic damage to left insular cortex, a dopamine-rich brain region, which could disrupt dopamine synthesis, release, and/or metabolism, leading to decreased urinary HVA levels.<sup>199</sup> The resulting dopaminergic dysfunction reflects widespread brain impairment and potentially linked to bradycardia and cardiac dysfunction in SHS due to its role in regulating cardiac contractility.<sup>200</sup>

Besides autonomic dysregulation, cytokine profiling revealed altered levels of proinflammatory cytokines, particularly CXCL13, ICAM-1, and TIMP-1 in plasma with a more pronounced response in male tMCAO mice. These molecules have been previously implicated in neuroinflammation and positively correlate to stroke severity.<sup>201–203</sup> In addition to their role in stroke-induced inflammation, our protein-protein interaction analysis indicates that these cytokines may influence A $\beta$  pathology. CXCL13, ICAM-1, and TIMP-1 have been linked to TNF- $\alpha$  and IFN- $\gamma$  signaling, which are known to promote A $\beta$  production and contribute to AD pathogenesis.<sup>204</sup> Given that systemic A $\beta$  accumulation and pathology have been reported in various chronic diseases including AD, type 2 diabetes and heart failure<sup>167,169,205,206</sup>, this raises the question of whether stroke-induced systemic inflammation facilitates oligomer accumulation in the post-stroke myocardium, warranting further investigation. Collectively, these findings highlight a complex interplay between parasympathetic dominance, dopamine dysregulation, and systemic inflammation in SHS. Understanding these mechanisms could identify targeted therapeutic strategies to mitigate cardiac complications in stroke patients.

## **5.3 Systemic accumulation of oligomers and protein misfolding during AIS**

Protein misfolding and aggregation have a prominent role in the pathogenesis of both neurodegenerative and cardiovascular diseases, with growing evidence suggesting their involvement in systemic organ dysfunction through the metastatic spreading behavior of misfolded proteins, as observed in cardiac amyloidosis.<sup>166</sup> However, their potential

contribution in brain-heart interactions, particularly in the context of ischemic stroke, remains poorly understood.

In this study, we detected an accumulation of A $\beta$ -positive oligomers in the ipsilateral brain hemisphere following AIS, consistent with previous findings that protein aggregation occurs in acute neuronal injury and contributes to neuronal death after brain ischemia.<sup>207</sup> Beyond the brain, we detected the presence of oligomers in post-stroke myocardial tissue, indicating their systemic presence in both the primary site of damage and the peripheral organ as the heart. Dot blot analysis further confirmed elevated oligomer levels in both the injured brain regions and the heart, reinforcing the concept of systemic protein misfolding. Together with previous observations in patients with AD where A $\beta$  accumulates in the heart and is associated with cardiac diastolic and myocyte damage, our findings raise the possibility of oligomers contribution to stroke-induced cardiac dysfunction. Moreover, the transient increase in oligomers within axillary lymph nodes in male tMCAO mice may suggest a potential route for oligomers spreading. Further investigation into the presence of oligomers in additional anatomical structures such as kidney, spleen as well as circulating blood compartments is warranted to better understand their systemic fate. In addition, the tissue origin of these oligomers - whether they originate primarily from the ischemic brain or the heart - remains to be elucidated.

#### **5.4 Impairment of local PQC mechanisms in the post-stroke heart**

Given that disrupted proteostasis leads to the accumulation of protein aggregates which is known to exacerbate cardiac pathologies<sup>130</sup>, it is tempting to speculate that myocardial protein homeostasis might be altered in response to AIS. In support of this idea, our findings revealed a compromised myocardial PQC network characterized by a series of molecular alterations in the UPR signaling, autophagic activity and oxidative stress response, which may contribute to post-stroke cardiac dysfunction.

A key observation was the significant downregulation of HSP90 in both male and female hearts following AIS, suggesting an impaired adaptive response to proteotoxic stress. Given the multifaceted role of HSP90 in assisting protein folding<sup>208</sup>, stabilizing UPR components<sup>209</sup> and regulating autophagy<sup>210</sup>, its reduction is likely to disrupt multiple signaling pathways. Specifically, the decline in HSP90 may compromise UPR activation, as indicated by reduced ATF6 cleavage. However, other UPR markers including p-IRE1, p-PERK and spliced-XBP1 (XBP1s) remain unaltered, suggesting a selective impairment of the ATF6-dependent UPR

branch. This is further supported by a tendency toward decreased GRP78 levels, a classical ATF6-inducible chaperone. However, CHOP, a marker of ER stress-mediated apoptosis, remained unchanged, indicating that the myocardial ER stress response was not fully dysregulated during acute stage of injury. This may increase myocardial susceptibility to proteotoxic damage without inducing cardiomyocyte death, a process previously documented in the heart following chronic ischemic stroke.<sup>211</sup>

In addition to UPR dysregulation, HSP90 downregulation can triggers autophagic regulation, likely through AKT inactivation.<sup>210</sup> This aligns with our results showing reduced p-AKT, a negative regulator of autophagy, accompanied by an increased LC3B-II/I ratio, indicating enhanced autophagic flux. This response may serve as a compensatory mechanism to counteract AIS-induced stress in the heart. The role of autophagy in cardiac homeostasis is well documented, particularly in clearing protein aggregates and maintaining cardiac proteostasis under pathological conditions.<sup>212</sup> Previous study reported that the control of cardiac alterations by ischemic stroke has been linked to the autophagic pathway.<sup>211</sup> While moderate autophagy is protective, its excessive activation has been associated with various cardiac diseases including AF<sup>213</sup>, highlighting its dual role in cardiac health. Given this complexity, further investigation is required to elucidate the precise impact of autophagy on post-stroke cardiac dysfunction taking into consideration side, extension and lack/presence of reperfusion.

Despite the reduction in cATF6, we observed an upregulation of catalase, a noncanonical-ATF6 inducible protein and a key antioxidant defense enzyme, in both male and female hearts following AIS. Given that the crucial role of catalase in neutralizing reactive oxygen species (ROS)<sup>214</sup>, its upregulation may serve as a compensatory mechanism against oxidative damage potentially triggered by ER dysfunction and excessive autophagic flux. However, the presence of increased oxidative stress markers in post-stroke hearts requires further validation in this model.

While both sexes exhibited broad proteotoxic stress responses, sex-specific differences in post-stroke myocardial damage were presented with male hearts exhibiting more pronounced dysregulation in certain UPR components including cATF6, LC3B, ATF4 and phosphorylated mTOR (Ser2448), suggesting a greater imbalance in ER stress responses in males than females. The underlying mechanisms driving this sex-specific susceptibility remain unclear, but several possibilities warrant consideration. One potential explanation is the difference in

cerebral infarct volume, with females generally exhibiting smaller infarcts following ischemic stroke<sup>215</sup>, which may reduce the extent of cardiac impairment. However, in this study, sex-specific differences in infarct size were not statistically significant, likely due to small sample size. Alternatively, female hearts may possess inherently stronger compensatory mechanisms that enhance their ability to manage proteotoxic stress.

In addition to previous studies showing AIS-induced myocardial vulnerability by altering cardioprotective pathways<sup>216</sup>, our findings suggest that the heart following ischemic stroke also experiences broad disruptions in PQC mechanisms, characterized by HSP90 downregulation, selective impairment of the ATF6-dependent UPR, AKT inactivation, autophagy induction, and oxidative stress adaptation. Notably, sex-specific differences in these biological responses may influence disease progression, suggesting potential variations in cardiac resistance to proteotoxicity. Given the concurrent accumulation of misfolded oligomers in the post-stroke myocardium of our tMCAO mice, these results raise the critical question of whether oligomer accumulation is a cause or consequence of these molecular alterations. Future studies are needed to address the role of oligomers in these processes, and it is interesting to determine whether these findings translate to clinical outcomes.

### **5.5 Differential ubiquitin dynamics in the brain and heart**

In the brain, the accumulation of ubiquitin aggregates in the ischemic hemisphere provides clear evidence of AIS-induced proteotoxic stress. This scenario could be the result of UPS dysfunction, which inhibits clearance of polyubiquitinated proteins, thereby exacerbating protein aggregation and cellular stress or more likely to the overwhelming damage elicited by ischemia which cannot be properly counteracted by compensatory mechanisms.<sup>179</sup> To confirm this hypothesis, future studies should investigate the proteasomal activity in the ischemic brain. Interestingly, no such ubiquitin accumulation was observed in the myocardium, suggesting distinct regulation following AIS between these two organs. Unlike the brain, the heart may counteract proteotoxic stress through alternative degradation pathways, such as increased autophagic activity, which facilitates the removal of excessive misfolded proteins and mitigates oligomer toxicity<sup>129</sup>, as evidenced by increased LC3B-II/I ratio observed in our previous studies. Meanwhile, the unchanged levels of free ubiquitin in both tissues demonstrate that AIS does not lead to a global depletion of ubiquitin pools. Instead, the selective accumulation of ubiquitin conjugates in the brain points to a tissue-specific impairment in ubiquitin-dependent protein degradation, likely due to the overwhelming

molecular damage within this organ. In contrast, the heart appears to adapt through enhanced autophagy to maintain proteostasis.

## 5.6 The biological relevance of oligomers on human cardiomyocytes

Our findings in the tMCAO model underscore the complex pathophysiology of ischemic stroke with oligomer accumulation appears as a characteristic feature in both the ischemic brain and the heart. However, it remains unclear whether oligomers per se are the direct toxic mediator in this complex scenario.

It is interesting to note that oligomer-induced cardiac dysfunction occurs through common pathological mechanisms, independent of protein species.<sup>217</sup> To induce proteotoxic stress in our study, we employed *bona fide* A $\beta$ <sub>42</sub> oligomers due to their well-documented role in AD<sup>175,218–221</sup> and growing experimental evidence of their pathological effects beyond the brain including in the cardiovascular system.<sup>167,205,206,222</sup>

Our data shows that A $\beta$ <sub>42</sub> oligomers broadly dysregulated proteostasis-related genes and disrupted proteomic inflammatory responses with a pattern distinct from inflammatory (IFN- $\gamma$ ) and neurohormonal (epinephrine, haloperidol) stimuli. These molecular alterations in inflammation<sup>153</sup> and proteostasis<sup>223,224</sup> are also observed in damaged neurons as part of A $\beta$ <sub>42</sub> oligomer-induced neuropathology in AD, suggesting a broader pathophysiological framework in which A $\beta$ <sub>42</sub> oligomers may contribute to both cerebral and cardiac pathology through overlapped underlying mechanisms.

Despite comparable cell viability between sexes, the divergent transcriptional and proteomic patterns indicate the modulation of sex on cardiac susceptibility to proteotoxic stress. Interestingly, A $\beta$ <sub>42</sub> oligomers exposure led to a convergence of male and female proteomic profiles, suggesting a potent influence of oligomers that may diminish inherent sex-specific differences observed under vehicle-treated conditions, reinforcing the concept of A $\beta$ -related damage irrespectively of organ and sex.

However, these findings should be interpreted in light of certain limitations including a relatively small sample size, variability in cardiomyocyte populations and heterogeneity in cell sources. Future investigations incorporating additional biological replicates and consistent cell sources will be necessary to clarify sex-specific proteomic adaptations. While hiCM provides a physiologically relevant human model, they lack the systemic complexity of *in vivo* systems and exhibit genetic and phenotypic variability.<sup>225</sup> Nevertheless, these

preliminary findings reinforce the importance of incorporating sex as a biological variable in cardiac research to better understanding of sex-specific differences in stress responses and disease progression.

## **6. Conclusion and future perspectives**

This study unravels previously unrecognized systemic consequences of AIS on cardiac function, highlighting the complex interplay between protein misfolding, inflammation, and autonomic dysregulation in the pathology of SHS. The concurrent accumulation of oligomers in both the brain and heart along with impaired cardiac resistance to proteotoxicity, suggests a mechanistic connection between post-stroke neurodegeneration and cardiac dysfunction. Notably, sex-specific differences in the cardiac response to proteotoxic stress were identified, underscoring the importance of considering biological sex in the pathophysiology and treatment of SHS. Targeting protein homeostasis mechanisms may serve as a promising therapeutic approach to attenuate post-stroke cardiac impairment. Future research should aim to further determine the origin, systemic translocation and temporal dynamics of oligomer accumulation to better understand their role in stroke-induced cardiac dysfunction.

The complex biological response of hiCM to A $\beta$ <sub>42</sub> oligomers in vitro underscores the unique feature of oligomers impact on the human myocardium with potential sex-specific divergence. These findings emphasize the need to investigate broader proteotoxicity stressors beyond A $\beta$ <sub>42</sub> including other amyloidogenic proteins implicated in neurodegenerative and cardiac pathology which will be critical to identify therapeutic strategies that counteract oligomer-induced cardiac dysfunction. Additionally, the distinct susceptibility of male and female cardiomyocytes to oligomer toxicity should be investigated in more physiologically relevant models, such as engineered heart tissues, to better understand sex-specific vulnerabilities.

These findings have significant implications for understanding the systemic nature of ischemic stroke which is crucial for advancing therapeutic strategies aimed at preventing and managing stroke-related cardiac complications. It will also be of high importance to refine clinical management in short- and long-term and ultimately improve prognosis and life expectancy in stroke patients. Characterization of possible divergences between the two genders on AIS-induced cardiac events will offer a patient-centered tailored therapy with the wishful intention of personalized medicine outlook.

## 7. Limitation of the study

The primary findings of this study suggest a potential link between oligomers and post-stroke cardiovascular complications; however the causality of this relationship remains unclear. Due to the diverse mechanistic effects of oligomers, conducting rescue experiments with targeted interventions, such as chaperone-based therapies or proteostasis regulators, poses challenges in mitigating the complex oligomer-induced damages without causing off-target effects. This makes it difficult to determine whether protein misfolding is a direct driver of cardiac pathology or a secondary consequence of ischemic injury. However, ongoing studies on using both mouse and human cardiomyocytes exposed to A $\beta$ <sub>42</sub> oligomers aim to clarify the mechanistic contribution of protein misfolding to stroke-induced cardiac dysfunction in both species. On top of protein misfolding, systemic inflammation and autonomic dysregulation, other factors such as neuroendocrine signaling, oxidative stress, epigenetic modifications, and gut microbiota are implicated in the pathophysiology of SHS. The potential involvement of these additional mediators in brain-heart interactions following ischemic stroke cannot be excluded and warrants further investigation.

In lights of our *in vivo* model, this study evaluated the outcomes at a single time point of 48 h after reperfusion, which may not capture the full progression of stroke-induced cardiac dysfunction over time. Extending the analysis to later time points will be crucial for understanding the chronic effects of ischemic brain injury on the heart. Additionally, the use of young animals without any comorbidity for the stroke model in this study differs from human stroke which particularly affects elderly people who have various cerebrovascular risk factors. Older populations may exhibit distinct responses to ischemic injury, highlighting the need for future studies to incorporate age-dependent differences to better reflect clinical scenarios.

Although the investigation of sex-specific differences on post-stroke cardiac injury was not the primary objective of this study, our findings suggest the possibility for different responses to AIS between sexes particularly in morphometric changes and the modulation of cardiac protein homeostasis. However, due to the small sample size within each sex group, we were unable to identify sex-specific differences in several other parameters. This limitation highlights the importance of including larger sample sizes in future studies, as a more robust sample would improve the statistical power and enhance the ability to detect sex-based variations in organ-specific responses to stroke.

While our in vitro model provides insights into the effects of A $\beta$ <sub>42</sub> oligomers on human cardiomyocytes, it does not fully recapitulate the complex physiological environment of the heart. The absence of systemic sex hormone influences in vitro may constrain the interpretation of sex-specific susceptibility in a physiological context. Additionally, the concentration and duration of oligomer exposure in vitro may not accurately reflect in vivo conditions and species-specific differences in oligomer interactions with cardiomyocytes may limit the translational relevance of observed findings from mouse to humans. Furthermore, given the heterogeneity of oligomers, it is essential to investigate a broader spectrum of other amyloidogenic proteins beyond A $\beta$ <sub>42</sub> oligomers such as tau, transthyretin, Huntington,  $\alpha$ -synuclein, which are implicated in both neurodegenerative and cardiac diseases. This would provide a more comprehensive understanding of shared pathogenic mechanisms across different oligomeric species within the frame of brain-heart axis as well as uncover potential therapeutic strategies to mitigate oligomer-induced cardiac dysfunction.

## 8. Appendix I: Supplementary Figures

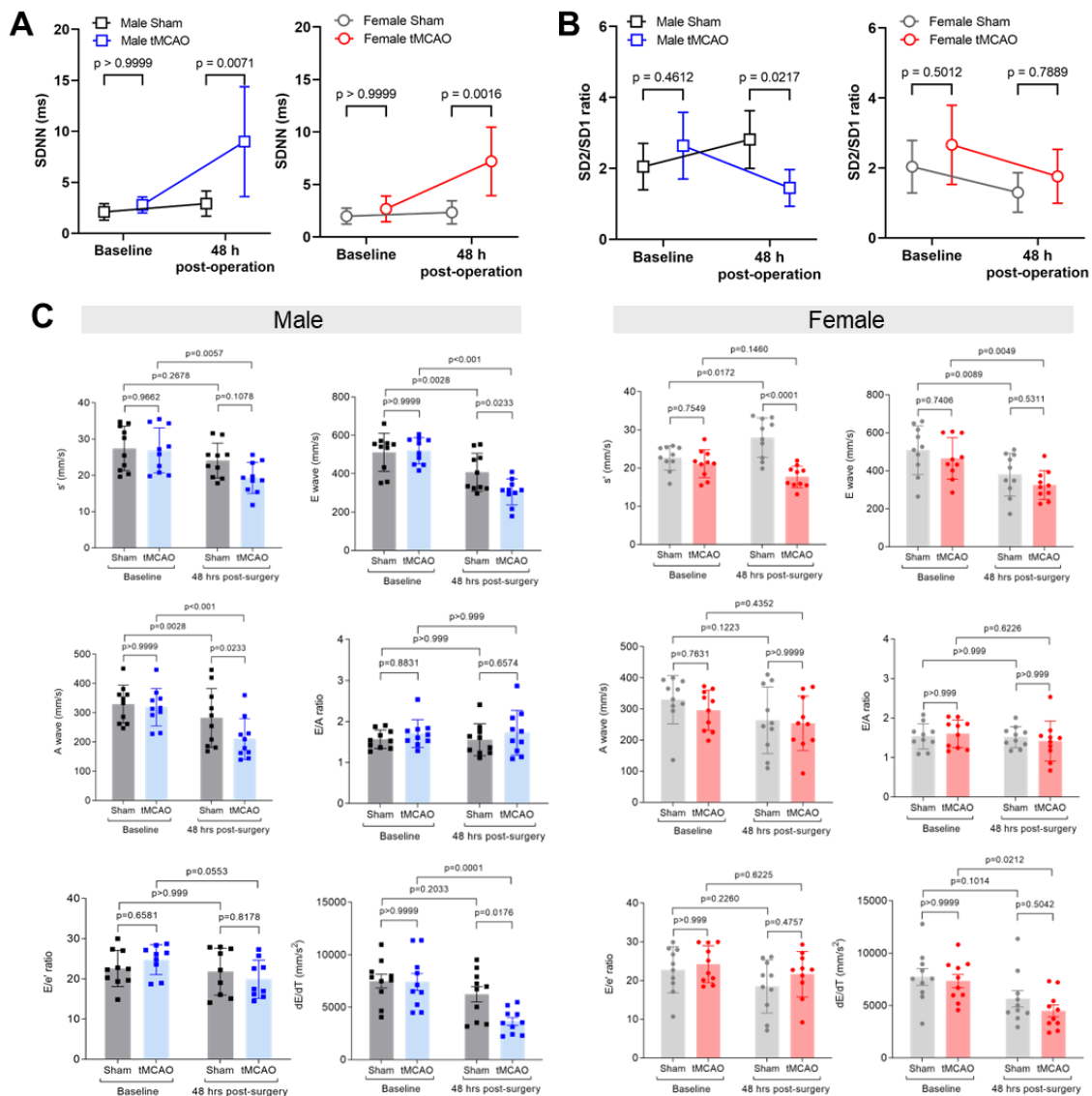


**Figure S1: Heart rate variability (HRV) and impaired diastolic functions in mice following AIS.** (A) HRV assessment showing increased standard deviation of all RR intervals (SDNN) in both sexes of tMCAO mice versus sham controls whereas (B) the ratio between long-term (SD2) and short-term (SD1) RR interval variability, which generally accepted as an index of autonomic balance, was decreased only in male mice post-stroke while the ratio remains stable in female mice post-stroke (N=5/group). (C) Echocardiographic assessments in both sexes of tMCAO mice compared to sham controls at baseline (pre-operation) and at 48 h-post operation (N=10/group). Female tMCAO mice showed a reduction in systolic velocity ( $s'$ ) while male tMCAO mice exhibited predominant alterations in some diastolic parameters including impaired mitral inflow velocity during early diastolic filling (E wave), mitral inflow velocity during atrial contraction (A wave) and the early diastolic acceleration rate (dE/dT). However, the ratio for absolute values of early-to-late diastolic flow velocity (E/A) and relationship between early diastolic mitral inflow velocity and diastolic mitral annular velocity at septal wall (E/E') remain unchanged. Data is presented as mean  $\pm$  SD. Each dot in the graph corresponds to individual data points from each mouse. (Figure legend continued)

**Figure S1:** (*Figure legend continued*) Two-group comparisons were performed using Student's two-tailed test. Multiple comparisons were performed by two-way ANOVA followed by Bonferroni *post-hoc* test. A *p*-value <0.05 was considered significant. p.o., Post-operation; h, hours; ms, Milliseconds; tMCAO, Transient-middle carotid artery.

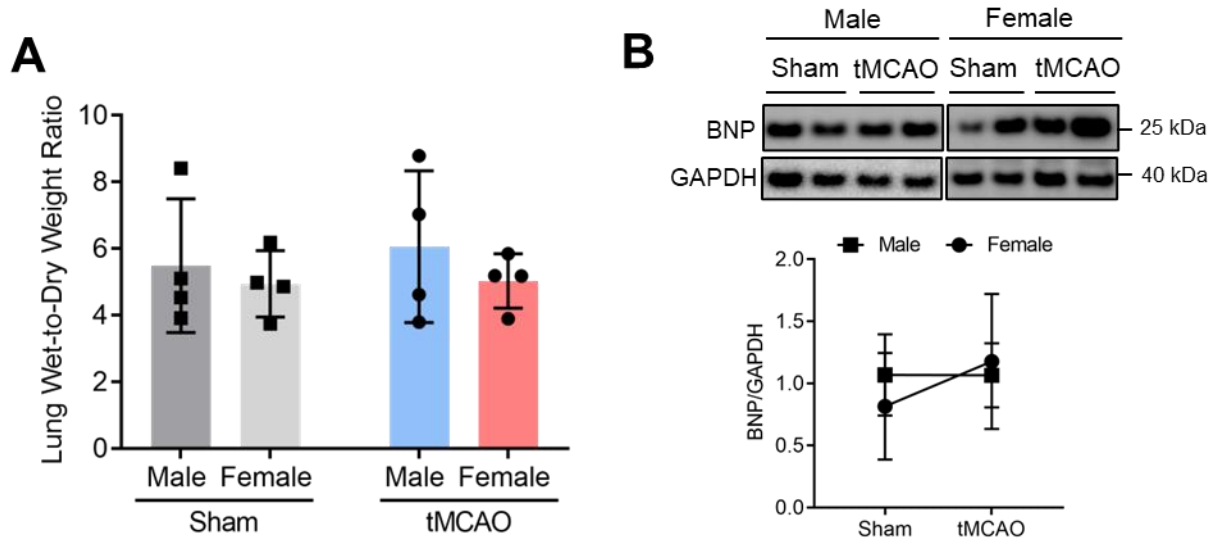


**Figure S2: No alterations in lung weight and BNP protein expression in the post-stroke heart.** (A) The ratio of lung wet/dry weight remain unchanged in both male and female tMCAO mice compared to sham controls (N=4/group). Bar graph represents mean  $\pm$  SD. Each dot in the graph corresponds to individual data points from each mouse. (B) Representative Western Blot and their respective densitometric quantification showing no alterations in BNP expression in the post-stroke hearts of male (closed square) and female (closed circle) mice compared to sham controls (N=10/group). Data represents mean  $\pm$  SD. Statistical comparisons between tMCAO and sex were performed by two-way ANOVA followed by Bonferroni's *post-hoc* test. A *p* value <0.05 was considered significant; kDa, Kilodalton; tMCAO, Transient-middle carotid artery.

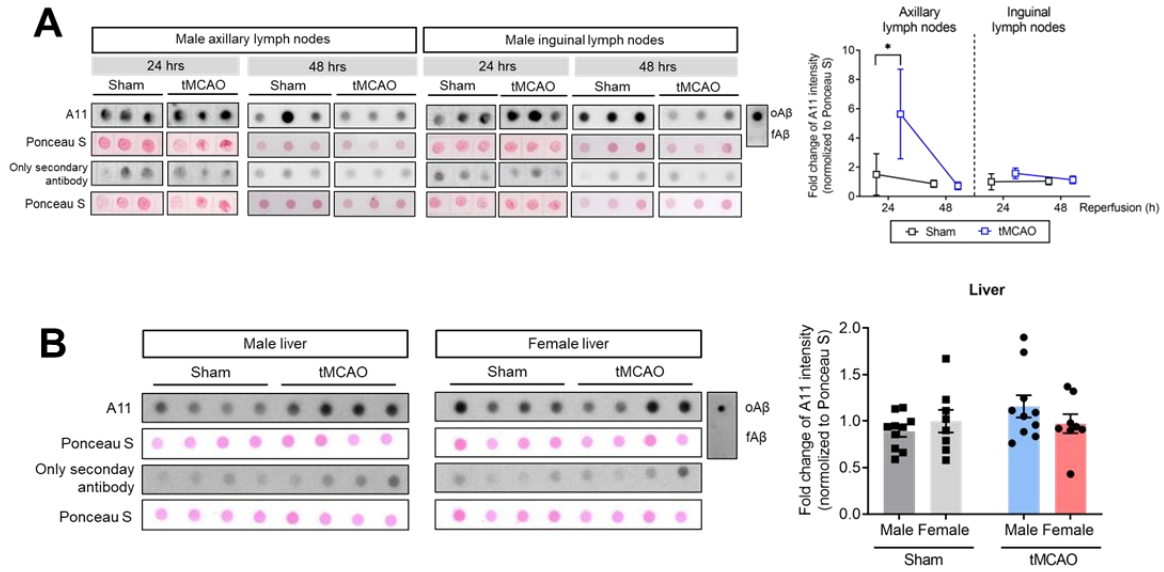


**Figure S3: The presence of oligomers accumulation in lymph nodes and plasma.** (A) Representative dot blot images and their relative densitometric quantification for the expression of oligomers using A11 antibody in the Triton-soluble fraction showing significant increase in levels of oligomers in axillary lymph nodes isolated from male tMCAO mice at 24 h of reperfusion and decreased at 48 h of reperfusion, while inguinal lymph nodes did not show any changes (N=10/group). Data are presented in mean  $\pm$  SD. Two-group comparisons were performed using an unpaired Student's t-test. A  $p$  value  $<0.05$  was considered significant. (B) Oligomer levels in liver remained unchanged in both sexes of mice upon AIS (N=10/group). Bar graph represents mean  $\pm$  SD. Each dot in the graph corresponds to individual data points from each mouse. Statistical comparisons between tMCAO and sex were performed by two-way ANOVA followed by Bonferroni's *post-hoc* test. A  $p$  value  $<0.05$  was considered significant. \* $p < 0.05$  sham vs. tMCAO; tMCAO, Transient-middle carotid artery.

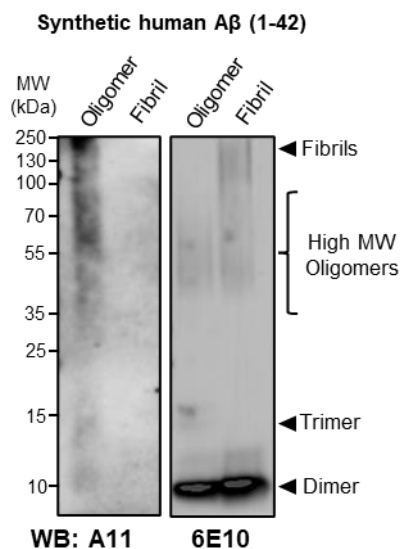


**Figure S4: Western blot analysis of synthetic human A $\beta$ <sub>42</sub> oligomers and fibrils.** Both oligomer and fiber samples were subjected to SDS-PAGE, transferred onto nitrocellulose membrane and probed with anti-oligomeric A11 and anti-A $\beta$  6E10 antibodies. A11 selectively (Figure legend continued)

**Figure S4:** (*Figure legend continued*) detected oligomeric samples, while 6E10 recognized both amyloid oligomers and fibrils, revealing multiple bands ranging from dimers up to high molecular weight (MW) aggregates that accumulate at the top of the gel. MW, Molecular weight; kDa, Kilodalton.

## 9. Appendix II: Supplementary Tables

Gene	Forward	Reverse
<b>Mouse</b>		
<i>Actb</i>	CCTTCTTGGGTATGGAATCCTG	AGCACTGTGTTGGCATAGAG
<i>Hspa2</i>	ACAGTGCAGTCCGATATGAAG	GAAATCTCCTCAGGGAAGAAGG
<i>Hspa5</i>	TGGATAAGAGAGAGGGAGAGAAG	CACCACTTCAAAGACACCATTG
<i>Hspd1</i>	TGAGCAGCTAGACATCACAAC	TCACTTGTTCCTCCAACCTTC
<i>Hsp90aa1</i>	CATCGGACGCTCTGGATAAA	CTGTTTGCTGGGAATGAGATTG
<i>Hsf1</i>	CCCTGAAGAGTGAGGACATAAA	GAGTCCATACACCCTGTTTCC
<i>Atf6</i>	GTCACTGGTCCTGGAACAA	GGCGCTGCTGGAAGTAATA
<i>Ern1</i>	CCCAAATGTGATCCGCTACT	CCTTCTGCTCCACATACTCTTG
<i>Eif2ak3</i>	GTTACACAGCCAGCGAAGAA	GGCCTCTGTACATCCCTAAGTA
<i>Xbp1</i>	CAAGTTGGACCCTGTTCATGT	GAAGTAGGTCCTTCTGGGTAGA
<i>Mbtps1</i>	CTACTGCTCCAGCCTATCTA	CCACTCAGGCTTATCCACAAT
<i>Mbtps2</i>	GTCCTTGCTCTCCTTGGTATTT	CCTCTGCGACTTCAGTGATAAG
<i>Atf4</i>	GAGCTAGGCAGTGAAGTTGAT	GGAGTGTCTTCTCCTTTACAC
<i>Ddit3</i>	CCAGGAAACGAAGAGGAAGAA	TTTGGGATGTGCGTGTGA
<i>Syvn1</i>	CCTACTACCTCAAACACCAGTTC	AAGAGGAAGACAAGGACAAAGG
<i>Hdac6</i>	CAGACTTCCATCTACTGCACTC	CGGCTTCTTCCACTTCATCT
<i>Prnp</i>	AAGGAGTCCCAGGCCTATTA	CACGATCAGGAAGATGAGGAAG
<i>Clu</i>	CCAGGGAGTGAAGCACATAAA	CTCCAGAGCATCCTCTTTCTTC
<i>Cat</i>	GATGGTAACTGGGATCTTGTGG	GTGGGTTTCTCTTCTGGCTATG
<i>Map1lc3b</i>	ACTCCCATCTCCGAAGTGTA	ATTGCTGTCCCGAATGTCTC
<i>Atf7</i>	CCTGTGAGCTTGGATCAAAGGC	GAGCAAGGAGACCAGAACAGTG
<i>Sod2</i>	TAACGCGCAGATCATGCAGCTG	AGGCTGAAGAGCGACCTGAGTT
<i>Mtor</i>	CGGGACTACAGAGAGAAGAAGA	CATCAACGTCAGGTGGTCATAG
<i>Dapk1</i>	TGATGACCAGTCCACCAAAG	GAAGTACACAGGGTTTCCAGAG
<i>Becn1</i>	AAACCAGGAGAGACCCAGGAG	TTCTGTAGACATCATCCTGGCTGG
<b>Human</b>		
<i>GAPDH</i>	CCCTTCATTGACCTCAACTACA	ATGACAAGCTTCCCCTTCTC
<i>HSPA5</i>	CCTTCGATGTGTCTCTTCTCAC	ACGCTGGTCAAAGTCTTCTC
<i>HSPD1</i>	TACTGTACTGGCAGCTCTA	CTCACAACCTCTCCTGATTCC
<i>HSPA2</i>	CAAGAGCACCCGGTAAGGAAA	CGTCTGCTTGATGTTGTAGGTA
<i>HSP90AA1</i>	GGAGATAAACCTGACCATTCC	GACAGGAGCGCAGTTTCATA
<i>ATF6</i>	CTCCAGCCTCCTCAAGTTATTC	ACTAGAAGACAAATCCAACCTC
<i>EIF2AK3</i>	GGTTGGAGACTTTGGGTTAGT	GTCCTGTGTGTCTGGCATAA
<i>XBP1</i>	AGATCGAAAGAAGGCTCGAATG	CCCAAGCGCTGTCTTAACT
<i>MBTPS1</i>	TGGGAGTCACAGGAAGAATTG	TAAGACCGAGGAGTAGGAGAAG
<i>ATF4</i>	GTCCTCCACTCCAGATCATTC	CAGTGTAGTCTGGCTTCTATC
<i>DDIT3</i>	TCACTCTCCAGATTCCAGTCA	ACCACTCTGTTTCCGTTTCC
<i>HDAC6</i>	CTATTTCTCCATCCACCGCTAC	TGGTTCCAAGGCACATTGA
<i>PRNP</i>	CGTGGTTGAGCAGATGTGTA	ATCACAGGTGGAGAGGAGAA
<i>CLU</i>	CAGCCCTTCTTGAGATGATAC	TCGCCTTCTCGTATGAATTCTG
<i>MAP1LC3B</i>	CGCACCTTCGAACAAAGAGTA	GCTGCTTCTCACCCTTGTATC

**Table S1:** Mouse and human primers used for qPCR analysis

Antibodies	Source	Catalog number	Working dilution
Vinculin	Invitrogen	MA5-11690	1/10,000
ATF6	Novus Biologicals	NBP1-40256	1/4,000
GRP78	Abcam	ab21685	1/1,000
HSP90	Santa Cruz	sc-13119	1/1,000
Catalase	Cell Signaling	14097	1/2,000
LC3B	Cell Signaling	27755	1/1,000
PERK	Santa Cruz	sc-13073	1/500
HSP60	Santa Cruz	sc-13115	1/500
GAPDH	Sigma-Aldrich	MAB374	1/10,000
$\beta$ -actin	Sigma-Aldrich	A1978	1/10,000
Ubi-1	Invitrogen	13-1600	1/2,000
BNP	Abbexa	abx102416	1/1,000
Akt	Cell Signaling	9272	1/2,000
p-Akt (Ser473)	Cell Signaling	4060	1/2,000
mTOR	Cell Signaling	2893	1/1,000
p-mTOR (Ser2481)	Cell Signaling	2974	1/1,000
p-mTOR (Ser2448)	Cell Signaling	5536	1/1,000
IRE1- $\alpha$	Invitrogen	PA5-20189	1/1,000
p-IRE1- $\alpha$ (Ser724)	Invitrogen	PA1-16927	1/1,000
ATF-4	Santa Cruz	sc-390063	1/1,000
SOD2	Cell Signaling	13194	1/2,000
CHOP	Cell Signaling	2895	1/1,000
PP2AB	Cell Signaling	5689	1/1,000
XBP1	Abcam	EPR22004	1/1,000
p-eIF2a (Ser51)	Cell Signaling	3398	1/1,000
eIF2a	Cell Signaling	5324	1/1,000
p-PERK (Thr980)	Cell Signaling	3179	1/500
PERK	Santa Cruz	sc-377400	1/500
MBTSP1	Invitrogen	PA5-109948	1/1,000
MBTSP2	Cell Signaling	2157	1/1,000
PHLPP	ProteinTech	22789-1-AP	1/3,000
ATG7	Santa Cruz	sc-376212	1/2,000

**Table S2:** List of antibodies used for Western blot analysis

<b>Biomarker (92)</b>	<b>UniProt ID</b>	<b>Gene name</b>
Cobalamin binding intrinsic factor	P27352	CBLIF (GIF, IFMH)
Interleukin-18	Q14116	IL18 (IGIF, IL1F4)
Polymeric immunoglobulin receptor	P01833	PIGR
Superoxide dismutase [Mn], mitochondrial	P04179	SOD2
Fibroblast growth factor 23	Q9GZV9	FGF23 (HYPF)
Spondin-2	Q9BUD6	SPON2 (DIL1)
Lactoylglutathione lyase	Q04760	GLO1
Pappalysin-1	Q13219	PAPPA
Renin	P00797	REN
Tyrosine-protein kinase Mer	Q12866	MERTK (MER)
Thrombospondin-2	P35442	THBS2 (TSP2)
Thrombomodulin	P07204	THBD (THRM)
Interleukin-6	P05231	IL6 (IFNB2)
Pro-adrenomedullin	P35318	ADM (AM)
SLAM family member 7	Q9NQ25	SLAMF7 (CS1)
A disintegrin and metalloproteinase with thrombospondin motifs 13	Q76LX8	ADAMTS13 (C9orf8)
Interleukin-4 receptor subunit alpha	P24394	IL4R (IL4RA)
Interleukin-1 receptor antagonist protein	P18510	IL1RN (IL1F3, IL1RA)
Bone morphogenetic protein 6	P22004	BMP6 (VGR)
Alpha-L-iduronidase	P35475	IDUA
Proteinase-activated receptor 1	P25116	F2R (CF2R, PAR1, TR)
Serine protease 27	Q9BQR3	PRSS27 (MPN)
Tissue factor	P13726	F3
Platelet-derived growth factor subunit B	P01127	PDGFB (PDGF2, SIS)
Interleukin-27	Q14213_Q8NEV9	EBI3_IL27 (IL-27a, IL-27b, IL27A, IL27A, IL27B, IL30, IL30)
Lipoprotein lipase	P06858	LPL (LIPD)
Decorin	P07585	DCN (SLRR1B)
Low affinity immunoglobulin gamma Fc region receptor II-b	P31994	FCGR2B (CD32, FCG2, IGFR2)
C-C motif chemokine 3	P10147	CCL3 (G0S19-1, MIP1A, SCYA3)
C-C motif chemokine 17	Q92583	CCL17 (SCYA17, TARC)
Galectin-9	O00182	LGALS9
Kit ligand	P21583	KITLG (MGF, SCF)
Fibroblast growth factor 21	Q9NSA1	FGF21

**Table S3:** Protein targets available from the Olink Target 96 Cardiovascular II panel (continued)

Biomarker (92)	UniProt ID	Gene name
Advanced glycosylation end product-specific receptor	Q15109	AGER (RAGE)
Chymotrypsin-C	Q99895	CTRC (CLCR)
Oxidized low-density lipoprotein receptor 1	P78380	OLR1 (CLEC8A, LOX1)
Follistatin	P19883	FST
SLAM family member 5	Q9UIB8	CD84 (SLAMF5)
Serpin A12	Q8IW75	SERPINA12
2,4-dienoyl-CoA reductase, mitochondrial	Q16698	DECR1 (DECR, SDR18C1)
Hepatitis A virus cellular receptor 1	Q96D42	HAVCR1 (KIM1, TIM1, TIMD1)
Somatotropin	P01241	GH1
Growth-regulated alpha protein	P09341	CXCL1 (GRO, GRO1, GROA, MGSA, SCYB1)
Angiopoietin-1	Q15389	ANGPT1 (KIAA0003)
CD40 ligand	P29965	CD40LG (CD40L, TNFSF5, TRAP)
Placenta growth factor	P49763	PGF (PGFL, PLGF)
Brother of CDO	Q9BWV1	BOC
Proto-oncogene tyrosine-protein kinase Src	P12931	SRC (SRC1)
Interleukin-17D	Q8TAD2	IL17D
Serine/threonine-protein kinase 4	Q13043	STK4 (KRS2, MST1)
Tumor necrosis factor receptor superfamily member 11A	Q9Y6Q6	TNFRSF11A (RANK)
Tumor necrosis factor receptor superfamily member 10B	O14763	TNFRSF10B (DR5, KILLER, TRAILR2, TRICK2, ZTNFR9)
Angiopoietin-1 receptor	Q02763	TEK (TIE2, VMCM, VMCM1)
Interleukin-1 receptor-like 2	Q9HB29	IL1RL2 (IL1RRP2)
Tumor necrosis factor receptor superfamily member 10A	O00220	TNFRSF10A (APO2, DR4, TRAILR1)
Prostasin	Q16651	PRSS8
Dickkopf-related protein 1	O94907	DKK1
Integrin beta-1-binding protein 2	Q9UKP3	ITGB1BP2
Matrilysin	P09237	MMP7 (MPSL1, PUMP1)
Agouti-related protein	O00253	AGRP (AGRT, ART)
Pentraxin-related protein PTX3	P26022	PTX3 (TNFAIP5, TSG14)
Carcinoembryonic antigen-related cell adhesion molecule 8	P31997	CEACAM8 (CGM6)
Pro-interleukin-16	Q14005	IL16
Heme oxygenase 1	P09601	HMOX1 (HO, HO1)

**Table S3:** Protein targets available from the Olink Target 96 Cardiovascular II panel (continued)

<b>Biomarker (92)</b>	<b>UniProt ID</b>	<b>Gene name</b>
Protein AMBP	P02760	AMBP (HCP, ITIL)
V-set and immunoglobulin domain-containing protein 2	Q96IQ7	VSIG2 (CTH, CTXL)
Fatty acid-binding protein, intestinal	P12104	FABP2 (FABPI)
Vascular endothelial growth factor D	O43915	VEGFD (FIGF)
T-cell surface glycoprotein CD4	P01730	CD4
Carbonic anhydrase 5A, mitochondrial	P35218	CA5A (CA5)
Protein-glutamine gamma-glutamyltransferase 2	P21980	TGM2
Tumor necrosis factor receptor superfamily member 13B	O14836	TNFRSF13B (TACI)
Programmed cell death 1 ligand 2	Q9BQ51	PDCD1LG2 (B7DC, CD273, PDCD1L2, PDL2)
Macrophage metalloelastase	P39900	MMP12 (HME)
Gastrotropin	P51161	FABP6 (ILBP, ILLBP)
Thrombopoietin	P40225	THPO (MGDF)
Hydroxyacid oxidase 1	Q9UJM8	HAO1 (GOX1, HAOX1)
Sortilin	Q99523	SORT1
Lymphotactin	P47992	XCL1 (LTN, SCYC1)
Prolargin	P51888	PRELP (SLRR2A)
P-selectin glycoprotein ligand 1	Q14242	SELPLG
Proheparin-binding EGF-like growth factor	Q99075	HBEGF (DTR, DTS, HEGFL)
Poly [ADP-ribose] polymerase 1	P09874	PARP1 (ADPRT, PPOL)
NF-kappa-B essential modulator	Q9Y6K9	IKBKG (FIP3, NEMO)
Heat shock protein beta-1	P04792	HSPB1 (HSP27, HSP28)
Leptin	P41159	LEP (OB, OBS)
Growth/differentiation factor 2	Q9UK05	GDF2 (BMP9)
Cathepsin L1	P07711	CTSL (CTSL1)
Angiotensin-converting enzyme 2	Q9BYF1	ACE2
Natriuretic peptides B	P16860	NPPB
Macrophage receptor MARCO	Q9UEW3	MARCO (SCARA2)
Osteoclast-associated immunoglobulin-like receptor	Q8IYS5	OSCAR

**Table S3:** Protein targets available from the Olink Target 96 Cardiovascular II panel

## 10. Appendix III: Buffer Preparations

This appendix provides detailed compositions and preparations steps for the buffers used in this study.

### 10.1 Phosphate-Buffered Saline (PBS, 10x, pH 7.4)

Composition:

- 1.37 M NaCl
- 27 mM KCl
- 100 mM Na<sub>2</sub>HPO<sub>4</sub>
- 18 mM KH<sub>2</sub>PO<sub>4</sub>

Preparation:

1. Dissolve NaCl (8.0 g), KCl (0.2 g), Na<sub>2</sub>HPO<sub>4</sub> (1.44 g), and KH<sub>2</sub>PO<sub>4</sub> (0.24 g) in ultrapure water and adjust the pH to 7.4 using HCl or NaOH.
2. Adjust the final volume to 1 L with ultrapure water and dilute into 1:10 with ultrapure water.
3. Store at 4°C.

### 10.2 Tris-Buffered Saline (TBS, 10x, pH 7.6)

Composition:

- 1.5 M NaCl
- 200 mM Tris

Preparation:

1. Dissolve NaCl (88 g), and Tris (24 g) in ultrapure water and adjust the pH to 7.6 using HCl or NaOH.
2. Adjust the final volume to 1 L with distilled water and dilute into 1:10 with ultrapure water.
3. Store at room temperature.

### 10.3 Tris-Buffered Saline, 0.1% Tween-20 (TBST)

Composition:

- 100 mL TBS 10x
- 900 mL distilled water
- 1 mL Tween-20

Preparation:

- Mix all components thoroughly and store at room temperature

#### **10.4 Lysis buffer for Triton-X soluble and insoluble protein aggregates**

Composition:

- 15 mM Tris-HCl pH 7.6
- 250 mM sucrose
- 1 mM MgCl<sub>2</sub>
- 2.5 mM EDTA
- 1mM EGTA
- 20 mM N-ethylmaleimide
- 1% Triton X-100

Preparation:

4. Dissolve all components in 10 mL ultrapure water and mix thoroughly.
5. Make 958 µl aliquots and store at -20°C
6. Add the mixture of proteases and phosphatase inhibitors (5 mM NaF, 10 µM leupeptin, 1.5 µM aprotinin, 0.1 mM Na<sub>3</sub>VO<sub>4</sub> and 1 mM PMSF) freshly before use.

#### **10.5 RIPA Lysis buffer for Western Blot**

Composition:

- 50 mM Tris-HCl pH 7.5
- 150 mM NaCl
- 1 mM EDTA
- 0.5% NP-40

Preparation:

7. Dissolve all components in 10 mL ultrapure water and mix thoroughly.
8. Make 967 µl aliquots and store at -20°C
9. Add 1 mM DTT and the mixture of proteases and phosphatase inhibitors (1 mM NaF, 0.01 mM leupeptin, 1.5 µM aprotinin, 0.1 mM Na<sub>3</sub>VO<sub>4</sub> and 1 mM PMSF) freshly before use.

#### **10.6 Lysis buffer for Olink proteomics**

Composition:

- 50 mM Tris-HCl pH 7.4
- 150 mM NaCl

- 1 mM EDTA
- 1% Triton X-100
- 0.1% deoxycholate

Preparation:

10. Dissolve all components in 10 mL ultrapure water and mix thoroughly.
11. Make 967  $\mu$ l aliquots and store at  $-20^{\circ}\text{C}$
12. Add the mixture of proteases and phosphatase inhibitors (1 mM NaF, 10  $\mu$ M leupeptin, 1.5  $\mu$ M aprotinin, 0.1 mM  $\text{Na}_3\text{VO}_4$  and 1 mM PMSF) freshly before use.

## **11. Acknowledgements**

I would like to express my sincere gratitude to all those who have supported and contributed to the success of this project.

Firstly, I am deeply grateful to my main supervisor, Dr. med. Marco Luciani, for his intellectual and emotional guidance, unwavering motivation, constant encouragement and support throughout my PhD journey. His insights and constructive feedback have been invaluable in shaping the direction of this study. I could not have imagined a better advisor and mentor.

I would also like to thank all of my research colleagues involved in this project for their collaborative efforts, dedication and support in every aspect of the research process. Without their effort, this project would never have been possible.

My deepest gratitude extends to my PhD committee for their invaluable input on this project and for continuous support throughout my PhD.

I extend my sincere gratitude to the University of Zürich and the University Zürich Hospital for providing essential resources for my research. Additionally, I acknowledge the support of the Forschungskredit, Hartmann Müller funding, International Society for Heart Research travel grants, GRC career grant and Swiss Heart Foundation for funding my PhD project and enabling my participation in conferences.

My sincere thanks go also to all members of the CTEC and CMC. Your friendship and unwavering support have created a wonderful working environment. The memories and experiences I have gathered during my time here will always remain cherished.

Last but not least, I would like to acknowledge the endless support of my family, my boyfriend and friends. To mom, dad, P'Peace and Max, your boundless trust, encouragement and understanding have been my source of strength through the most challenging moment of my life. To my dear friends, you have become like my family, filling my life with beautiful memories and helping me overcome homesickness. Special thanks to P'Nes for always sharing me delicious Thai food which has comforted me during the tough time.

Lastly, big thanks to myself for always giving my best and never giving up even when I felt like it.

## 12. References

1. Feigin VL, Stark BA, Johnson CO, et al. Global, regional, and national burden of stroke and its risk factors, 1990–2019: a systematic analysis for the Global Burden of Disease Study 2019. *Lancet Neurol.* 2021;20(10):795-820. doi:10.1016/S1474-4422(21)00252-0
2. Murray CJL, Vos T, Lozano R, et al. Disability-adjusted life years (DALYs) for 291 diseases and injuries in 21 regions, 1990-2010: a systematic analysis for the Global Burden of Disease Study 2010. *Lancet.* 2012;380(9859):2197-2223. doi:10.1016/S0140-6736(12)61689-4
3. Feigin VL, Brainin M, Norrving B, et al. World Stroke Organization (WSO): Global Stroke Fact Sheet 2022. *International Journal of Stroke.* 2022;17(1):18-29. doi:10.1177/17474930211065917
4. Ospel J, Singh N, Ganesh A, Goyal M. Sex and Gender Differences in Stroke and Their Practical Implications in Acute Care. *J Stroke.* 2023;25(1):16-25. doi:10.5853/jos.2022.04077
5. Murphy SJ, Werring DJ. Stroke: causes and clinical features. *Medicine (Abingdon).* 2020;48(9):561. doi:10.1016/J.MPMED.2020.06.002
6. Liu S, Levine SR, Winn R. Targeting ischemic penumbra: part I - from pathophysiology to therapeutic strategy. *J Exp Stroke Transl Med.* 2010;3(1):47. doi:10.6030/1939-067X-3.1.47
7. Moskowitz MA, Lo EH, Iadecola C. The science of stroke: Mechanisms in search of treatments. *Neuron.* 2010;67(2):181-198. doi:10.1016/J.NEURON.2010.07.002/ASSET/BD795236-56FA-490E-B707-E60D99D634AA/MAIN.ASSETS/GR2.JPG
8. Hollist M, Morgan L, Cabatbat R, Au K, Kirmani MF, Kirmani BF. Acute Stroke Management: Overview and Recent Updates. *Aging Dis.* 2021;12(4):1000. doi:10.14336/AD.2021.0311
9. Qin C, Yang S, Chu YH, et al. Signaling pathways involved in ischemic stroke: molecular mechanisms and therapeutic interventions. doi:10.1038/s41392-022-01064-1
10. Bindal P, Kumar V, Kapil L, Singh C, Singh A. Therapeutic management of ischemic stroke. *Naunyn Schmiedebergs Arch Pharmacol.* 2024;397(5):2651-2679. doi:10.1007/s00210-023-02804-y
11. Adams HP, Del Zoppo G, Alberts MJ, et al. Guidelines for the Early Management of Adults With Ischemic Stroke. *Stroke.* 2007;38(5):1655-1711. doi:10.1161/STROKEAHA.107.181486
12. Cui P, Mccullough LD, Hao J. Brain to periphery in acute ischemic stroke: Mechanisms and clinical significance. doi:10.1016/j.yfrne.2021.100932
13. Gallacher KI, Batty GD, McLean G, et al. Stroke, multimorbidity and polypharmacy in a nationally representative sample of 1,424,378 patients in Scotland: implications for treatment burden. *BMC Med.* 2014;12(1):1-9. doi:10.1186/S12916-014-0151-0
14. Yousufuddin M, Bartley AC, Alsawas M, et al. Impact of Multiple Chronic Conditions in Patients Hospitalized with Stroke and Transient Ischemic Attack. *Journal of Stroke and Cerebrovascular Diseases.* 2017;26(6):1239-1248. doi:10.1016/j.jstrokecerebrovasdis.2017.01.015
15. Balch MHH, Nimjee SM, Rink C, Hannawi Y. Beyond the brain: The systemic pathophysiological response to acute ischemic stroke. *J Stroke.* 2020;22(2):159-172. doi:10.5853/jos.2019.02978

16. Gallacher KI, McQueenie R, Nicholl B, Jani BD, Lee D, Mair FS. Risk Factors and Mortality Associated with Multimorbidity in People with Stroke or Transient Ischaemic Attack: A Study of 8,751 UK Biobank Participants. *J Comorb.* 2018;8(1):1. doi:10.15256/JOC.2018.8.129
17. Byer E, Ashman R, Toth LA. Electrocardiograms with large, upright T waves and long Q-T intervals. *Am Heart J.* 1947;33(6):796-806. doi:10.1016/0002-8703(47)90025-2
18. Manea MM, Comsa M, Minca A, Dragos D, Popa C. Brain-heart axis - Review Article. *J Med Life.* 2015;8(3):266. Accessed May 30, 2022. /pmc/articles/PMC4556904/
19. Sposato LA, Lam M, Allen B, Richard L, Shariff SZ, Saposnik G. First-ever ischemic stroke and increased risk of incident heart disease in older adults Is incident stroke associated with increased risk of major adverse cardiovascular events? CME Course. Published online 2020. doi:10.1212/WNL.00000000000009234
20. Thom M, Boldrini M, Bundock E, Sheppard MN, Devinsky O. Review: The past, present and future challenges in epilepsy-related and sudden deaths and biobanking. *Neuropathol Appl Neurobiol.* 2018;44:32-55. doi:10.1111/nan.12453
21. Pelliccia F, Pasceri V, Patti G, et al. Long-Term Prognosis and Outcome Predictors in Takotsubo Syndrome A Systematic Review and Meta-Regression Study. Published online 2019. doi:10.1016/j.jchf.2018.10.009
22. Buckley BJR, Harrison SL, Hill A, Underhill P, Lane DA, Lip GYH. Stroke-Heart Syndrome: Incidence and Clinical Outcomes of Cardiac Complications Following Stroke. *Stroke.* 2022;53(5):1759-1763. doi:10.1161/STROKEAHA.121.037316
23. Wira Iii CR, Rivers E, Martinez-Capolino C, et al. Cardiac Complications in Acute Ischemic Stroke. doi:10.5811/westjem.2011.2.1765
24. Scheitz JF, Nolte CH, Doehner W, Hachinski V, Endres M. Stroke–heart syndrome: clinical presentation and underlying mechanisms. *Lancet Neurol.* 2018;17(12):1109-1120. doi:10.1016/S1474-4422(18)30336-3
25. Scheitz JF, Sposato LA, Schulz-Menger J, Nolte CH, Backs J, Endres M. Stroke–Heart Syndrome: Recent Advances and Challenges. *J Am Heart Assoc.* 2022;11(17):26528. doi:10.1161/JAHA.122.026528
26. Sposato LA, Hilz MJ, Aspberg S, et al. Post-Stroke Cardiovascular Complications and Neurogenic Cardiac Injury: JACC State-of-the-Art Review. *J Am Coll Cardiol.* 2020;76(23):2768-2785. doi:10.1016/J.JACC.2020.10.009
27. Héloïse Kenmogne-Domning G, Kamtchum-Tatuene J, Noumegni SR, Maxime Fokoua-Dongmo C, Zafack JG, Noubiap JJ. Cardiac complications after stroke: protocol for a systematic review and meta-analysis. doi:10.1136/bmjopen-2017-021416
28. Sörös P, Hachinski V. Cardiovascular and neurological causes of sudden death after ischaemic stroke. *Lancet Neurol.* 2012;11(2):179-188. doi:10.1016/S1474-4422(11)70291-5
29. Goldstein DS. The electrocardiogram in stroke: relationship to pathophysiological type and comparison with prior tracings. *Stroke.* 1979;10(3):253-259. doi:10.1161/01.STR.10.3.253
30. Togha M, Sharifpour A, Ashraf H, Moghadam M, Sahraian MA. Electrocardiographic abnormalities in acute cerebrovascular events in patients with/without cardiovascular disease. *Ann Indian Acad Neurol.* 2013;16(1):66. doi:10.4103/0972-2327.107710

31. Villa A, Bacchetta A, Milani O, Omboni E. QT interval prolongation as predictor of early mortality in acute ischemic stroke patients. *Am J Emerg Med.* 2001;19(4):332-333. doi:10.1053/AJEM.2001.24450
32. Ibrahim AA, Mohamed Taha S, Hussien KA, et al. Electrocardiographic Changes and Serum Troponin Levels in Patients with Acute Stroke: A Prospective Cross-Sectional Study Changes and Serum Troponin Levels in Patients with Acute Stroke: A Prospective Cross-Sectional Study. *Ethiop J Health Sci.* 2021;32(3):549. doi:10.4314/ejhs.v32i3
33. Cerasuolo JO, Cipriano LE, Sposato LA. The complexity of atrial fibrillation newly diagnosed after ischemic stroke and transient ischemic attack: Advances and uncertainties. *Curr Opin Neurol.* 2017;30(1):28-37. doi:10.1097/WCO.0000000000000410
34. Migdady I, Russman A, Buletko AB. Atrial Fibrillation and Ischemic Stroke: A Clinical Review. *Semin Neurol.* 2021;41(4):348-364. doi:10.1055/S-0041-1726332/ID/JR200064-16/BIB
35. Sposato LA, Klein FR, Jáuregui A, et al. Newly Diagnosed Atrial Fibrillation after Acute Ischemic Stroke and Transient Ischemic Attack: Importance of Immediate and Prolonged Continuous Cardiac Monitoring. *Journal of Stroke and Cerebrovascular Diseases.* 2012;21(3):210-216. doi:10.1016/J.JSTROKECEREBROVASDIS.2010.06.010
36. Vingerhoets F, Bogouslavsky J, Regli F, Van Melle G. Atrial fibrillation after acute stroke. *Stroke.* 1993;24(1):26-30. doi:10.1161/01.STR.24.1.26
37. Sposato LA, Riccio PM, Hachinski V. Poststroke atrial fibrillation: Cause or consequence?: Critical review of current views. *Neurology.* 2014;82(13):1180-1186. doi:10.1212/WNL.000000000000265/SUPPL\_FILE/SPOSATO\_1180.PDF
38. Wang Y, Qian Y, Smerin D, Zhang S, Zhao Q, Xiong X. Newly Detected Atrial Fibrillation after Acute Stroke: A Narrative Review of Causes and Implications. *Cardiology.* 2019;144(3-4):112-121. doi:10.1159/000502971
39. Siedler G, Sommer K, Macha K, et al. Heart Failure in Ischemic Stroke: Relevance for Acute Care and Outcome. *Stroke.* 2019;50(11):3051-3056. doi:10.1161/STROKEAHA.119.026139
40. Lee M, Oh JH, Lee KB, et al. Clinical and Echocardiographic Characteristics of Acute Cardiac Dysfunction Associated With Acute Brain Hemorrhage – Difference From Takotsubo Cardiomyopathy –. *Circulation Journal.* 2016;80(9):2026-2032. doi:10.1253/CIRCJ.CJ-16-0395
41. Salem R, Vallée F, Dépret F, et al. Subarachnoid hemorrhage induces an early and reversible cardiac injury associated with catecholamine release: One-week follow-up study. *Crit Care.* 2014;18(5):1-10. doi:10.1186/S13054-014-0558-1/FIGURES/2
42. Wrigley P, Houry J, Eckerle B, et al. Prevalence of Positive Troponin and Echocardiogram Findings and Association with Mortality in Acute Ischemic Stroke. *Stroke.* 2017;48(5):1226-1232. doi:10.1161/STROKEAHA.116.014561/FORMAT/EPUB
43. Kim WJ, Nah HW, Kim DH, Cha JK. Association between Left Ventricular Dysfunction and Functional Outcomes at Three Months in Acute Ischemic Stroke. *Journal of Stroke and Cerebrovascular Diseases.* 2016;25(9):2247-2252. doi:10.1016/J.JSTROKECEREBROVASDIS.2016.05.004

44. Park HK, Kim BJ, Yoon CH, Yang MH, Han MK, Bae HJ. Left Ventricular Diastolic Dysfunction in Ischemic Stroke: Functional and Vascular Outcomes. Published online 2016. doi:10.5853/jos.2015.01669
45. Ghadri JR, Wittstein IS, Prasad A, et al. International Expert Consensus Document on Takotsubo Syndrome (Part I): Clinical Characteristics, Diagnostic Criteria, and Pathophysiology. *Eur Heart J*. 2018;39(22):2032. doi:10.1093/EURHEARTJ/EHY076
46. Mori H, Ishikawa S, Kojima S, et al. Increased responsiveness of left ventricular apical myocardium to adrenergic stimuli. *Cardiovasc Res*. 1993;27(2):192-198. doi:10.1093/CVR/27.2.192
47. Templin C, Hänggi J, Klein C, et al. Altered limbic and autonomic processing supports brain-heart axis in Takotsubo syndrome. *Eur Heart J*. 2019;40(15):1183. doi:10.1093/EURHEARTJ/EHZ068
48. Jung JM, Kim JG, Kim J Bin, et al. Takotsubo-like myocardial dysfunction in ischemic stroke: A hospital-based registry and systematic literature review. *Stroke*. 2016;47(11):2729-2736. doi:10.1161/STROKEAHA.116.014304
49. Sudden cardiac death : report of a WHO scientific group [meeting held in Geneva from 24 to 27 October 1984]. Accessed March 29, 2024. <https://iris.who.int/handle/10665/39554>
50. Fineschi V, Michalodimitrakis M, D'Errico S, et al. Insight into stress-induced cardiomyopathy and sudden cardiac death due to stress. A forensic cardio-pathologist point of view. *Forensic Sci Int*. 2010;194(1-3):1-8. doi:10.1016/J.FORSCIINT.2009.10.025
51. Rabinstein AA. Sudden cardiac death. *Handb Clin Neurol*. 2014;119:19-24. doi:10.1016/B978-0-7020-4086-3.00002-3
52. Tokgözoğlu SL, Batur MK, Topçuoğlu MA, Saribas O, Kes S, Oto A. Effects of Stroke Localization on Cardiac Autonomic Balance and Sudden Death. *Stroke*. 1999;30(7):1307-1311. doi:10.1161/01.STR.30.7.1307
53. Powers WJ, Rabinstein AA, Ackerson T, et al. 2018 Guidelines for the Early Management of Patients With Acute Ischemic Stroke: A Guideline for Healthcare Professionals From the American Heart Association/American Stroke Association. *Stroke*. 2018;49(3):e46-e110. doi:10.1161/STR.0000000000000158/FORMAT/EPUB
54. Twerenbold R, Boeddinghaus J, Nestelberger T, et al. Clinical Use of High-Sensitivity Cardiac Troponin in Patients With Suspected Myocardial Infarction. *J Am Coll Cardiol*. 2017;70(8):996-1012. doi:10.1016/J.JACC.2017.07.718
55. Scheitz JF, Mochmann HC, Erdur H, et al. Prognostic relevance of cardiac troponin T levels and their dynamic changes measured with a high-sensitivity assay in acute ischaemic stroke: Analyses from the TRELAS cohort. *Int J Cardiol*. 2014;177(3):886-893. doi:10.1016/J.IJCARD.2014.10.036
56. Krause T, Werner K, Fiebach JB, et al. Stroke in right dorsal anterior insular cortex Is related to myocardial injury. *Ann Neurol*. 2017;81(4):502-511. doi:10.1002/ANA.24906
57. Thygesen K, Alpert JS, Jaffe AS, et al. Fourth Universal Definition of Myocardial Infarction (2018). *Circulation*. 2018;138(20):e618-e651. doi:10.1161/CIR.0000000000000617

58. Yip HK, Sun CK, Chang LT, Chen MC, Liou CW. Time Course and Prognostic Value of Plasma Levels of N-Terminal Pro-Brain Natriuretic Peptide in Patients After Ischemic Stroke. *Circulation Journal*. 2006;70(4):447-452.
59. Etgen T, Baum H, Sander K, Sander D. Cardiac Troponins and N-Terminal Pro-Brain Natriuretic Peptide in Acute Ischemic Stroke Do Not Relate to Clinical Prognosis. *Stroke*. 2005;36(2):270-275. doi:10.1161/01.STR.0000151364.19066.A1
60. Giannakoulas G, Hatzitolios A, Karvounis H, et al. N-Terminal Pro-Brain Natriuretic Peptide Levels Are Elevated in Patients with Acute Ischemic Stroke. <http://dx.doi.org/10.1177/000331970505600610>. 2005;56(6):723-730. doi:10.1177/000331970505600610
61. Bunevicius A, Kazlauskas H, Raskauskiene N, et al. Role of N-Terminal Pro-B-Type Natriuretic Peptide, High-Sensitivity C-Reactive Protein, and Interleukin-6 in Predicting a Poor Outcome after a Stroke. *Neuroimmunomodulation*. 2015;22(6):365-372. doi:10.1159/000381218
62. Chen Z, Venkat P, Seyfried D, Chopp M, Yan T, Chen J. Brain-Heart Interaction: Cardiac Complications after Stroke. *Circ Res*. 2017;121(4):451-468. doi:10.1161/CIRCRESAHA.117.311170
63. Chen Z, Venkat P, Seyfried D, Chopp M, Yan T, Chen J. Brain-heart interaction: cardiac complications after stroke. *Circ Res*. 2017;121(4):451. doi:10.1161/CIRCRESAHA.117.311170
64. Dorrance AM, Fink G. Effects of stroke on the autonomic nervous system. *Compr Physiol*. 2015;5(3):1241-1263. doi:10.1002/CPHY.C140016
65. Nayani S, Sreedharan SE, Namboodiri N, Sarma PS, Sylaja PN. Autonomic dysfunction in first ever ischemic stroke: Prevalence, predictors and short term neurovascular outcome. *Clin Neurol Neurosurg*. 2016;150:54-58. doi:10.1016/J.CLINEURO.2016.08.022
66. De Raedt S, De Vos A, De Keyser J. Autonomic dysfunction in acute ischemic stroke: An underexplored therapeutic area? *J Neurol Sci*. 2015;348(1-2):24-34. doi:10.1016/J.JNS.2014.12.007
67. ESTIMATION OF MYOCARDIAL INTERSTITIAL NOREPINEPHRINE RELEASE... : Transplantation. Accessed March 29, 2024. [https://journals.lww.com/transplantjournal/abstract/1994/02150/estimation\\_of\\_myocardial\\_interstitial.10.aspx](https://journals.lww.com/transplantjournal/abstract/1994/02150/estimation_of_myocardial_interstitial.10.aspx)
68. Hachinski VC, Smith KE, Silver MD, Gibson CJ, Ciriello J. Acute myocardial and plasma catecholamine changes in experimental stroke. *Stroke*. 1986;17(3):387-390. doi:10.1161/01.STR.17.3.387
69. Saini HK, Tripathi ON, Zhang S, Elimban V, Dhalla NS. Involvement of Na<sup>+</sup>/Ca<sup>2+</sup> exchanger in catecholamine-induced increase in intracellular calcium in cardiomyocytes. *Am J Physiol Heart Circ Physiol*. 2006;290(1):373-380. doi:10.1152/AJPHEART.00613.2005/ASSET/IMAGES/LARGE/ZH40010664080006.JPEG
70. Du Y, Demillard LJ, Ren J. Catecholamine-induced cardiotoxicity: A critical element in the pathophysiology of stroke-induced heart injury. *Life Sci*. 2021;287:120106. doi:10.1016/J.LFS.2021.120106
71. Sörös P, Hachinski V, Sörös P, Hachinski V. *Cardiovascular and Neurological Causes of Sudden Death after Ischaemic Stroke*. Vol 11.; 2012. <http://www.qtdrugs.org>

72. Cheshire WP, Saper CB. The insular cortex and cardiac response to stroke. *Neurology*. 2006;66(9):1296-1297. doi:10.1212/01.WNL.0000219563.87204.7D
73. Ozdemir O, Hachinski V. Brain lateralization and sudden death: Its role in the neurogenic heart syndrome. *J Neurol Sci*. 2008;268(1-2):6-11. doi:10.1016/J.JNS.2007.11.009
74. Tokgözoğlu SL, Batur MK, Topçuoğlu MA, Saribas O, Kes S, Oto A. Effects of Stroke Localization on Cardiac Autonomic Balance and Sudden Death. *Stroke*. 1999;30(7):1307-1311. doi:10.1161/01.STR.30.7.1307
75. Hunt D, Gore I. Myocardial lesions following experimental intracranial hemorrhage: Prevention with propranolol. *Am Heart J*. 1972;83(2):232-236. doi:10.1016/0002-8703(72)90142-1
76. Savitz SI, Erhardt JA, Anthony J V., et al. The novel  $\beta$ -blocker, carvedilol, provides neuroprotection in transient focal stroke. *Journal of Cerebral Blood Flow and Metabolism*. 2000;20(8):1197-1204. doi:10.1097/00004647-200008000-00005/FORMAT/EPUB
77. Smith SM, Vale WW. The role of the hypothalamic-pituitary-adrenal axis in neuroendocrine responses to stress. *Dialogues Clin Neurosci*. 2006;8:383-395. Accessed March 31, 2024. www.dialogues-cns.org
78. Kageyama K, Iwasaki Y, Daimon M. Hypothalamic regulation of corticotropin-releasing factor under stress and stress resilience. *Int J Mol Sci*. 2021;22(22). doi:10.3390/ijms222212242
79. Olsson T, Åström M, Eriksson S, Forssell Å. Hypercortisolism revealed by the dexamethasone suppression test with acute ischemic stroke. *Stroke*. 1989;20(12):1685-1690. doi:10.1161/01.STR.20.12.1685
80. Fassbender K, Schmidt R, Mößner R, Daffertshofer M, Hennerici M. Pattern of activation of the hypothalamic-pituitary-adrenal axis in acute stroke: Relation to acute confusional state, extent of brain damage, and clinical outcome. *Stroke*. 1994;25(6):1105-1108. doi:10.1161/01.STR.25.6.1105
81. Christensen H, Boysen G, Johannesen HH. Serum-cortisol reflects severity and mortality in acute stroke. *J Neurol Sci*. 2004;217(2):175-180. doi:10.1016/J.JNS.2003.09.013
82. Gulyaeva N V., Onufriev M V., Moiseeva Y V. Ischemic Stroke, Glucocorticoids, and Remote Hippocampal Damage: A Translational Outlook and Implications for Modeling. *Front Neurosci*. 2021;15. doi:10.3389/fnins.2021.781964
83. Melville KI, Shister HE, Silver MD, Montreal C. *Experimental' Studies Cardiac Ischemic Changes and Arrhythmias Induced by Hypothalamic Stimulation\**.
84. O'Connell GC, Walsh KB, Burrage E, Adeoye O, Chantler PD, Barr TL. Translational and Precision Medicine: High-throughput profiling of the circulating proteome suggests sexually dimorphic corticosteroid signaling following ischemic stroke. *Physiol Genomics*. 2018;50(10):876. doi:10.1152/PHYSIOLGENOMICS.00058.2018
85. Doll DN, Barr TL, Simpkins JW. Cytokines: Their Role in Stroke and Potential Use as Biomarkers and Therapeutic Targets. *Aging Dis*. 2014;5(5):294. doi:10.14336/AD.2014.0500294
86. Simats A, Liesz A. Systemic inflammation after stroke: implications for post-stroke comorbidities. *EMBO Mol Med*. 2022;14(9). doi:10.15252/emmm.202216269

87. Yang C, Hawkins KE, Doré S, Candelario-Jalil XE. Neuroinflammatory mechanisms of blood-brain barrier damage in ischemic stroke. *Am J Physiol Cell Physiol*. 2019;316:135-153. doi:10.1152/ajp
88. Liu P, Prabhu SD. Cytokine-Induced Modulation of Cardiac Function. *Circ Res*. 2004;95(12):1140-1153. doi:10.1161/01.RES.0000150734.79804.92
89. Mann DL. Innate immunity and the failing heart: The cytokine hypothesis revisited. *Circ Res*. 2015;116(7):1254-1268. doi:10.1161/CIRCRESAHA.116.302317/-/DC1
90. Boltze J, Ochoa-Reparaz J, He Y, et al. Gut Microbiota in Acute Ischemic Stroke: From Pathophysiology to Therapeutic Implications. *Frontiers in Neurology* | [www.frontiersin.org](http://www.frontiersin.org). 2020;1:598. doi:10.3389/fneur.2020.00598
91. Singh V, Roth S, Llovera G, et al. Neurobiology of Disease Microbiota Dysbiosis Controls the Neuroinflammatory Response after Stroke. Published online 2016. doi:10.1523/JNEUROSCI.1114-16.2016
92. Wen Wen S, Y Wong CH. An unexplored brain-gut microbiota axis in stroke. *Gut Microbes*. 2017;8. doi:10.1080/19490976.2017.1344809
93. Nam HS. Gut Microbiota and Ischemic Stroke: The Role of Trimethylamine N-Oxide. *J Stroke*. 2019;21(2):151-159. doi:10.5853/JOS.2019.00472
94. Wang Z, Klipfell E, Bennett BJ, et al. Gut flora metabolism of phosphatidylcholine promotes cardiovascular disease. *Nature*. 2011;472(7341):57. doi:10.1038/NATURE09922
95. Zhu W, Gregory JC, Org E, et al. Gut Microbial Metabolite TMAO Enhances Platelet Hyperreactivity and Thrombosis Risk. *Cell*. 2016;165(1):111-124. doi:10.1016/J.CELL.2016.02.011
96. Li X jin, You X yu, Wang C ying, et al. Bidirectional Brain-gut-microbiota Axis in increased intestinal permeability induced by central nervous system injury. *CNS Neurosci Ther*. 2020;26(8):783-790. doi:10.1111/cns.13401
97. Lundström A, Fariborz Mobarrez &, Rooth E, et al. Prognostic Value of Circulating Microvesicle Subpopulations in Ischemic Stroke and TIA. doi:10.1007/s12975-019-00777-w
98. Schrick D, Molnár T, Tókécs-Füzesi M, Molnár A, Ezer E. Circulating Microvesicles in Convalescent Ischemic Stroke Patients: A Contributor to High-On-Treatment Residual Platelet Reactivity? *Frontiers in Bioscience - Landmark*. 2022;27(5):158. doi:10.31083/J.FBL2705158
99. Huo S, Kränkel N, Heinrich Nave A, et al. Endothelial and Leukocyte-Derived Microvesicles and Cardiovascular Risk After Stroke PROSCIS-B Class of Evidence Criteria for rating therapeutic and diagnostic studies. Published online 2020. doi:10.1212/WNL.00000000000011223
100. Schoch B, Regel JP, Wichert M, Gasser T, Volbracht L, Stolke D. Analysis of intrathecal interleukin-6 as a potential predictive factor for vasospasm in subarachnoid hemorrhage. *Neurosurgery*. 2007;60(5):828-835. doi:10.1227/01.NEU.0000255440.21495.80
101. Sinauridze EI, Kireev DA, Popenko NY, et al. Platelet microparticle membranes have 50- to 100-fold higher specific procoagulant activity than activated platelets. *Thromb Haemost*. 2007;97(3):425-434. doi:10.1160/TH06-06-0313
102. Porro C, Trotta T, Panaro MA. Microvesicles in the brain: Biomarker, messenger or mediator? Published online 2015. doi:10.1016/j.jneuroim.2015.09.006

103. Zhao Z, Wang M, Tian Y, et al. Cardiolipin-mediated procoagulant activity of mitochondria contributes to traumatic brain injury–associated coagulopathy in mice. *Blood*. 2016;127(22):2763. doi:10.1182/BLOOD-2015-12-688838
104. Wang S, Aurora AB, Johnson BA, et al. The Endothelial-Specific MicroRNA miR-126 Governs Vascular Integrity and Angiogenesis. *Dev Cell*. 2008;15(2):261-271. doi:10.1016/J.DEVCEL.2008.07.002
105. Chen J, Cui C, Yang X, et al. MiR-126 Affects Brain-Heart Interaction after Cerebral Ischemic Stroke. *Transl Stroke Res*. 2017;8(4):374-385. doi:10.1007/s12975-017-0520-z
106. Jia L, Hao F, Wang W, Qu Y. Circulating miR-145 is associated with plasma high-sensitivity C-reactive protein in acute ischemic stroke patients. *Cell Biochem Funct*. 2015;33(5):314-319. doi:10.1002/CBF.3116
107. Ashraf GM, Greig NH, Khan TA, et al. Protein misfolding and aggregation in Alzheimer’s disease and Type 2 Diabetes Mellitus. *CNS Neurol Disord Drug Targets*. 2014;13(7):1280. doi:10.2174/1871527313666140917095514
108. Wu S, Du L. Protein Aggregation in the Pathogenesis of Ischemic Stroke. *Cell Mol Neurobiol*. 2021;41:1183-1194. doi:10.1007/s10571-020-00899-y
109. Ge P, Luo Y, Liu CL, Hu B. Protein Aggregation and Proteasome Dysfunction After Brain Ischemia. *Stroke*. 2007;38(12):3230-3236. doi:10.1161/STROKEAHA.107.487108
110. Knowles TPJ, Vendruscolo M, Dobson CM. The amyloid state and its association with protein misfolding diseases. *Nat Rev Mol Cell Biol*. 2014;15(6):384-396. doi:10.1038/nrm3810
111. Chiti F, Dobson CM. Protein Misfolding, Amyloid Formation, and Human Disease: A Summary of Progress Over the Last Decade. *Annu Rev Biochem*. 2017;86(1):27-68. doi:10.1146/annurev-biochem-061516-045115
112. Ishimaru D, Andrade LR, Teixeira LSP, et al. Fibrillar Aggregates of the Tumor Suppressor p53 Core Domain †. Published online 2003. doi:10.1021/bi034218k
113. Koga H, Kaushik S, Cuervo AM. Protein homeostasis and aging: The importance of exquisite quality control. *Ageing Res Rev*. 2011;10(2):205-215. doi:10.1016/j.arr.2010.02.001
114. Dobson CM. Protein folding and misfolding. *Nature* 2003 426:6968. 2003;426(6968):884-890. doi:10.1038/nature02261
115. Ponomarenko EA, Poverennaya E V, Ilgisonis E V, et al. The Size of the Human Proteome: The Width and Depth. Published online 2016. doi:10.1155/2016/7436849
116. Hartl FU, Bracher A, Hayer-Hartl M. Molecular chaperones in protein folding and proteostasis. *Nature*. 2011;475(7356):324-332. doi:10.1038/nature10317
117. Douglas PM, Cyr DM. Review Interplay Between Protein Homeostasis Networks in Protein Aggregation and Proteotoxicity. Published online 2009. doi:10.1002/bip.21304
118. Labbadia J, Morimoto RI. The Biology of Proteostasis in Aging and Disease. doi:10.1146/annurev-biochem-060614-033955
119. Chen B, Retzlaff M, Roos T, Frydman J. Cellular Strategies of Protein Quality Control. *Cold Spring Harb Perspect Biol*. 2011;3(8):1-14. doi:10.1101/CSHPERSPECT.A004374

120. Kim YE, Hipp MS, Bracher A, Hayer-Hartl M, Ulrich Hartl F. Molecular Chaperone Functions in Protein Folding and Proteostasis. <https://doi.org/10.1146/annurev-biochem-060208-092442>. 2013;82:323-355. doi:10.1146/ANNUREV-BIOCHEM-060208-092442
121. Hetz C, Zhang K, Kaufman RJ. Mechanisms, regulation and functions of the unfolded protein response. *Nat Rev Mol Cell Biol.* 2020;21(8):421-438. doi:10.1038/s41580-020-0250-z
122. Glembotski CC. Endoplasmic reticulum stress in the heart. *Circ Res.* 2007;101(10):975-984. doi:10.1161/CIRCRESAHA.107.161273
123. Wang S, Binder P, Fang Q, et al. Endoplasmic reticulum stress in the heart: insights into mechanisms and drug targets. *Br J Pharmacol.* 2018;175(8):1293-1304. doi:10.1111/bph.13888
124. Naidoo N. ER and aging-Protein folding and the ER stress response. *Ageing Res Rev.* 2009;8(3):150-159. doi:10.1016/j.arr.2009.03.001
125. Ciechanover A, Kwon YT ae. Degradation of misfolded proteins in neurodegenerative diseases: therapeutic targets and strategies. *Exp Mol Med.* 2015;47(3):e147. doi:10.1038/emm.2014.117
126. Vilchez D, Saez I, Dillin A. The role of protein clearance mechanisms in organismal ageing and age-related diseases. *Nature Communications 2014 5:1.* 2014;5(1):1-13. doi:10.1038/ncomms6659
127. Dantuma NP, Lindsten K. SPOTLIGHT REVIEW Stressing the ubiquitin-proteasome system. doi:10.1093/cvr/cvp255
128. Brodsky and, Travers KJ, Patil CK, et al. Functional and Genomic Analyses Reveal an Essential Coordination between the Unfolded Protein Response and ER-Associated Degradation ERAD requires a number of dedi-cated ER-resident factors, including the proteins Der1p, Der3p/Hrd1p, and Hrd3p (Hampton et al ERAD substrates pass. *Cell.* 2000;101:249-258. Accessed July 14, 2024. <http://www.cell.com/cgi/content/full/101/3/249/DC1>.
129. Wang X, Robbins J. Proteasomal and Lysosomal Protein Degradation and Heart Disease. *J Mol Cell Cardiol.* 2013;0:16. doi:10.1016/J.YJMCC.2013.11.006
130. Diteepeng T, del Monte F, Luciani M. The long and winding road to target protein misfolding in cardiovascular diseases. *Eur J Clin Invest.* 2021;51(5). doi:10.1111/eci.13504
131. Herczenik E, Gebbink MFBG. Molecular and cellular aspects of protein misfolding and disease. *The FASEB Journal.* 2008;22(7):2115-2133. doi:10.1096/fj.07-099671
132. Sipe JD, Cohen AS. Review: History of the amyloid fibril. *J Struct Biol.* 2000;130(2-3):88-98. doi:10.1006/jsbi.2000.4221
133. Buxbaum JN, Dispenzieri A, Eisenberg DS, et al. Amyloid nomenclature 2022: update, novel proteins, and recommendations by the International Society of Amyloidosis (ISA) Nomenclature Committee. *Amyloid.* 2022;29(4):213-219. doi:10.1080/13506129.2022.2147636
134. Ross CA, Poirier MA. Protein aggregation and neurodegenerative disease. *Nat Med.* 2004;10(7):S10. doi:10.1038/NM1066
135. Verma M, Vats A, Taneja V. Toxic species in amyloid disorders: Oligomers or mature fibrils. *Ann Indian Acad Neurol.* 2015;18(2):138-145. doi:10.4103/0972-2327.144284

136. Bucciantini M, Giannoni E, Chiti F, et al. *Inherent Toxicity of Aggregates Implies a Common Mechanism for Protein Misfolding Diseases.*; 2002. [www.nature.com](http://www.nature.com)
137. Conway KA, Lee SJ, Rochet JC, Ding TT, Williamson RE, Lansbury PT. Acceleration of oligomerization, not fibrillization, is a shared property of both  $\alpha$ -synuclein mutations linked to early-onset Parkinson's disease: Implications for pathogenesis and therapy. *Proc Natl Acad Sci U S A.* 2000;97(2):571. doi:10.1073/PNAS.97.2.571
138. Haass C, Selkoe DJ. Soluble protein oligomers in neurodegeneration: Lessons from the Alzheimer's amyloid  $\beta$ -peptide. *Nat Rev Mol Cell Biol.* 2007;8(2):101-112. doi:10.1038/nrm2101
139. Diociaiuti M, Bonanni R, Cariati I, Frank C, D'arcangelo G. Amyloid Prefibrillar Oligomers: The Surprising Commonalities in Their Structure and Activity. *Int J Mol Sci.* 2021;22(12). doi:10.3390/IJMS22126435
140. Gandy S, Simon AJ, Steele JW, et al. Days to criterion as an indicator of toxicity associated with human Alzheimer amyloid- $\beta$  oligomers. *Ann Neurol.* 2010;68(2):220-230. doi:10.1002/ANA.22052
141. Pattison JS, Sanbe A, Maloyan A, Osinska H, Klevitsky R, Robbins J. Cardiomyocyte expression of a polyglutamine preamyloid oligomer causes heart failure. *Circulation.* 2008;117(21):2743-2751. doi:10.1161/CIRCULATIONAHA.107.750232
142. Denny RA, Gavrin LK, Saiah E. Recent developments in targeting protein misfolding diseases. *Bioorg Med Chem Lett.* 2013;23(7):1935-1944. doi:10.1016/j.bmcl.2013.01.089
143. Kaye R, Head E, Thompson JL, et al. Common structure of soluble amyloid oligomers implies common mechanism of pathogenesis. *Science (1979).* 2003;300(5618):486-489. doi:10.1126/SCIENCE.1079469/SUPPL\_FILE/KAYED.SOM.PDF
144. Lambert MP, Barlow AK, Chromy BA, et al. Diffusible, nonfibrillar ligands derived from A $\beta$ 1-42 are potent central nervous system neurotoxins. *Proc Natl Acad Sci U S A.* 1998;95(11):6448-6453. doi:10.1073/PNAS.95.11.6448/ASSET/D2009379-CA04-49AC-AF86-501F246A174A/ASSETS/GRAPHIC/PQ1082409005.JPEG
145. Sengupta U, Nilson AN, Kaye R. The Role of Amyloid- $\beta$  Oligomers in Toxicity, Propagation, and Immunotherapy. *EBioMedicine.* 2016;6:42. doi:10.1016/J.EBIOM.2016.03.035
146. Chiti F, Dobson CM. Protein Misfolding, Amyloid Formation, and Human Disease: A Summary of Progress Over the Last Decade. *Annu Rev Biochem.* 2017;86(1):27-68. doi:10.1146/annurev-biochem-061516-045115
147. Stefani M. Biochemical and biophysical features of both oligomer/fibril and cell membrane in amyloid cytotoxicity. *FEBS J.* 2010;277(22):4602-4613. doi:10.1111/J.1742-4658.2010.07889.X
148. Rinauro DJ, Chiti F, Vendruscolo M, Limbocker R. Misfolded protein oligomers: mechanisms of formation, cytotoxic effects, and pharmacological approaches against protein misfolding diseases. *Mol Neurodegener.* 2024;19(1). doi:10.1186/s13024-023-00651-2
149. Ghio S, Camilleri A, Caruana M, et al. Cardiolipin Promotes Pore-Forming Activity of Alpha-Synuclein Oligomers in Mitochondrial Membranes. *ACS Chem Neurosci.* 2019;10(8):3815-3829. doi:10.1021/ACSCHEMNEURO.9B00320/SUPPL\_FILE/CN9B00320\_SI\_001.PDF

150. Cheignon C, Tomas M, Bonnefont-Rousselot D, Faller P, Hureau C, Collin F. Oxidative stress and the amyloid beta peptide in Alzheimer's disease. *Redox Biol.* 2018;14:450-464. doi:10.1016/J.REDOX.2017.10.014
151. Angelova PR, Choi ML, Berezhnov A V., et al. Alpha synuclein aggregation drives ferroptosis: an interplay of iron, calcium and lipid peroxidation. *Cell Death Differ.* 2020;27(10):2781. doi:10.1038/S41418-020-0542-Z
152. Greenough MA, Camakaris J, Bush AI. Metal dyshomeostasis and oxidative stress in Alzheimer's disease. *Neurochem Int.* 2013;62(5):540-555. doi:10.1016/J.NEUINT.2012.08.014
153. Salminen A, Ojala J, Kauppinen A, Kaarniranta K, Suuronen T. Inflammation in Alzheimer's disease: Amyloid- $\beta$  oligomers trigger innate immunity defence via pattern recognition receptors. *Prog Neurobiol.* 2009;87(3):181-194. doi:10.1016/J.PNEUROBIO.2009.01.001
154. Benilova I, Karran E, De Strooper B. The toxic A $\beta$  oligomer and Alzheimer's disease: An emperor in need of clothes. *Nat Neurosci.* 2012;15(3):349-357. doi:10.1038/nn.3028
155. Evangelisti E, Cecchi C, Cascella R, et al. Membrane lipid composition and its physicochemical properties define cell vulnerability to aberrant protein oligomers. *J Cell Sci.* 2012;125(10):2416-2427. doi:10.1242/JCS.098434/258430/AM/MEMBRANE-LIPID-COMPOSITION-AND-ITS-PHYSICOCHEMICAL
156. Kulenkampff K, Wolf Perez AM, Sormanni P, Habchi J, Vendruscolo M. Quantifying misfolded protein oligomers as drug targets and biomarkers in Alzheimer and Parkinson diseases. *Nature Reviews Chemistry* 2021 5:4. 2021;5(4):277-294. doi:10.1038/s41570-021-00254-9
157. Morales R, Moreno-Gonzalez I, Soto C. Cross-Seeding of Misfolded Proteins: Implications for Etiology and Pathogenesis of Protein Misfolding Diseases. *PLoS Pathog.* 2013;9(9):e1003537. doi:10.1371/JOURNAL.PPAT.1003537
158. Soto C, Pritzkow S. Protein misfolding, aggregation, and conformational strains in neurodegenerative diseases. *Nat Neurosci.* 2018;21(10):1332-1340. doi:10.1038/s41593-018-0235-9
159. Domert J, Rao SB, Agholme L, et al. Spreading of amyloid- $\beta$  peptides via neuritic cell-to-cell transfer is dependent on insufficient cellular clearance. *Neurobiol Dis.* 2014;65:82-92. doi:10.1016/j.nbd.2013.12.019
160. Lim YJ, Lee SJ. Are exosomes the vehicle for protein aggregate propagation in neurodegenerative diseases? *Acta Neuropathol Commun.* 2017;5(1):64. doi:10.1186/s40478-017-0467-z
161. Gibbons GS, Lee VMY, Trojanowski JQ. Mechanisms of Cell-to-Cell Transmission of Pathological Tau: A Review. *JAMA Neurol.* 2019;76(1):101-108. doi:10.1001/JAMANEUROL.2018.2505
162. Costanzo M, Zurzolo C. The cell biology of prion-like spread of protein aggregates: mechanisms and implication in neurodegeneration. *Biochemical Journal.* 2013;452(1):1-17. doi:10.1042/BJ20121898
163. Wang MJ, Yi S, Han JY, et al. Oligomeric forms of amyloid- $\beta$  protein in plasma as a potential blood-based biomarker for Alzheimer's disease. *Alzheimers Res Ther.* 2017;9(1):1-10. doi:10.1186/S13195-017-0324-0/FIGURES/4

164. De S, Whiten DR, Ruggeri FS, et al. Soluble aggregates present in cerebrospinal fluid change in size and mechanism of toxicity during Alzheimer's disease progression. *Acta Neuropathol Commun.* 2019;7(1):120. doi:10.1186/S40478-019-0777-4/FIGURES/4
165. Guo JL, Lee VMY. Cell-to-cell transmission of pathogenic proteins in neurodegenerative diseases. *Nature Medicine* 2014 20:2. 2014;20(2):130-138. doi:10.1038/nm.3457
166. Ruberg FL, Berk JL. Transthyretin (TTR) Cardiac Amyloidosis. *Circulation.* 2012;126(10):1286. doi:10.1161/CIRCULATIONAHA.111.078915
167. Troncone L, Luciani M, Coggins M, et al. A $\beta$  Amyloid Pathology Affects the Hearts of Patients With Alzheimer's Disease. *J Am Coll Cardiol.* 2016;68(22):2395-2407. doi:10.1016/j.jacc.2016.08.073
168. Luciani M, Montalbano M, Troncone L, et al. Big tau aggregation disrupts microtubule tyrosination and causes myocardial diastolic dysfunction: from discovery to therapy. *Eur Heart J.* 2023;44(17):1560-1570. doi:10.1093/eurheartj/ehad205
169. Zhu F, Wolters FJ, Yaqub A, et al. Plasma Amyloid- $\beta$  in Relation to Cardiac Function and Risk of Heart Failure in General Population. *JACC Heart Fail.* 2023;11(1):93-102. doi:10.1016/J.JCHF.2022.09.006
170. Kahl A, Blanco I, Jackman K, et al. Cerebral ischemia induces the aggregation of proteins linked to neurodegenerative diseases. *Sci Rep.* 2018;8(1):2701. doi:10.1038/s41598-018-21063-z
171. Cao Z, Jia Y, Zhu B. BNP and NT-proBNP as diagnostic biomarkers for cardiac dysfunction in both clinical and forensic medicine. *Int J Mol Sci.* 2019;20(8):18-20. doi:10.3390/ijms20081820
172. Battaglini D, Robba C, Lopes Da Silva A, et al. Brain-heart interaction after acute ischemic stroke. *Crit Care.* 2020;24(1):163. doi:10.1186/s13054-020-02885-8
173. Hampel H, Hardy J, Blennow K, et al. The Amyloid- $\beta$  Pathway in Alzheimer's Disease. *Molecular Psychiatry* 2021 26:10. 2021;26(10):5481-5503. doi:10.1038/s41380-021-01249-0
174. Bernini F, Malferrari D, Pignataro M, et al. Pre-amyloid oligomers budding: a metastatic mechanism of proteotoxicity. *Nature Publishing Group.* Published online 2016. doi:10.1038/srep35865
175. Esparza TJ, Wildburger NC, Jiang H, et al. Soluble Amyloid-beta Aggregates from Human Alzheimer's Disease Brains. *Scientific Reports* 2016 6:1. 2016;6(1):1-16. doi:10.1038/srep38187
176. Su H, Wang X. The ubiquitin-proteasome system in cardiac proteinopathy: A quality control perspective. *Cardiovasc Res.* 2010;85(2):253-262. doi:10.1093/cvr/cvp287
177. Hanna J, Leggett DS, Finley D. Ubiquitin Depletion as a Key Mediator of Toxicity by Translational Inhibitors. *Mol Cell Biol.* 2003;23(24):9251-9261. doi:10.1128/MCB.23.24.9251-9261.2003
178. Wu S, Du L. Protein Aggregation in the Pathogenesis of Ischemic Stroke. *Cell Mol Neurobiol.* 2021;41(6):1183-1194. doi:10.1007/S10571-020-00899-Y/FIGURES/1
179. Hochrainer K, Jackman K, Anrather J, Iadecola C. Reperfusion rather than ischemia drives the formation of ubiquitin aggregates after middle cerebral artery occlusion. *Stroke.* 2012;43(8):2229-2235. doi:10.1161/STROKEAHA.112.650416

180. Wang SM, Kang DW, Um YH, et al. Plasma oligomer beta-amyloid is associated with disease severity and cerebral amyloid deposition in Alzheimer's disease spectrum. *Alzheimers Res Ther.* 2024;16(1):1-11. doi:10.1186/S13195-024-01400-3/FIGURES/5
181. Veltkamp R, Uhlmann S, Marinescu M, et al. Experimental ischaemic stroke induces transient cardiac atrophy and dysfunction. Published online 2018. doi:10.1002/jcsm.12335
182. Kallmünzer B, Breuer L, Kahl N, et al. Serious cardiac arrhythmias after stroke: Incidence, time course, and predictors-a systematic, prospective analysis. *Stroke.* 2012;43(11):2892-2897. doi:10.1161/STROKEAHA.112.664318/ASSET/EB4CEFE9-73EE-4461-81AE-A54A6C7E830B/ASSETS/GRAPHIC/2892FIG02.JPEG
183. Oppenheimer SM, Gelb A, Girvin JP, Hachinski VC. *The Johns Hopkins Hospital, 600 North Wolfe Street.* Vol 42.; 1992. <https://www.neurology.org>
184. Lubjuhn J, Gastens A, von Wilpert G, et al. Functional testing in a mouse stroke model induced by occlusion of the distal middle cerebral artery. *J Neurosci Methods.* 2009;184(1):95-103. doi:10.1016/J.JNEUMETH.2009.07.029
185. Oppenheimer SM, Cechetto DF. Cardiac chronotropic organization of the rat insular cortex. *Brain Res.* 1990;533(1):66-72. doi:10.1016/0006-8993(90)91796-J
186. Vornholz L, Nienhaus F, Gliem M, et al. Acute Heart Failure After Reperfused Ischemic Stroke: Association With Systemic and Cardiac Inflammatory Responses. *Front Physiol.* 2021;12:782760. doi:10.3389/FPHYS.2021.782760/FULL
187. Hilz MJ, Dütsch M, Perrine K, Nelson PK, Rauhut U, Devinsky O. Hemispheric influence on autonomic modulation and baroreflex sensitivity. *Ann Neurol.* 2001;49(5):575-584. doi:10.1002/ANA.1006
188. Sposato LA, Chaturvedi S, Hsieh CY, Morillo CA, Kamel H. Atrial Fibrillation Detected after Stroke and Transient Ischemic Attack: A Novel Clinical Concept Challenging Current Views. *Stroke.* 2022;53(2):E94-E103. doi:10.1161/STROKEAHA.121.034777/SUPPL\_FILE/STR\_STROKE-2021-034777\_SUPP2.PDF
189. Goldberger JJ, Arora R, Buckley U, Shivkumar K. Autonomic Nervous System Dysfunction: JACC Focus Seminar. *J Am Coll Cardiol.* 2019;73(10):1189-1206. doi:10.1016/J.JACC.2018.12.064
190. Vornholz L, Nienhaus F, Gliem M, et al. Acute Heart Failure After Reperfused Ischemic Stroke: Association With Systemic and Cardiac Inflammatory Responses. *Front Physiol.* 2021;12. doi:10.3389/FPHYS.2021.782760
191. Buckley U, Shivkumar K. Stress-induced cardiac arrhythmias: The heart-brain interaction. *Trends Cardiovasc Med.* 2015;26(1):78. doi:10.1016/J.TCM.2015.05.001
192. Vaseghi M, Shivkumar K. The Role of the Autonomic Nervous System in Sudden Cardiac Death. *Prog Cardiovasc Dis.* 2008;50(6):404. doi:10.1016/J.PCAD.2008.01.003
193. Bieber M, Werner RA, Tanai E, et al. Stroke-induced chronic systolic dysfunction driven by sympathetic overactivity. *Ann Neurol.* 2017;82(5):729-743. doi:10.1002/ana.25073
194. Kerkelä R, Ulvila J, Magga J. Natriuretic Peptides in the Regulation of Cardiovascular Physiology and Metabolic Events. *Journal of the American Heart Association: Cardiovascular and Cerebrovascular Disease.* 2015;4(10):2423. doi:10.1161/JAHA.115.002423

195. Scherbakov N, Dirnagl U, Doehner W. Body weight after stroke lessons from the obesity paradox. *Stroke*. 2011; 42(12):3646-3650. doi:10.1161/STROKEAHA.111.619163/ASSET/FF3A6C86-4D48-4261-9720-C2F94570850E/ASSETS/GRAPHIC/ZHS0121162480002.JPEG
196. Haley MJ, Mullard G, Hollywood KA, Cooper GJ, Dunn WB, Lawrence CB. Adipose tissue and metabolic and inflammatory responses to stroke are altered in obese mice. *Dis Model Mech*. 2017;10(10):1229. doi:10.1242/DMM.030411
197. Haley MJ, White CS, Roberts D, et al. Stroke Induces Prolonged Changes in Lipid Metabolism, the Liver and Body Composition in Mice. *Transl Stroke Res*. 2020;11(4):837-850. doi:10.1007/S12975-019-00763-2/FIGURES/6
198. Chen Z, Venkat P, Seyfried D, Chopp M, Yan T, Chen J. Brain-Heart Interaction: Cardiac Complications after Stroke. *Circ Res*. 2017;121(4):451-468. doi:10.1161/CIRCRESAHA.117.311170
199. Chiang T, Messing RO, Chou WH. Mouse Model of Middle Cerebral Artery Occlusion. *J Vis Exp*. 2011;(48):2761. doi:10.3791/2761
200. Neumann J, Hofmann B, Dhein S, Gergs U. Role of Dopamine in the Heart in Health and Disease. *Int J Mol Sci*. 2023;24(5):5042. doi:10.3390/IJMS24055042
201. Zheng K, Chen M, Xu X, et al. Chemokine CXCL13–CXCR5 signaling in neuroinflammation and pathogenesis of chronic pain and neurological diseases. *Cell Mol Biol Lett*. 2024;29(1):134. doi:10.1186/S11658-024-00653-Y
202. Wang L, Chen Y, Feng D, Wang X. Serum ICAM-1 as a Predictor of Prognosis in Patients with Acute Ischemic Stroke. *Biomed Res Int*. 2021;2021(1):5539304. doi:10.1155/2021/5539304
203. Rayasam A, Kijak JA, Kissel L, et al. CXCL13 expressed on inflamed cerebral blood vessels recruit IL-21 producing TFH cells to damage neurons following stroke. *J Neuroinflammation*. 2022;19(1):125. doi:10.1186/S12974-022-02490-2
204. Alasmari F, Alshammari MA, Alasmari AF, Alanazi WA, Alhazzani K. Neuroinflammatory Cytokines Induce Amyloid Beta Neurotoxicity through Modulating Amyloid Precursor Protein Levels/Metabolism. *Biomed Res Int*. 2018;2018. doi:10.1155/2018/3087475
205. Aishwarya R, Abdullah CS, Remex NS, et al. Diastolic dysfunction in Alzheimer’s disease model mice is associated with A $\beta$ -amyloid aggregate formation and mitochondrial dysfunction. *Sci Rep*. 2024;14(1). doi:10.1038/s41598-024-67638-x
206. Hall LG, Czczor JK, Connor T, et al. Amyloid beta 42 alters cardiac metabolism and impairs cardiac function in male mice with obesity. *Nat Commun*. 2024;15(1). doi:10.1038/s41467-023-44520-4
207. Wu S, Du L. Protein Aggregation in the Pathogenesis of Ischemic Stroke. *Cell Mol Neurobiol*. 2021;41(6):1183-1194. doi:10.1007/S10571-020-00899-Y/FIGURES/1
208. Schopf FH, Biebl MM, Buchner J. The HSP90 chaperone machinery. *Nature Reviews Molecular Cell Biology* 2017 18:6. 2017;18(6):345-360. doi:10.1038/nrm.2017.20
209. Marcu MG, Doyle M, Bertolotti A, Ron D, Hendershot L, Neckers L. Heat Shock Protein 90 Modulates the Unfolded Protein Response by Stabilizing IRE1 $\alpha$ . *Mol Cell Biol*. 2002;22(24):8506. doi:10.1128/MCB.22.24.8506-8513.2002

210. Mori M, Hitora T, Nakamura O, et al. Hsp90 inhibitor induces autophagy and apoptosis in osteosarcoma cells. *Int J Oncol*. 2014;46(1):47. doi:10.3892/IJO.2014.2727
211. Ishikawa H, Tajiri N, Vasconcellos J, et al. Ischemic stroke brain sends indirect cell death signals to the heart. *Stroke*. 2013;44(11):3175-3182. doi:10.1161/STROKEAHA.113.001714
212. Bhuiyan S, Pattison JS, Osinska H, et al. Enhanced autophagy ameliorates cardiac proteinopathy. *J Clin Invest*. 2013;123(12):5284. doi:10.1172/JCI70877
213. Matsui Y, Takagi H, Qu X, et al. Distinct roles of autophagy in the heart during ischemia and reperfusion: roles of AMP-activated protein kinase and Beclin 1 in mediating autophagy. *Circ Res*. 2007;100(6):914-922. doi:10.1161/01.RES.0000261924.76669.36
214. Nandi A, Yan LJ, Jana CK, Das N. Role of Catalase in Oxidative Stress- and Age-Associated Degenerative Diseases. *Oxid Med Cell Longev*. 2019;2019(1):9613090. doi:10.1155/2019/9613090
215. Brait VH, Jackman KA, Walduck AK, et al. Mechanisms contributing to cerebral infarct size after stroke: gender, reperfusion, T lymphocytes, and Nox2-derived superoxide. *J Cereb Blood Flow Metab*. 2010;30(7):1306-1317. doi:10.1038/JCBFM.2010.14
216. Meloux A, Rigal E, Rochette L, Cottin Y, Bejot Y, Vergely C. Ischemic Stroke Increases Heart Vulnerability to Ischemia-Reperfusion and Alters Myocardial Cardioprotective Pathways. *Stroke*. 2018;49(11):2752-2760. doi:10.1161/STROKEAHA.118.022207
217. Sanbe A, Osinska H, Villa C, et al. Reversal of amyloid-induced heart disease in desmin-related cardiomyopathy. *Proc Natl Acad Sci U S A*. 2005;102(38):13592-13597. doi:10.1073/PNAS.0503324102/ASSET/476DBDEE-7C7D-4419-95A7-895A12FED9F3/ASSETS/GRAPHIC/ZPQ0390596240006.JPEG
218. Ding Y, Zhao J, Zhang X, et al. Amyloid Beta Oligomers Target to Extracellular and Intracellular Neuronal Synaptic Proteins in Alzheimer's Disease. *Front Neurol*. 2019;10:1140. doi:10.3389/FNEUR.2019.01140/BIBTEX
219. Bernabeu-Zornoza A, Coronel R, Palmer C, López-Alonso V, Liste I. Oligomeric and Fibrillar Species of A $\beta$ 42 Diversely Affect Human Neural Stem Cells. *Int J Mol Sci*. 2021;22(17). doi:10.3390/IJMS22179537
220. Tomic JL, Pensalfini A, Head E, Glabe CG. Soluble fibrillar oligomer levels are elevated in Alzheimer's disease brain and correlate with cognitive dysfunction. *Neurobiol Dis*. 2009;35(3):352-358. doi:10.1016/J.NBD.2009.05.024
221. Wang MJ, Yi S, Han J young, et al. Oligomeric forms of amyloid- $\beta$  protein in plasma as a potential blood-based biomarker for Alzheimer's disease. *Alzheimers Res Ther*. 2017;9(1):98. doi:10.1186/s13195-017-0324-0
222. Gallart-Palau X, Serra A, Pasinetti G, et al. Beta-Amyloid Instigates Dysfunction of Mitochondria in Cardiac Cells. *Cells 2022, Vol 11, Page 373*. 2022;11(3):373. doi:10.3390/CELLS11030373
223. Alberdi E, Wyssenbach A, Alberdi M, et al. Ca(2+) -dependent endoplasmic reticulum stress correlates with astrogliosis in oligomeric amyloid  $\beta$ -treated astrocytes and in a model of Alzheimer's disease. *Aging Cell*. 2013;12(2):292-302. doi:10.1111/ACEL.12054

224. Casas-Tinto S, Zhang Y, Sanchez-Garcia J, Gomez-Velazquez M, Rincon-Limas DE, Fernandez-Funez P. The ER stress factor XBP1s prevents amyloid-beta neurotoxicity. *Hum Mol Genet.* 2011;20(11):2144-2160. doi:10.1093/HMG/DDR100
225. Ivashchenko CY, Pipes GC, Lozinskaya IM, et al. Human-induced pluripotent stem cell-derived cardiomyocytes exhibit temporal changes in phenotype. *Am J Physiol Heart Circ Physiol.* 2013; 305 ( 6 ) : 9 1 3 - 9 2 2 . doi:10.1152/AJPHEART.00819.2012/ASSET/IMAGES/LARGE/ZH40181308670006.JPEG